LBL--27912

DE91 004142

Use of Integrated Geologic and Geophysical Information for Characterizing the Structure of Fracture Systems at the US/BK Site, Grimsel Laboratory, Switzerland

Stephen J. Martel and John E. Peterson Jr.

Earth Sciences Division
Lawrence Berkeley Laboratory
University of California
Berkeley, California 94720

May 1990

This work was supported by the Manager, Chicago Operations, Repository Technology Program, Repository Technology and Transportation Division, of the U.S. Department of Energy under Contract No. DE-AC03-76SF00098 and by the Swiss National Cooperative for the Storage of Nuclear Waste (NAGRA).

Preface

This report is one of a series documenting the results of the Nagra-DOE Cooperative (NDC-I) research program in which the cooperating scientists explore the geological, geophysical, hydrological, geochemical, and structural effects anticipated from the use of a rock mass as a geologic repository for nuclear waste. This program was sponsored by the U. S. Department of Energy (DOE) through the Lawrence Berkeley Laboratory (LBL) and the Swiss Nationale Genossenschaft für die Lagerung radioaktiver Abfälla (Nagra) and concluded in September 1989. The principal investigators are Jane C. S. Long, Ernest L. Majer, Karsten Pruess, Kenzi Karasaki, Chalon Carnahan and Chin-Fu Tsang for LBL and Piet Zuidema, Peter Blümling, Peter Hufschmied and Stratis Vomvoris for Nagra. Other participants will appear as authors of the individual reports. Technical reports in this series are listed below.

1. Determination of Fracture Inflow Parameters with a Borehole Fluid Conductivity Logging Method by Chin-Fu Tsang, Peter Hufschmied, and Frank V. Hale (NDC-1, LBL-24752).
2. A Code to Compute Borehole Fluid Conductivity Profiles with Multiple Feed Points by Frank V. Hale and Chin-Fu Tsang (NDC-2, LBL-24928; also NTB 88-21).
3. Numerical Simulation of Alteration of Sodium Bentonite by Diffusion of Ionic Groundwater Components by Janet S. Jacobsen and Chalon L. Carnahan (NDC-3, LBL-24494).
4. P-Wave Imaging of the FRI and BK Zones at the Grimsel Rock Laboratory by Ernest L. Majer, John E. Peterson Jr., Peter Blümling, and Gerd Sattel (NDC-4, LBL-28807).
5. Numerical Modeling of Gas Migration at a Proposed Repository for Low and Intermediate Level Nuclear Wastes at Oberbauenstock, Switzerland by Karsten Pruess (NDC-5, LBL-25413).
6. Analysis of Well Test Data from Selected Intervals in Leuggern Deep Borehole — Verification and Application of PTST Method by Kenzi Karasaki (NDC-6, LBL-27914).
7. Shear Wave Experiments at the U. S. Site at the Grimsel Laboratory by Ernest L. Majer, John E. Peterson Jr., Peter Blümling, and Gerd Sattel (NDC-7 LBL-28808).
8. The Application of Moment Methods to the Analysis of Fluid Electrical Conductivity Logs in Boreholes by Simon Loew, Chin-Fu Tsang, Frank V. Hale, and Peter Hufschmied (NDC-8, LBL-28809).
9. Numerical Simulation of Cesium and Strontium Migration through Sodium Bentonite Altered by Cation Exchange with Groundwater Components by Janet S. Jacobsen and Chalon L. Carnahan (NDC-9, LBL-26395).
10. Theory and Calculation of Water Distribution in Bentonite in a Thermal Field by Chalon L. Carnahan (NDC-10, LBL-26058).
11. Prematurely Terminated Slug Tests by Kenzi Karasaki (NDC-11, LBL-27528).
12. Hydrologic Characterization of Fractured Rocks — An Interdisciplinary Methodology by Jane C. S. Long, Ernest L. Majer, Stephen J. Martel, Kenzi Karasaki, John E. Peterson Jr., Amy Davey, and Kevin Hestir, (NDC-12, LBL-27863).
13. Exploratory Simulations of Multiphase Effects in Gas Injection and Ventilation Tests in an Underground Rock Laboratory by Stefan Finsterle, Erika Schlueter, and Karsten Pruess (NDC-13, LBL-28810).
14. Joint Seismic, Hydrogeological, and Geomechanical Investigations of a Fracture Zone in the Grimsel Rock Laboratory, Switzerland by Ernest L. Majer, Larry R. Myer, John E. Peterson Jr., Kenzi Karasaki, Jane C. S. Long, Stephen J. Martel, Peter Blümling, and Stratis Vomvoris (NDC-14, LBL-27913).
15. Analysis of Hydraulic Data from the MI Fracture Zone at the Grimsel Rock Laboratory, Switzerland by Amy Davey, Kenzi Karasaki, Jane C.S. Long, Martin Landsfeld, Antoine Mensch, and Stephen J. Martel (NDC-15, LBL-27864).
16. Use of Integrated Geologic and Geophysical Information for Characterizing the Structure of Fracture Systems at the US/BK Site, Grimsel Laboratory, Switzerland by Stephen J. Martel and John E. Peterson Jr. (NDC-16, LBL-27912).

Table of Contents

List of Figures

List of Tables

Abstract

Fracture systems form the primary fluid flow paths in a number of rock types, including some of those being considered for high level nuclear waste repositories. In some cases, flow along fractures must be modeled explicitly as part of a site characterization effort. Fractures commonly are concentrated in fracture zones, and even where fractures are seemingly ubiquitous, the hydrology of a site can be dominated by a few discrete fracture zones. We have implemented a site characterization methodology that combines information gained from geophysical and geologic investigations. The general philosophy is to identify and locate the major fracture zones, and then to characterize their systematics. Characterizing the systematics means establishing the essential and recurring patterns in which fractures are organized within the zones. We make a concerted effort to use information on the systematics of the fracture systems to link the site-specific geologic, borehole and geophysical information. The better the structural systematics can be defined, the more confidence can be placed in the interpretation of the site.

The procedure generally is applied to a specific site in a four-step sequence. First, information on the region encompassing the site is assembled and a model of the geologic structure in the vicinity of the target site is prepared. The major structures that might intersect the site are identified in this stage. Second, detailed geologic mapping is conducted to define the structural systematics of the major fracture zones near the site and to gain insight into how fluid might flow along the zones. Third, a preliminary geologic model of the major structures at the site is prepared using the regional information together with geologic mapping and borehole surveys along the target site perimeter. Finally, the model can be refined based on borehole information, Vertical Seismic Profiling (VSP), and geophysical tomography investigations.

This methodology was applied at the US/BK site at the Grimsel underground rock laboratory in Switzerland, situated in granitic rock. The US/BK site is bounded on the north and south by boreholes that are about 150 m long that are spaced about 150 m apart. The site is bounded on the east by the main tunnel at the laboratory. We modeled the structure within the site by projecting the major features exposed in the tunnels adjacent to the site using borehole information and geophysical tomograms. The major elements in our model all dip steeply. They are: 1) A discontinuous northeast-striking shear zone that intersects the northeast corner of the site. Three echelon shear zone segments occur within the site. 2) A lamprophyre-bearing fault zone that strikes west through the center of the site. This prominent feature separates the northern and central shear zone segments. 3) A few northwest-striking lamprophyres in the south-central and northwest parts of the site. The southern lamprophyres separate the central and southern shear zone segments; 4) A west-striking fault zone midway between the first fault zone and the southern boundary of the site. The anastamosing fractures in the shear zones should provide a well connected network for flow. We expect that fluid would not be conducted readily across the lamprophyre-bearing fault zones and the lamprophyres, but it could be conducted along them. Flow in the west-striking fault zone probably occurs most readily in the steps between echelon fault segments where fractures are particularly abundant.

This model is consistent with the results of two brine tracer injection tests conducted at the US/BK site. The brine was tracked using two-dimensional radar difference tomography. The difference tomography does suggest that a detectable portion of the flow at the site occurs along fractures that do not form major throughgoing zones.

In many aspects Grimsel was an ideal place to apply the methodology outlined here. Geologic and geophysical information was abundant and the fracture zones were very well exposed in several places at the surface and in the subsurface. In many places excellent exposures will not be readily available and it may be extremely difficult (or too expensive) to determine the sys-

tematics of the fracture systems. In such cases, studies of structures in geologically analogous areas may be useful, even if those areas are distant from the target site.

We strongly recommend that those modeling a site personally visit the site, have access to all the original raw data, and be able to collect new data through the course of an investigation. Those who collect the initial field data should clearly highlight features that appear particularly interesting, important, or unusual to ensure that important factors are brought into the modeling at an early stage. We highly recommend that geologic and geophysical investigators cooperate closely in all stages of experimental design, data collection, and interpretation.

Acknowledgements

Many people have helped us carry out this study. Foremost is Dr. Jane Long of Lawrence Berkeley Laboratory who tirelessly promoted the approach taken in this study and also served as a tenacious and conscientious editor of this report. This report is certainly a reflection of her encouragement and perseverance. Discussions with other members of the fracture hydrology group at LBL, notably Kenzi Karasaki and Amy Davey, also aided this study. Peter Blümling and Paul Bossart of Nagra also contributed constructive reviews of this report. Finally, Piet Zuidema, Peter Blümling, Stratis Vomvoris, and Paul Bossart of Nagra and the technical staff at the Grimsel Laboratory established a friendly and supportive climate for the fieldwork and served as gracious hosts during our stays in Switzerland.

1.0. INTRODUCTION

Geologic heterogeneities can strongly influence groundwater flow and are important factors in a variety of problems involving the transport of hazardous waste in groundwater and the evaluation of prospective high-level nuclear waste repositories. Indeed, at many sites (such as those in rocks with low matrix permeability) fluid flow occurs most readily along geologic heterogeneities and not the background medium. However, it is extremely difficult, if not impossible, to uniquely identify the heterogeneities at a given site based on hydrologic data alone; in general many different hydrologic models will be consistent with the available hydrologic data. Without using additional information, the most realistic hydrologic models may be obscured by a host of others that are actually incompatible with the site geology.

One way to help focus the hydrologic modeling effort is to apply information on the geologic heterogeneities early in the modeling process. Both geologic observations and geophysical measurements can contribute to a better knowledge of the geologic framework. The geologic and geophysical information can also be used throughout a modeling program to identify critical places to test competing hydrologic models.

This report illustrates how geologic and geophysical information on geologic heterogeneities can be integrated to guide the development of hydrologic models. The report focuses on fractures, a particularly common type of geologic heterogeneity. However, many aspects of the methodology we present can be applied to other geologic heterogeneities as well.

Fractures are a particularly ubiquitous type of geologic heterogeneity. They occur in all rock types over a broad range of scales. Fractures also pose a formidable hydrologic modeling problem, for even where they are abundant, they commonly are not sufficiently interconnected for the rock to behave as a porous medium. As a result, porous media models may not reliably

describe fracture flow (Long et al., 1982); in some cases they severely underpredict flow rates (Geldon, written communication, 1989). In certain situations, fracture flow must be considered explicitly in the hydrologic characterization of a site.

Part of the difficulty in modeling the hydrology of a fracture system stems from the abundance of fractures. In many places fractures are so numerous and of so many different sizes and orientations that it is impossible to evaluate each fracture individually. This has encouraged some investigators to use a statistically-based approach (e.g. Rouleau and Gale, 1985; Dershowitz, 1984; Robinson, 1984; Long and Billaux, 1987; Billaux et al., 1989; Howard and Nolen-Hoeksema, 1990). In these approaches, a small sample of individual fractures is observed in excavations or drill cores and their location, orientation, trace length, aperture, etc. recorded. The distributions of these parameters are then treated statistically, and the distributions extrapolated to cover the volume of the site under consideration. To build a realistic model one must infer the fracture geometry from the statistics, and that is very hard to do. Although these approaches are useful for revealing how different distributions can affect fluid flow, they can lead to misleading conclusions regarding the hydrology at a specific site for a variety of reasons. There are two particularly persistent problems. One is the difficulty of characterizing the three-dimensional fracture structure of even small samples from what are essentially one- or two-dimensional data. The other is of scale; fracture networks are in many aspects not scale-independent and extrapolations must be made using a sample size that is too small.

We have used a different approach that recognizes that fractures commonly are organized into discrete fracture zones. These zones can dominate the hydrologic behavior of large volumes of rock, volumes that are the size of a repository or larger, even where fracturing appears pervasive (Long et al., 1989). For example, at a test block in the Stripa mine in Sweden, fracture zones in the granite occupy approximately 4% of the rock volume yet account for 94% of the hydraulic transmissivity (Olsson et al., 1988). Most of the water-producing zones in boreholes at Yucca Mountain also are associated with fracture zones (Geldon, 1989). Findings such as these have motivated our effort to devise a methodology for characterizing the geologic structure of

fracture zones to assist in hydrologic modeling.

As discussed in section 2.0, fracture zones commonly exhibit some kind of regular organized internal structure. We make a major effort to determine the systematic structural patterns in the fracture zones, and we use that information to guide us in our structural modeling. As we will discuss below, a knowledge of fracture zone systematics can help in several aspects of an integrated geologic/geophysical site evaluation. The fracture zone approach should be time-effective because we can bypass much of the need to collect data on each individual fracture. Finally, we try to address scaling problems by examining fracture zone systematics at a variety of scales. Large regions that enclose a site are examined as well as small regions within it or adjacent to it.

We have had the good fortune to be able to develop our methodology in a location well suited for the task, the Grimsel Rock Laboratory in Switzerland. The Swiss National Cooperative for the Storage of Radioactive Waste (NAGRA) has hosted a variety of experiments in the past few years at the Grimsel Laboratory directed towards improving site characterization techniques and the understanding of fracture flow. A broad variety of geologic and geophysical information is available on the fracture systems there, and the fracture systems are well exposed. This laboratory is located inside a mountain (the Juchlistock) in the Bernese Alps near the headwaters of the Aare River (Figure 1.1). The laboratory is at an elevation of ~1730 m, a few hundred meters below the surface. Several test sites occur at the laboratory; they are located using a code designating the host tunnel and the distance along that tunnel from its entrance. We have modeled the geologic fracture structure at the US/BK site (Figure 1.2). This site contains the BK room room, which branches from the main laboratory tunnel between L174.5 and L184. In map view the US/BK site has dimensions of approximately 150 m on a side.

The body of the report has five sections:

(1) A brief discussion of fracture zones, related geologic structures, and factors controlling fracture patterns in fracture zones;

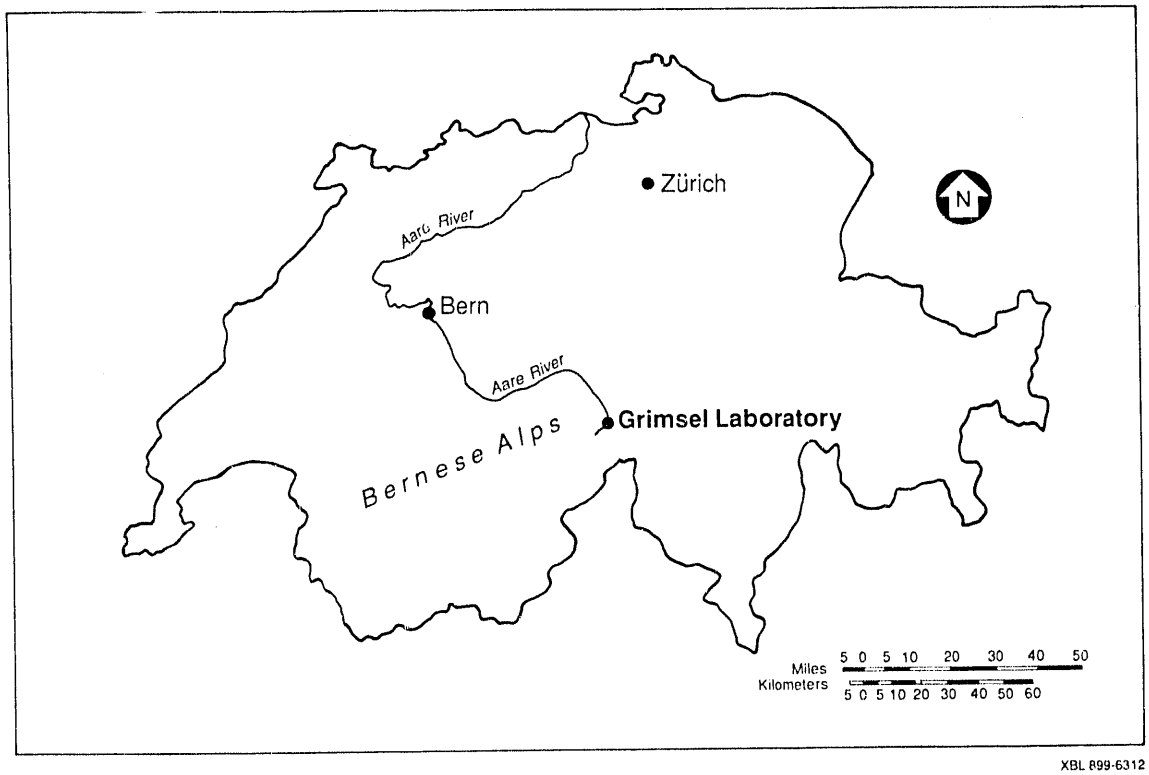

Figure 1.1. Location of the Grimsel laboratory in Switzerland.

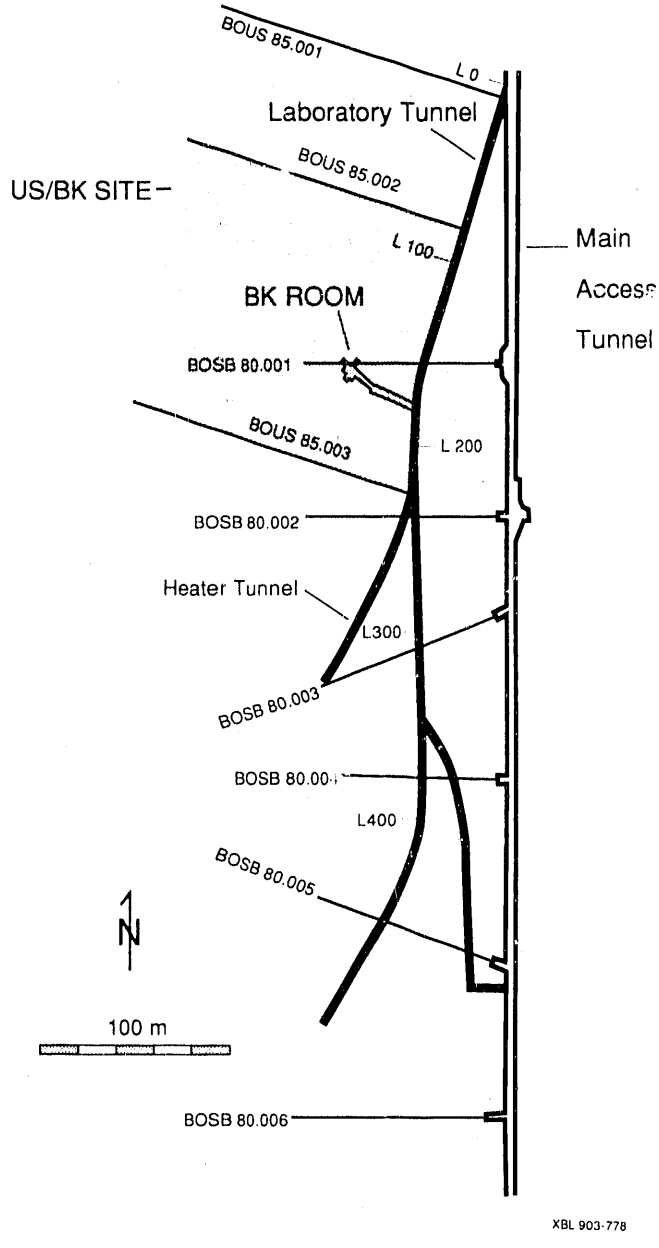

Figure 1.2. Map of the Grimsel rock laboratory showing the location of the US/BK site, the first six exploratory (BOSB) boreholes drilled from the main access tunnel, and the BOUS boreholes. BOUS 85.002 and BOUS 85.003 bound the US/BK site. Modified from NTB 87-14, Plate 3.

(2) Overview of current LBL methodology for modeling fracture systems as part of a hydrogeologic characterization;

(3) The application of this methodology for the construction of a conceptual model at the US/BK site;

(4) Analysis of radar difference tomography used to test our model of the US/BK site;

(5) Conclusions on the applicability of our methodology.

An appendix contains some of the borehole fracture data we used in constructing our model.

2.0. FRACTURE ZONE PATTERNS AND GROWTH MECHANICS

Three classes of relatively planar structures are common in a variety of rock types and geologic settings: fracture zones, shear zones, and igneous dikes (Figure 2.1). Certain fracture patterns commonly develop in or along these features. These patterns reflect to a large extent the control that the stress state and the presence of pre-existing weaknesses exert on fracture growth.

Fractures are structural discontinuities; a feature cut by fractures cannot be traced continuously across them. There are two major kinds of fractures, joints or dilatant fractures (Figure 2.1a) and faults (Figure 2.1b). The relative displacement of the opposing walls of a joint is predominantly perpendicular to the joint; relative displacement parallel to the joint is minimal. Joint walls may dilate in response to either a remote tensile stress or an internal pressure (such as from a fluid) that exceeds the compressive stress perpendicular to the joint (Pollard and Segall, 1987). The relative displacement of the opposing walls of a fault is predominantly parallel to the fault. Shear zones (Figure 2.1c), like faults, accommodate shear deformation, but unlike faults, deformation across shear zones is continuous. The mineral grains in a shear zone characteristically are preferentially oriented subparallel to the zone, so the rock in shear zones is anisotropic. Ductile shear zones presumably form under higher temperature/pressure conditions or lower strain rates than fractured fault zones. Still, many fault zones are probably rooted in ductile shear zones (e.g. Sibson, 1977) or develop from them. Igneous dikes (Figure 2.1d) can either intrude pre-existing fractures or form their own (Delaney et al., 1986). Many dikes have a maximum thickness greater than a meter, whereas most joints have a maximum thickness of less than a centimeter. It is not uncommon for dikes to serve as nuclei for shear zones (Lisle, 1989) or for deformation of dikes to cause fracturing in the adjacent rock.

Traditionally, fractures in the earth have been considered to be a product of shear failure in response to remote loads. The growth of joints and dikes and the spatial variation of fracturing

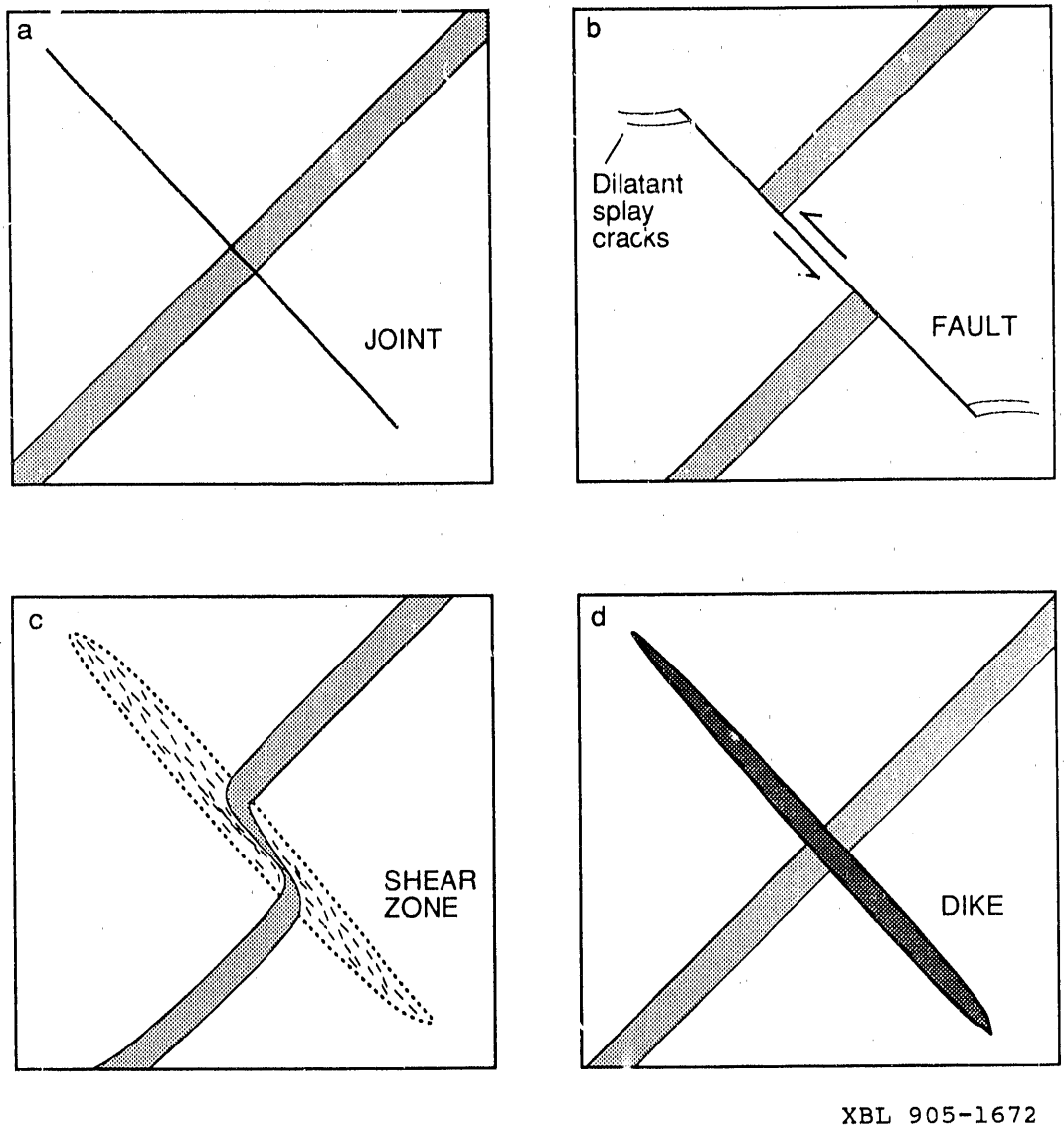

Figure 2.1. Four examples of common planar geologic structures. The feature in light grey is an arbitrary marker: (a) joint, (b) fault, (c) shear zone, and (d) dike.

along faults are difficult to account for from this perspective. We consider fractures from the standpoint of fracture mechanics, which deals with the remote stresses and the stress concentrations near a fracture tip. Theoretically, the near-tip stress field will be very heterogeneous, with large shear, compressive, and tensile stresses occurring; tensile near-tip stresses can arise no matter how large the regional compressive principal stresses are (Lawn and Wilshaw, 1975). Rock properties together with the local stress state will govern whether fracture growth occurs by shear or tensile failure.

Joints probably are the most common type of rock fracture. In relatively isotropic rocks like massive sandstone or granite, an isolated joint typically will be very nearly planar. This probably reflects a remote stress state that is symmetric with respect to the joint, the least compressive stress being perpendicular to the joint. The theoretical near-tip tensile stress concentration is symmetric about the tip of a isolated, slowly-growing, dilatant fracture, but the shear stress concentration is asymmetric (Lawn and Wilshaw, 1975) Accordingly, in-plane growth would be favored if a joint grew due to tensile failure at its tip, and out-of-plane growth would be favored if it grew due to shear failure at the tip. The planar shape of a joint and the style of relative displacement across a joint indicate that joints propagate in response to localized tensile failure at their tips and not shear failure.

Joints usually occur in sets of nearly planar subparallel joints (Figure 2.2a). These observations are consistent with the hypothesis that the regional stresses strongly control the orientation of the joints, with the maximum compressive stress being significantly different in magnitude from the least compressive stress (Olson and Pollard, 1989). Without a strong contrast in the remote stresses, the stress perturbations caused by the presence of the joints themselves would cause the joints to have highly curved shapes (Olson and Pollard, 1989). Elastic analyses demonstrate that the growth of a given joint would diminish the stress driving the growth of most nearby joints; this shielding effect is most strongly exerted by the longest joints. As a result, the growth of the longer joints should be favored, and the resulting fracture pattern should contain many short joints and fewer long ones (Segall and Pollard, 1983a). This is precisely one of the

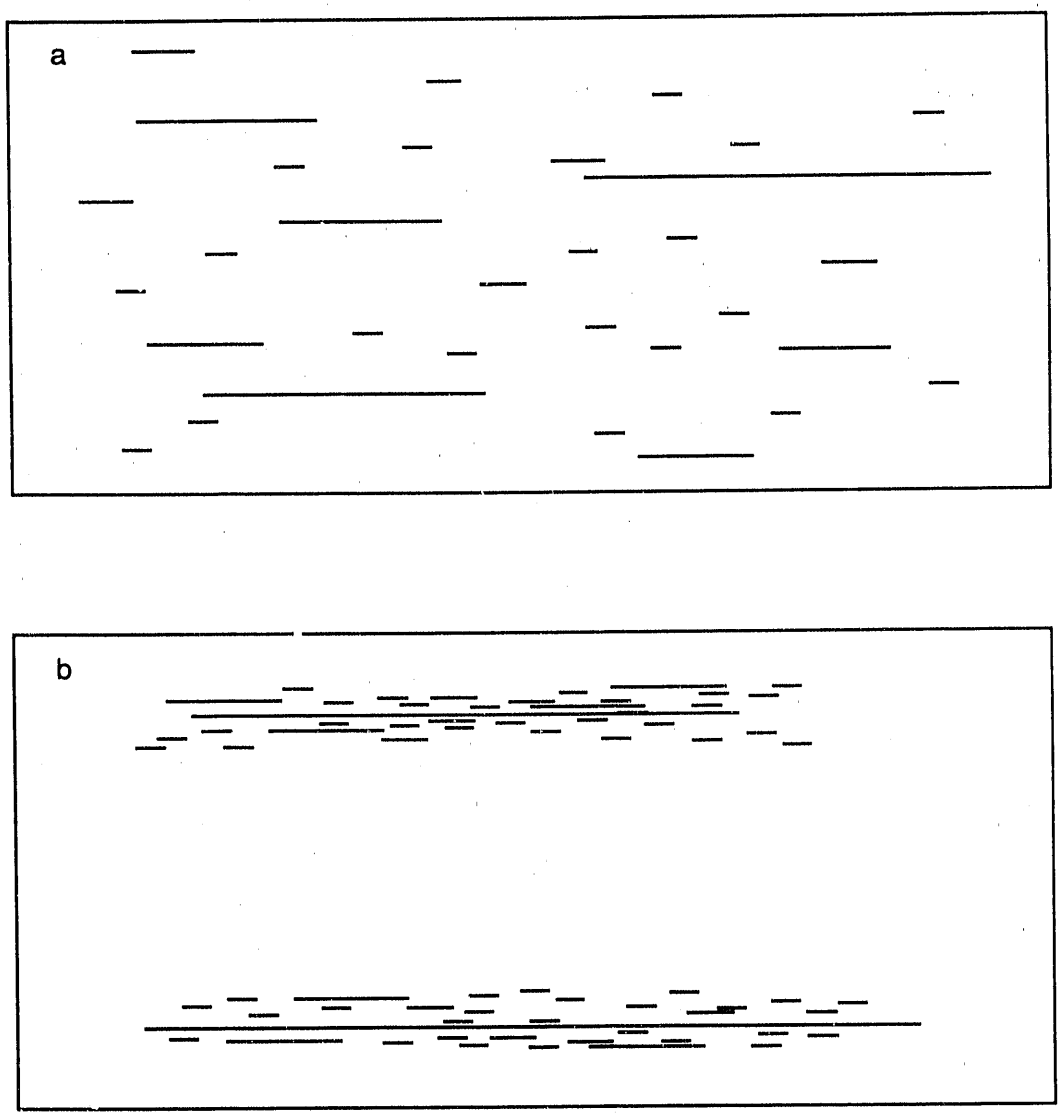

Figure 2.2. Examples of joint patterns: (a) joint set and (b) two joint zones. In the upper zone, joints have formed in front of the longest joint. In the lower zone, the longest joint has propagated past previously-formed flanking joints.

patterns most commonly observed.

Joint zones (Figure 2.2b) consist of clustered, overlapping, subparallel joints (Dyer, 1983) and form one kind of fracture zone. The spacing between joint zones is large relative to the spacing of joints within a zone. Both the zones and the joints in them are nearly planar. Joint zones resemble clusters of joints along some dikes, and both the zones and the clusters may form by a similar process. Some dike-parallel joints are inferred to open in response to the tensile stress concentration at the tip of a propagating dike (Delaney et al., 1986) and then be left in the wake of the dike tip as it advances. By analogy, a joint zone may form in response to the stress concentration at the tip of a particularly large joint.

Faults, the second major class of fractures, have traditionally been considered not only to accommodate shear displacement but also to *originate* as shear fractures (e.g. Sylvester, 1988). This perspective has developed largely as a result of shear fractures being formed in numerous laboratory compression tests on small rock samples. However, in recent years this view has come under increasing scrutiny. Detailed examinations of isotropic test specimens consistently show that shear fractures are not primary features. Instead, arrays of dilatant fractures first form parallel to the maximum compressive stress; only if deformation proceeds far enough do these fractures link up to form shear fractures (e.g. Peng and Johnson, 1972). Furthermore, attempts to propagate fractures in isotropic rocks under shear loads usually result in dilatant fractures propagating out-of plane from the fracture tips (Ingraffea, 1981). In laboratory compression tests on anisotropic rock, shear fractures do develop parallel to the anisotropy in the rock (Donath, 1961); these shear fractures may be primary structures. The laboratory compression tests thus imply that faults rarely originate as shear fractures in isotropic rock masses and that pre-existing dilatant fractures and rock anisotropy would strongly influence fault growth.

Field observations consistently show that faults of substantial size exploit pre-existing weaknesses as they develop (e.g. Muehlberger, 1986). In fact, we are aware of few examples (e.g. Aydin and Johnson, 1978) to the contrary. Faults and fault zones can originate from pre-existing joints (Segall and Pollard, 1983b; Martel et al., 1988). Faults can also develop from

pre-existing shear zones; shear zones in turn can develop from joints (Segall and Simpson, 1986) and dikes (Lisle, 1989). Systems of dilatant features (i.e. joints and dikes) can have lengths of many kilometers and can provide long planar flaws for long planar faults to develop from.

Fault zones can develop as originally discontinuous faults become linked together (Figure 2.3). Dilatant fractures that form as a result of fault slip can serve as links (Segall and Pollard, 1983; Martel et al., 1990); as may shear fractures (Sibson, 1986a). The secondary linking fractures occur in predictable locations. Elastic analyses indicate that secondary fractures are likely to form where extensional gradients are high along faults. High gradients would be expected at the ends of faults and at geometric irregularities along them, and numerous dilatant fractures do occur in those places (Sibson, 1986a; Martel et al., 1988; Martel and Peterson, 1989). Mineralization is common in regions such as these (Sibson, 1981) and provides direct evidence for pronounced fluid flow there. Secondary dilatant fractures also occur where geometric irregularities are not pronounced (Martel et al., 1988), presumably as a result of transient stress concentrations along the fault zones (Martel and Pollard, 1989). Both kinds of secondary dilatant fractures tend to be aligned perpendicular to the least compressive remote stress. Because the remote principal stresses would be oriented oblique to an activated fault zone, many of the fractures in fault zones can have orientations that are systematically oblique to the zones.

The laboratory compression tests on anisotropic rocks suggest that anisotropy in the earth may control the development of many fault zones. Swanson (1988) has documented aligned faults that developed along layering in metamorphosed sedimentary rocks. Anisotropy may also enhance the ability for aligned sets of fractures to subsequently form in shear zones (Figure 2.4). The fabric in ductile shear zones commonly has an anastamosing or braided form (Berthe et al., 1979), and anastamosing fractures are common in fault zones (Wallace and Morris, 1986).

Many fault zones have been reactivated under different stress regimes and different environmental conditions (Muehlberger, 1986; Sibson, 1986b). Some of the key factors influencing the growth of fractures in fault zones, such as the magnitude and orientation of the regional principal stresses, the mechanical behavior of the rock, and the fluid pressure, can

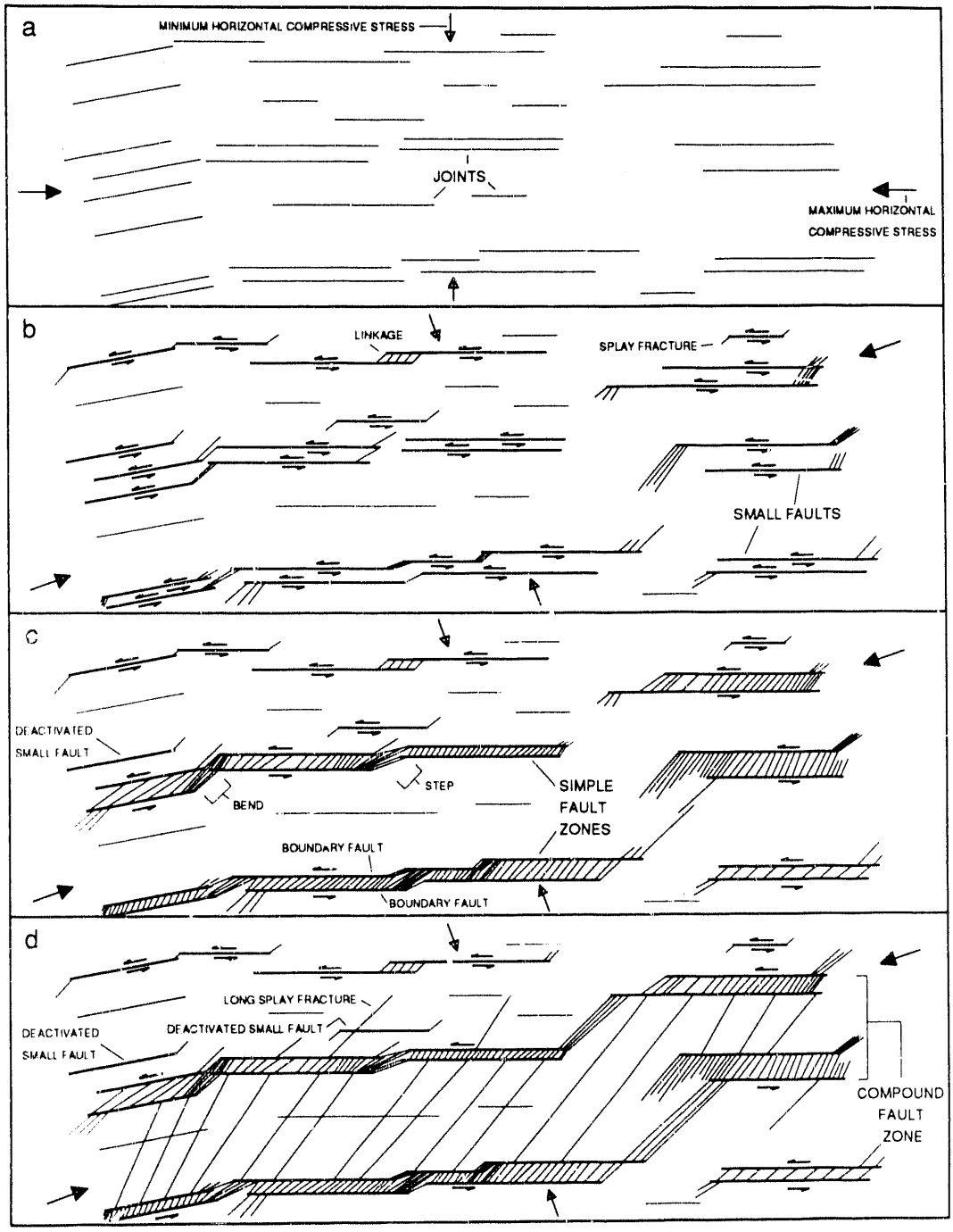

Figure 2.3. Growth of fault zones from a joint set: (a) opening of joints, (b) development of faults, (c) development of simple fault zones, and (d) formation of compound fault zones (from Martel, 1990).

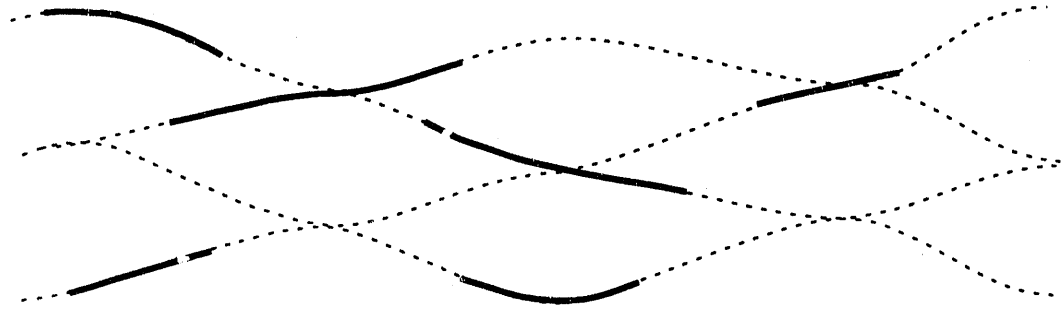

XBL 905-1676

Figure 2.4. Formation of fractures (heavy lines) in a shear zone. Light lines represent aligned minerals defining the foliation within the shear zone.

change with time. Many generations and orientations of internal fractures may form. As fractures become more numerous, the stress state in a fault zone is likely to become increasingly heterogeneous. Because of the varying conditions under which fracturing would occur, the fracture patterns that develop in many ancient reactivated fault zones are likely to be quite chaotic.

3.0. CURRENT LBL METHODOLOGY

The purpose of our combined geologic and geophysical investigation is to identify, locate, and characterize the major structures in a given area to aid in building hydrologic models. The geologic and geophysical contributions have different strengths and different limitations. To a large extent a weakness in one discipline is offset by strength in the other; this is a major reason why a joint investigation can be particularly fruitful. We first discuss the individual contributions and then give some examples of how the geologic and geophysical efforts operate in tandem.

3.1. Geologic Contribution

Surface and subsurface exposures allow geologists to directly observe fracture systems. The exposures can range from natural surface outcrops to subsurface excavations and boreholes. There are several goals for geologic observations for the purposes of this report. The first is to identify and locate major fracture systems. The second purpose is to to determine the systematics of their structure. Determining the systematics of a fracture system means characterizing the essential and recurring patterns in which fractures are organized within the system. A comprehensive evaluation of the systematics of a fracture zone would ideally account for the consistent patterns in the relative age, the spatial distribution, the mode of formation, and the orientation of fractures within the zone. A third goal is to project the structures from the area where they are visible to areas where they are not. This is commonly done in the form of geologic cross sections, and the fracture zones will typically be projected as planar features. Projections should be made with care and ideally should involve the geologist who makes the field observations. These projections can be tested using the results of geophysical investigations. A fourth objective is to use the observations to infer how water might flow along a given structure and from one structure to another.

It is fruitful to observe fracture zones at a variety of scales. This can reduce the chances of serious error in extrapolating data from one scale to another. Regional geologic mapping is important because it can be used to identify and locate major structures that might impact a site. Major features may be difficult to recognize if observations are only made in small exposures in the subsurface. At the other end of the spectrum, detailed large-scale geologic mapping can reveal the internal systematics of the major fracture zones; this information is useful for interpreting borehole records and for inferring how fluid might flow along the zones. Mapping at an intermediate scale can tie the small-scale and large-scale observations together.

Detailed geologic mapping plays an important role in our approach to characterizing fracture zone systematics. Detailed mapping is particularly effective in revealing the structural and age relationships of the fractures within a fracture zone, as well as their shapes, lengths, positions, and orientations. The maps present a system in the form of an integrated picture rather than a series of disconnected points. Moreover, the act of mapping forces the geologist to think about what the mapped patterns mean. Critical questions might not even be raised if one only records fracture locations and orientations on a logging form. Particularly well-exposed zones should be examined in detail a) to document the essential elements of their structure, b) to relate the style of their internal structures to their overall forms, and c) to assess their structural variability. Because precise, detailed mapping is time consuming, it must be done selectively. The focus of the detailed mapping should be on the outcrops with the largest and most complete exposures of the rock matrix and the major structures. Informative exposures can be found at or near some sites, but in many cases, exposures may be of insufficient quality or size to achieve the three objectives listed above. In such cases, mapping of fracture zones in analogous geologic settings can be useful, even if the exposures are well removed from the particular site in question.

Small-diameter boreholes provide the least expensive way to directly sample the geology within an unexposed volume of rock. They can be extremely useful in preparing or checking structural models made from maps and geophysical images. However, there are several limitations in using borehole data alone to construct models of fracture zones. Some problems stem

from the combination of small sample size and fracture irregularity. Unless a fracture is entirely confined within a borehole core, it is impossible to determine the dimensions of a fracture solely on the basis of borehole records. In some cases the relative thicknesses of fracture fillings may indicate the relative lengths of different fractures, but no universal quantitative relationships exist. Furthermore, although many fracture zones are relatively planar, the individual fractures within a zone can have irregular, nonplanar shapes. The orientation of a fracture at a point (i.e. where intersected by a borehole) thus can be a poor indicator of the orientation of the zone containing the fracture. Because of the uncertainties in fracture size and shape, an essentially unlimited number of fracture geometries would be compatible with a given borehole record. Figure 3.1 shows a simple example of how the same borehole fracture record can reflect entirely different fracture configurations. In one case (Figure 3.1a) the average orientation of a cluster of fractures encountered in a borehole can be a good indicator of the orientation of the zone as a whole. However, if the internal fractures are systematically oblique to the zone as a whole (Figure 3.1b), then this approach will yield a grossly incorrect zone orientation. In the case of Figure 3.1a the fractures are not hydrologically connected, whereas in Figure 3.1b they are. The actual sizes and shapes of the fractures clearly are important in determining the hydrologic behavior of the fracture zone. These factors can be exceedingly difficult to constrain from borehole data alone, even where boreholes are fairly numerous. The work on the structural systematics can reveal how individual fractures are arranged in fracture zones and therefore can be extremely valuable in interpreting borehole fracture data.

Another problem with borehole data is that of "borehole bias" (Terzaghi, 1965). The distribution of fracture orientations in a borehole depends on the orientation of the borehole itself. Fractures perpendicular to a borehole are more likely to be intersected than those parallel to it. Because of borehole bias, different boreholes may appear to encounter fracture zones with different orientations even if only one orientation occurs. Borehole bias effects highlight the importance of checking the interpretations of borehole data against independent findings wherever possible.

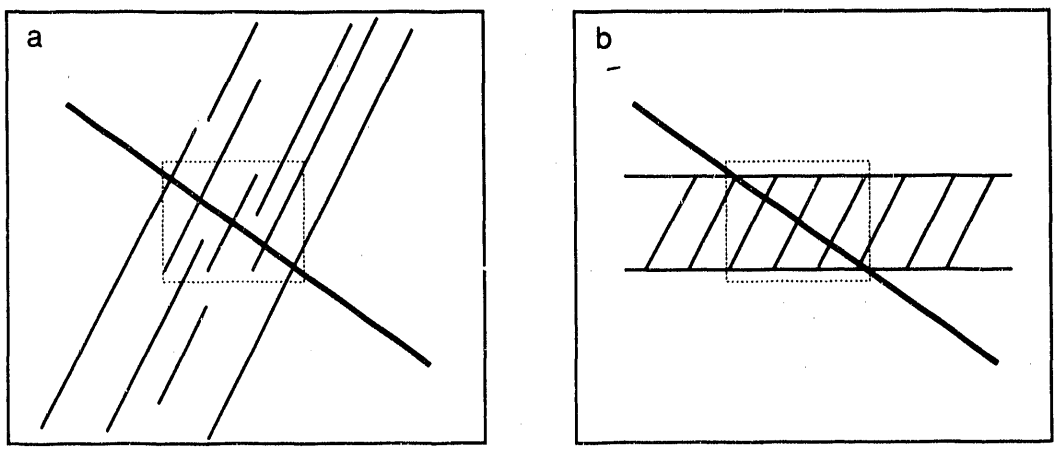

Figure 3.1. Two markedly different fracture zones can have the same appearance where they intersect a borehole (shown in heavy line): (a) a series of joints, and (b) a fault zone. Dotted box is for reference.

3.2. Geophysical Contribution

Geophysical techniques provide non-invasive ways to evaluate rock properties within a body of rock. In general, active geophysical techniques compare the responses of a body to a stimulus. Different elements of the body may respond differently, and by using signal processing techniques, the different elements can be identified and located. Seismic and electromagnetic techniques have been developed to sophisticated levels for this purpose. They can help project major features identified at the surface or in boreholes and can detect subsurface structures which were not previously identified. As a result, they provide a way to check and improve the structural model of a site. Geophysical investigations complement geologic work in that they are directed at unexposed portions of the site.

Seismic techniques are useful for evaluating the elastic properties of a rock mass and its density. These depend in turn on rock type, porosity, fluid content, and fracture distribution. For example, elastic wave velocities generally increase as a function of increasing rock stiffness. For a fixed saturation, an increase in rock porosity generally will decrease wave velocity. Wave velocities generally increase with the level of saturation. Signal attenuation is related to physical parameters in a complex manner.

Fractures can be detected by their effect on the velocity and attenuation of seismic signals. A zone of fractured material will usually be more compressible than the adjacent unfractured rock and thus have a lower velocity and higher attenuation. Even a single fracture can affect the signal depending on the stiffness of the fracture (Schoenberg, 1980, 1983). Compliant fractures will result in a lower velocities and increased attenuation relative to stiff fractures.

Electromagnetic techniques are used to sense variations in parameters such as electrical resistivity or conductivity, dielectric constant, and magnetic permeability (Telford et al., 1976). In many cases the electromagnetic properties of a rock mass are dominated not by the mineralogy of the rock, but instead by its water content. Therefore, the porosity and saturation of a rock mass will have relatively large effects on electromagnetic waves. This means electromagnetic waves are useful for evaluating the hydrologic properties of rock.

We focus here on techniques that use seismic and radar signals. These techniques are especially effective techniques for site characterization. Borehole logging techniques are useful for detecting properties at distances of a few meters or less from a transmitter. Reflection techniques, vertical seismic profiling (VSP), and tomography are effective over distances of at least one hundred meters.

Borehole logging reveals rock properties near a borehole. In geophysical borehole logging, a probe is lowered down a hole and it radiates a signal into the surrounding rock. The signals typically sample no more than a meter or so into the rock. Based on the signal return at the probe, parameters such as seismic velocities, electrical resistivity, porosity, and density of the rock along the borehole may be determined (Telford et al., 1976). These parameters can be altered by

the drilling process and may be different from undisturbed values away from the hole.

Reflection techniques are sensitive to impedance contrasts in the earth. The impedance of a rock is a product of the density and velocity of a rock; it is usually dominated by the velocity. Reflection surveys have traditionally used seismic signals to resolve large geologic structures and stratigraphic sequences. These seismic surveys use a transmitter and a series of receivers that together form a colinear array and are most effective in revealing subhorizontal structures parallel to the receiver array that have adequate impedance contrasts. Reflection surveys can also be done using radar signals, but radar signals typically penetrate much less than seismic signals. Downhole radar reflection techniques can be used to detect reflectors subparallel to a borehole. This can be an effective way to image fracture zones (Olsson et al., 1987).

Unlike conventional reflection techniques, in vertical seismic profiling (VSP) the receivers are down a deep vertical borehole instead of at the surface. The VSP transmitter typically is located within a few tens of meters of the borehole mouth. As with conventional reflection techniques, signals from the transmitter are reflected by features in the rock and detected by the borehole receivers. VSP is well-suited for detecting reflectors adjacent to a borehole or beyond it. VSP can thus help extend information provided by borehole logging further away from the hole. VSP signals will tend to be sharper than those from conventional reflection techniques because VSP signals pass through weathered near-surface rock only once instead of twice. The VSP geometry allows reflectors that dip steeply to be detected. Information on rock anisotropy and porosity can be obtained by using receivers that detect compressional waves and vertical and horizontal shear waves (Stewart, et al., 1981; Daley, et al., 1988). The three-component information can also allow fracture density and orientation to be estimated.

Cross-hole tomography is a particularly useful technique for non-destructively imaging seismic and electromagnetic properties of rock over distances as great as a few hundred meters. Signals are transmitted between transmitter and receiver arrays along either two coplanar boreholes or along a borehole and a coplanar line along the surface. Tomograms, images of the velocity and attenuation fields, are reconstructed by applying inverse techniques to the measured

signal travel times and amplitudes (Peterson, 1986). Distinctive geologic features in the imaged rock mass will be depicted on the processed tomograms as anomalies.

It is important to note that tomograms must be interpreted. Perceived anomalies on tomograms do not correspond uniquely to geologic features in a rock mass. There are two main reasons for this. First, anomalies on tomograms can correspond to a variety of geologic effects. Independent information on the geology can be used to determine which geologic features are most likely represented in the image. Second, the inversion process itself commonly produces artifacts that can be difficult to distinguish from the anomalies associated with real geologic structures. A knowledge of the techniques applied to collect and process tomographic data is vital in identifying artifacts. Artifacts are most numerous where raypaths are most sparse and at the edges of tomograms. The location and spacing of sources and receivers can be used in conjunction with a map of the ray paths to identify regions where raypaths are sparse.

3.3. Integration

Geologic and geophysical investigations clearly can complement each other. Geologic investigations are well-suited to identify, locate, and characterize exposed features, but they are limited in their ability 1) to determine how far to project known features and 2) to detect unexposed features. On the other hand, geophysical investigations can locate unexposed features, but are limited in their ability to uniquely determine the type of geologic features they detect. A clear use of geophysical information is to help project features within a site. A key contribution of geologic information is to prevent geophysical data from being interpreted blindly. If certain geologic features are known to be either exposed at the perimeter of a site or intersected within the site by boreholes, geophysical images should be interpreted with that information in mind.

3.4. Application

3.4.1. Reconnaissance

The first step in modeling the fracture structure at a given site is to review the existing information on the general geology in the vicinity of the site. The available material may range

from a single geologic reconnaissance map to an extensive literature that includes reports of site-specific geologic and geophysical investigations. Ideally this review will reveal the types and distributions of the major geologic features. The second step is to visit the site. This will allow those constructing the geologic model to get a hands-on feel of the complexity of the site and to assess the accuracy, level of detail, and extent of the previously conducted work.

3.4.2. Regional Modeling

The reconnaissance work sets the stage for regional modeling of the geology near the site. Regional geologic modeling has two main purposes:

(1) To identify structures which are likely to be encountered near the target site;

(2) To provide a larger context in which to view the site-specific model.

Only the gross external geometries of the major structures need be known at this stage. Detailed information on specific structures can be gathered once it is determined which structures are likely to be present at the target site. In cases where the major structures are exposed at the surface, the position and orientation of the major features would be established by the reconnaissance mapping. Projections such as geologic cross sections or block diagrams would show how the major structures might be arranged in the vicinity of the target site. Seismic reflection and VSP techniques, together with the drilling of deep boreholes, can aid in preparing a preliminary model of the major structures in the vicinity target site.

3.4.3. Selective Detailed Geologic Mapping

Selective detailed geologic mapping is done to determine the internal systematics of the major features that are likely to exist within the site. As noted above, the detailed mapping should focus on the outcrops with the largest and most complete exposures of major structures. In cases where local exposures are of insufficient quality or size to determine systematics, it can be useful to map similar structures in analogous geologic settings.

3.4.4. Site-specific Modeling

At this stage a preliminary model of the site structure is produced. Geologic structures either exposed in the site vicinity or inferred from geophysical data are projected into the site. The model is revised to incorporate the results of site-specific geophysical tests. Drill cores, core logs, and core photographs are also inspected to identify zones of abundant fractures and other structures (e.g. permeable dikes) within the site that may be important to the model. The geophysical and borehole information should be interpreted in a manner consistent with the systematics of the local structures. The model should be re-examined and refined as more site-specific information becomes available.

3.4.5. Constructing the Hydrologic Model

The resulting model of the major geologic features can be used as the basis for a hydrologic model. Both the gross arrangement of the major structures and the information on the internal systematics of the major structures should be considered in preparing hydrologic models. The structural information could also be used to help plan the siting of wells or boreholes for collecting hydrologic data.

4.0. APPLICATION OF LBL METHODOLOGY: THE US/BK SITE

We have applied the methodology of Chapter 3 to characterize the US/BK site at the Grimsel Rock Laboratory (Figure 1.2). We first review previously published material on the geology at Grimsel. We then present our work on the systematics of the major geologic structures near the laboratory. The geologic structures exposed in the subsurface workings adjacent to the US/BK site are described next. Finally, we build a model of the major geologic structures within the US/BK site based on surface and subsurface mapping, borehole data, and geophysical tomography. In Chapter 4 we compare this model against interpretations of the brine tracer difference tomograms.

4.1. Prior Studies of the Geology at Grimsel

NAGRA reports NTB 81-07, 85-46, and 87-14 served as our principal sources of information on the geology in the immediate area of the Grimsel Laboratory. These reports include surface and subsurface geologic data collected specifically for work at the laboratory. We relied most heavily on the maps, cross-sections, borehole logs and geometric information on the subsurface workings contained in the raw data appendices of a preliminary draft of NAGRA Technical Report 87-14. The three reports also provide a geologic model of the laboratory region and highlight some of the important features of the major structures. Finally, and perhaps more importantly, they show how the Grimsel fracture systems have been studied and how the understanding of the geologic structure at Grimsel has evolved.

4.1.1. NAGRA Technical Report 81-07 ("Sondierbohrungen Juchlistock Grimsel")

The preliminary geologic and hydrogeologic investigations of the Grimsel Laboratory were concluded in 1980 and are reported in NAGRA Technical Report 81-07. These investigations were conducted after the main access tunnel had been excavated, but before any laboratory

tunnels were bored and before detailed mapping of the surface had been conducted. The interpretation of the subsurface structure (Figure 4.1) relied primarily on information from the main access tunnel and six subhorizontal boreholes drilled west from the main access tunnel (Figure 1.2). The northernmost borehole (BOUS 80.001) was drilled above the site of the BK room.

The report identifies three main systems of geologic structures in the vicinity of the Grimsel laboratory: K-zones, S-zones and lamprophyre dikes (Table 4.1). The K-zones are steeply-dipping fracture zones that generally strike to the northwest, at high angles to the foliation of the rock, which strikes ~N65°E. The S-zones contain fractures that parallel the foliation in the rock. They commonly occur in biotite-rich shear zones, strike to the northeast, and generally dip steeply to the southeast. The youngest fractures in the S- and K- systems were considered to be of Alpine age (15-25 m.y.). The absolute ages of the oldest fractures and the relative ages of the fracture systems were not ascertained. On the basis of their orientation, the S-zones were subdivided into three groups (S1, S2, S3) and the K-zones into four (K1, K2, K3, K4); this orientation-based scheme is retained in NTB 85-46 and NTB 87-14. Some K-zone orientations overlap those of S-zones. Metamorphosed lamprophyres, mafic dikes that contain abundant micaceous material, were noted to parallel some K-zones. Intense deformation was observed locally along the contacts between some lamprophyres and the granitic host rock, and the lamprophyres are locally highly fractured. Fractures are thus associated with all of these geologic structures, and in places we shall refer to these structures as fracture systems or fracture zones.

The dominant features shown on the preliminary interpretation of the fracture structure near the eventual location of the BK room (Figure 4.1) are east-striking lamprophyres north of the room and a northeast-striking S-zone that intersects BOUS 80.001 near its west end. A preliminary geologic cross section in NTB 81-07 shows this S-zone extending to the surface.

4.1.2. NAGRA Technical Report 85-46 ("Grimsel Test Site: Overview and Test Programs")

The initial geologic, petrographic, and hydrogeologic studies of the Juchlistock area were completed in April of 1984. The key findings of these studies are presented in NAGRA Technical Report 85-46. This report was prepared after the laboratory tunnels were bored and the BK room

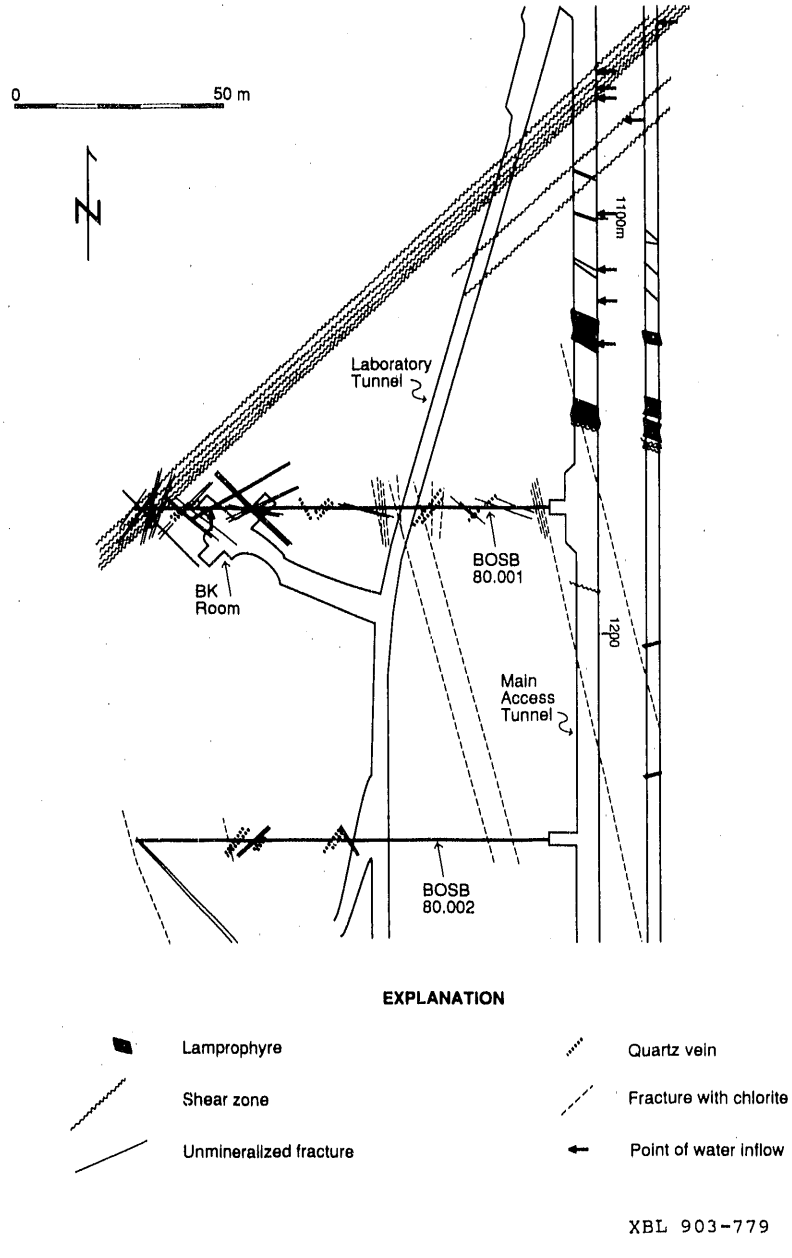

Figure 4.1. Structural interpretation of the US/BK site from NTB 81-07. This interpretation is based on logging of the main access tunnel, the cable tunnel, and boreholes BOSB 80.001 and BOSB 80.002. The laboratory tunnel and BK room did not exist when this interpretation was made and are shown here for reference only. Numbers along main access tunnel mark distance in meters from its north entrance.

Table 4.1. Structures Encountered in Borcholes BOSB 80.001-80.006

System	Average dip direction/ average dip (in degrees)	Number of fractures considered	Characteristics	Genetic interpretation
S_1	142/77	233	Parallel to schistosity (foliation) Shear zone	Youngest, Alpine schistosity
S_2	157/75	104		Older schistosity, possibly Hercynian-age
S_3	183/65	21	Scarce, marked by aligned biotite Shear zone in BOSB 80.005	Older schistosity
K_1	53 + 233/80	116		Most important fractures transverse to schistosity. Age unknown. May be Alpine or Hercynian.
K_2	19 + 199/78	39	Scarce, fractures with biotite and chlorite	Possibly Hercynian-age fractures
K_3	264/84	58	Scarce, open fractures typically coated with chlorite	Possibly Hercynian-age fractures
K_4	117/50	102		
L	216/80 and 242/80	17	Lamprophyre dike contacts	Parallel to K_1 and possibly K_2

was excavated, and it includes descriptions and maps of fractures in the laboratory tunnels and excavations.

The general conclusions of NTB 81-07 regarding the Grimsel fracture systems are echoed in NTB 85-46. Perhaps the most significant change is that two new sets of K-fracture orientations are classified in NTB 85-46. One of these sets consists of subhorizontal Alpine tension fissures (''Zerrklüfte''). These fissures are considered to be the youngest mineralized fractures and are approximately 13 million years old. The very youngest fractures are sheeting joints (T-fractures) that are subparallel to the topography. The report notes that most of the water circulation near the laboratory occurs along the most prominent S-fracture systems (S1 and S2), the margins of lamprophyres, and the Alpine tension fissures.

The report also contains a map of the geology near the US/BK site (Figure 4.2). The most numerous fractures shown in the vicinity of the BK room are classified as S2 fractures. The most prominent S2 zone is projected just west of the BK room; it is shown in the same location in NTB 81-07. Another prominent fracture zone (S3 in Figure 4.2) is exposed near the entrance to the room and strikes east-west. Based on borehole BOUS 80.001, numerous K4 fractures that dip to the west-northwest were inferred west of the BK room.

4.1.3. NAGRA Technical Report 87-14 (''Felslabor Grimsel: Geologie'')

The most recently released report on the geology of the entire Grimsel Laboratory is presented in the preliminary and final volumes of NAGRA Technical Report 87-14. This report was prepared after all portions of the laboratory tunnels were logged and after several hundred meters of borehole core were examined. It presents both a summary of the geologic literature on the Grimsel Pass region and the results of the site-specific geologic investigations conducted near the Grimsel Rock Laboratory between 1980 and 1987. The final volume was issued in February of 1989.

As in the previous two reports, NTB 87-14 relies primarily on orientation data from boreholes to characterize the fracture systems at Grimsel. Three ductile (S1, S2, S3) and six brit-

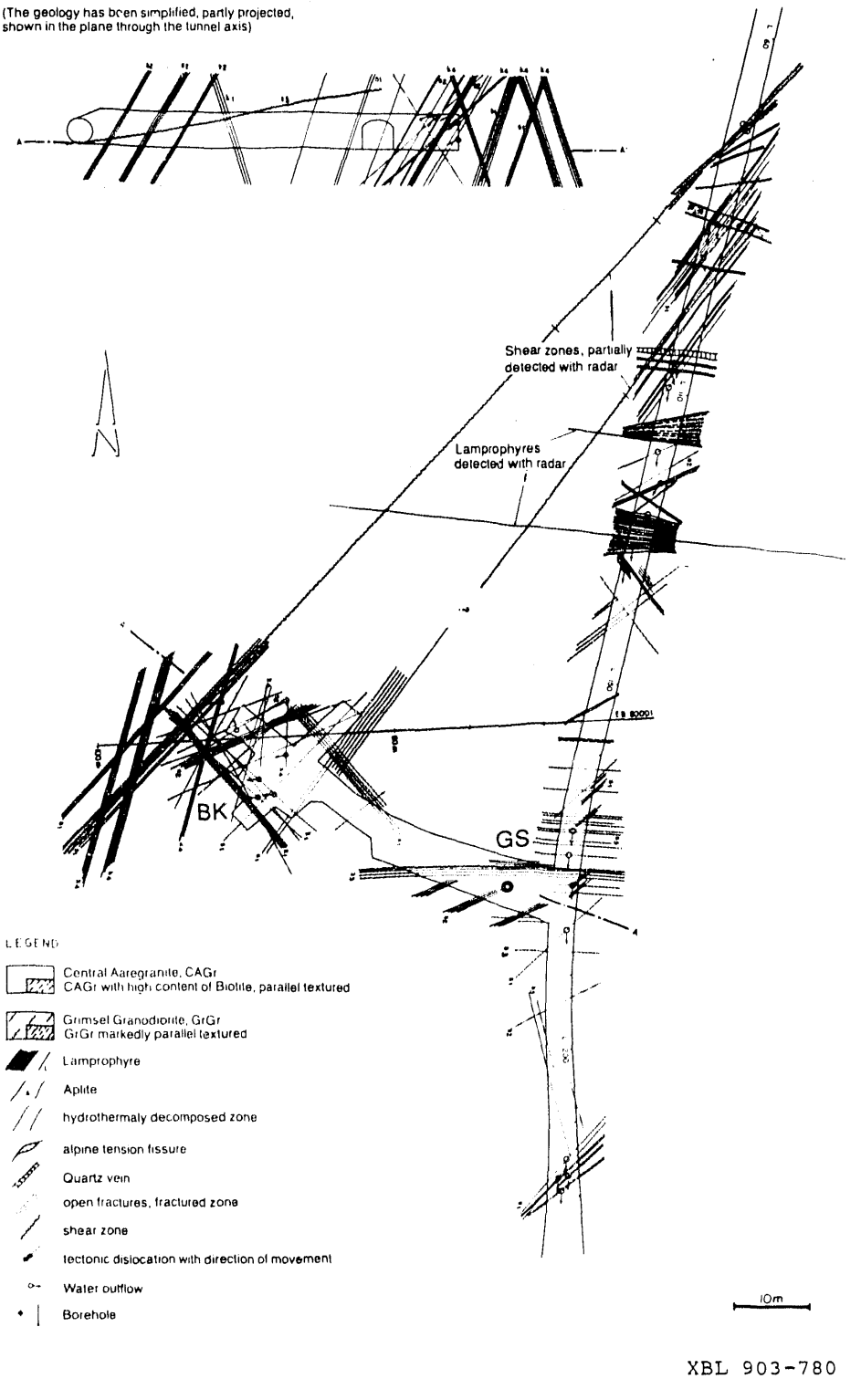

Figure 4.2. Structural interpretation of the US/BK site from NTB 85-46. Geology projected into plane through axis of laboratory tunnel. Inset figure is a vertical cross section along line A-A'.

tle (K1, K2/L, K3, S4/K4, S5, and subhorizontal tension fissures) fracture systems were classified based on fracture orientation data from subsurface boreholes. The orientations of the S1 and S2 systems overlap considerably, as do the orientations of the 1) K2 fractures and the lamprophyres (L), and 2) the S4 and K4 fractures.

The report indicates that the geologic structure largely reflects Alpine deformation between 25 and 15 m.y. During this interval the fracture systems developed and the granites acquired their foliation. Members in each of the four major fracture systems visible at the surface (S1/S2, S3, K2/L, and K3) have served as faults, and the displacements accommodated by faults of different orientation suggest either a multi-step or a nonuniform deformation. It is difficult to distinguish the relative ages of the fracturing events based on the mineralogy of the fracture-filling minerals, because most of the fractures are at least partly sealed with the same minerals (quartz and chlorite +/- epidote). The similar mineralogy in the fractures may indicate hydraulic communication among the different fracture zones. Only for the alpine tension fissures have the ambient pressure/temperature conditions at fracturing been established (~3 kilobars and 400- 450°C). This pressure corresponds to a depth of formation of 10-30 km. The S- and K-zones probably formed in this depth range or even deeper.

NTB 87-14 presents a three-dimensional model of the Juchlistock area through the combination of a geologic map of the surface (Figure 4.3), a slightly modified version of the geologic cross section of NTB 85-46 (Figure 4.4), and a block diagram (Figure 4.5). A salient aspect of these illustrations is that many of the major structures extend to depth as roughly planar features. This is consistent with the expression of the major structures in the mountainside above the laboratory. A particularly prominent feature shown on the geologic map (Figure 4.3) is a K-zone exposed at an elevation of 2100 m above the north end of the main laboratory tunnel. As did the cross section of NTB 85-46, the cross section of NTB 87-14 (Figure 4.4) shows the lamprophyres $L(k_2)$ exposed north of the BK room being connected to this K-zone. The report also includes a generalized map of the main fracture zones at the level of the Grimsel Laboratory (Figure 4.6); it is very similar to Figure 1 of NTB 85-46.

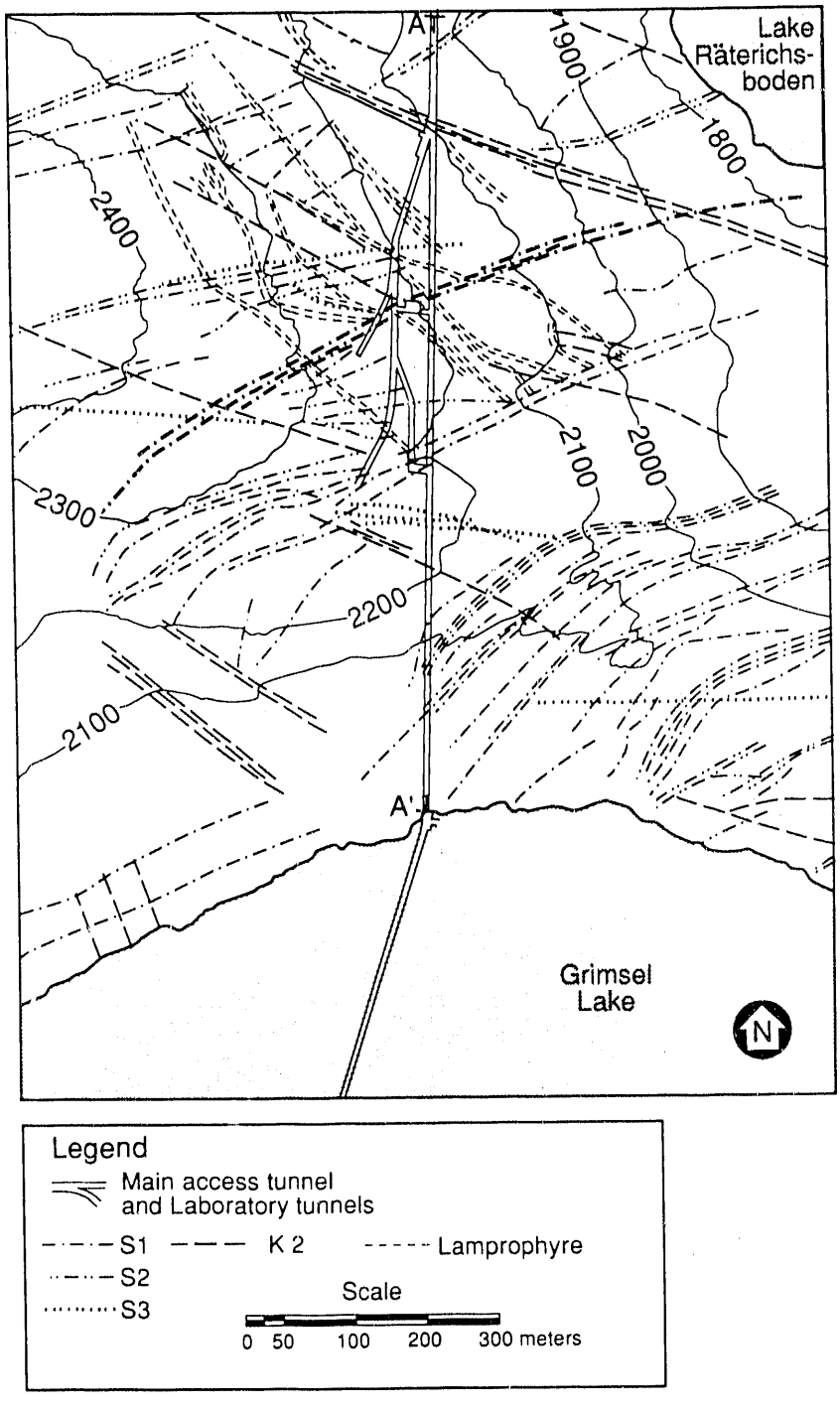

XBL 898-7692

Figure 4.3. Map showing traces of fracture zones at the surface above the Grimsel laboratory. Contour interval is 100 meters. Line A-A' marks line of cross section of Figure 4.4. Lake at upper left corner of map is the Ratrichsbodensee (from NTB 87-14).

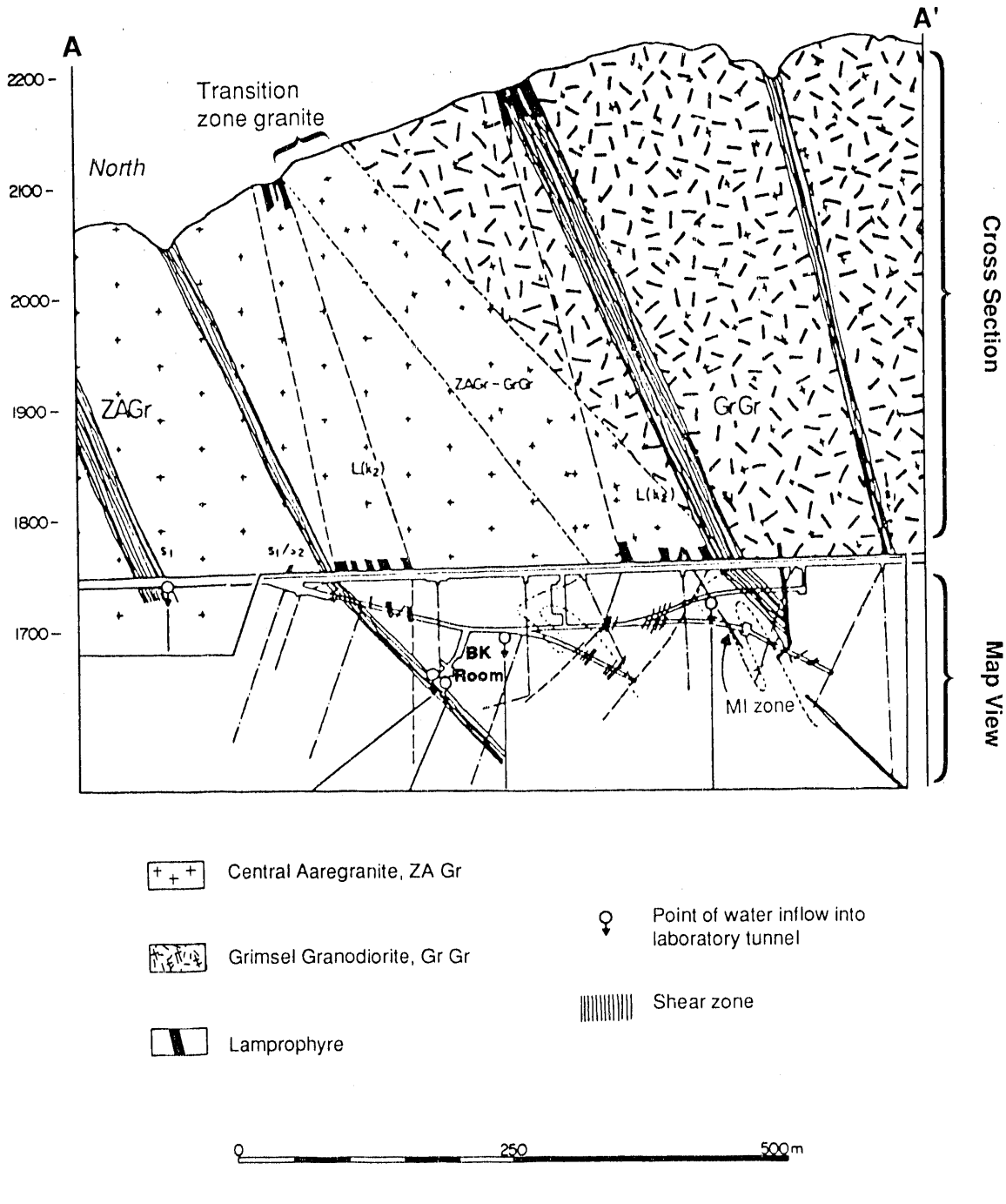

Figure 4.4. Geologic section along the main access tunnel to the Grimsel laboratory showing major fracture zones and simplified map showing major structures at the level of the laboratory tunnels. Line of cross section A-A' shown in Figure 4.3. Straight long-dashed lines in map view are boreholes (from NTB 87-14).

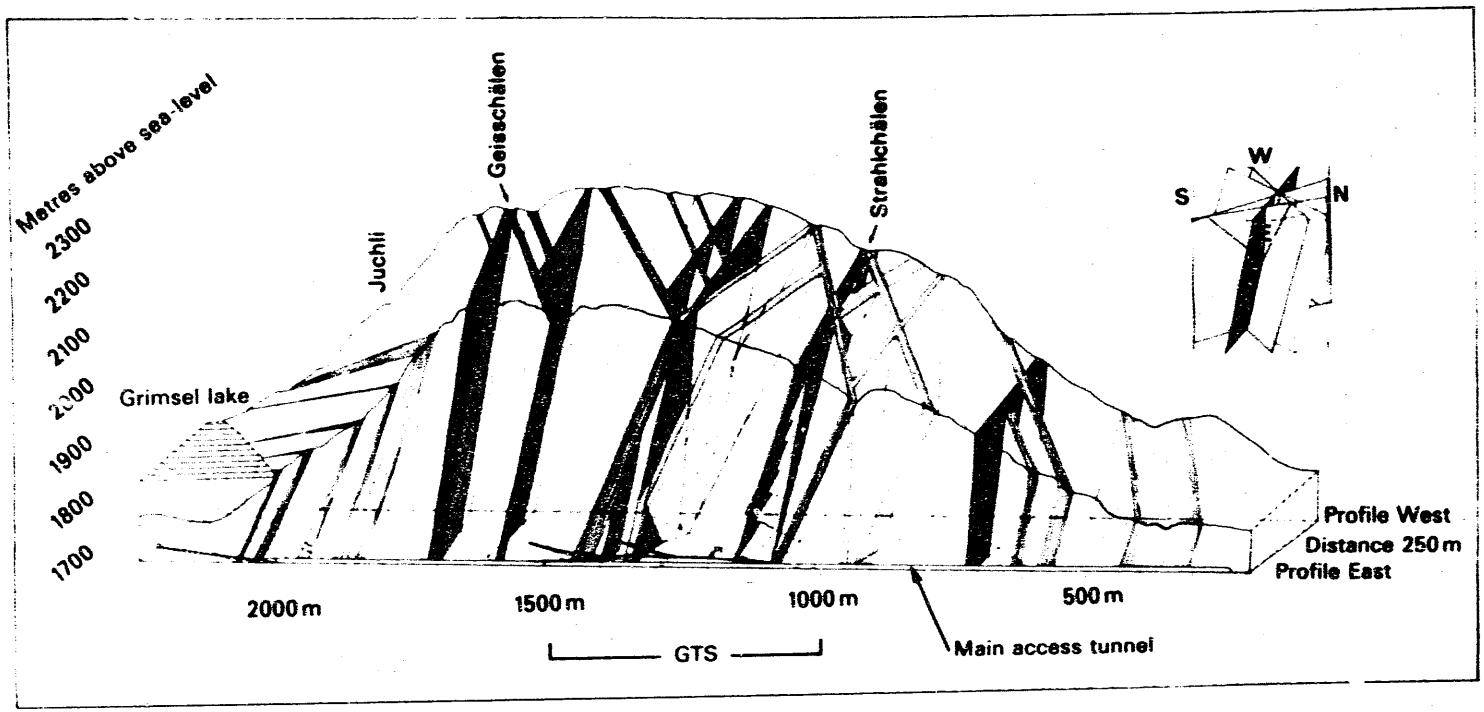

Figure 4.5. Block diagram showing major structures in the vicinity of the Grimsel laboratory (GTS). View is to the west. Zones shown with lined edges are S-zones. Structures marked by solid shading are K-zones and lamprophyre dikes. Numbers along main access tunnel mark distance in meters from its north entrance.

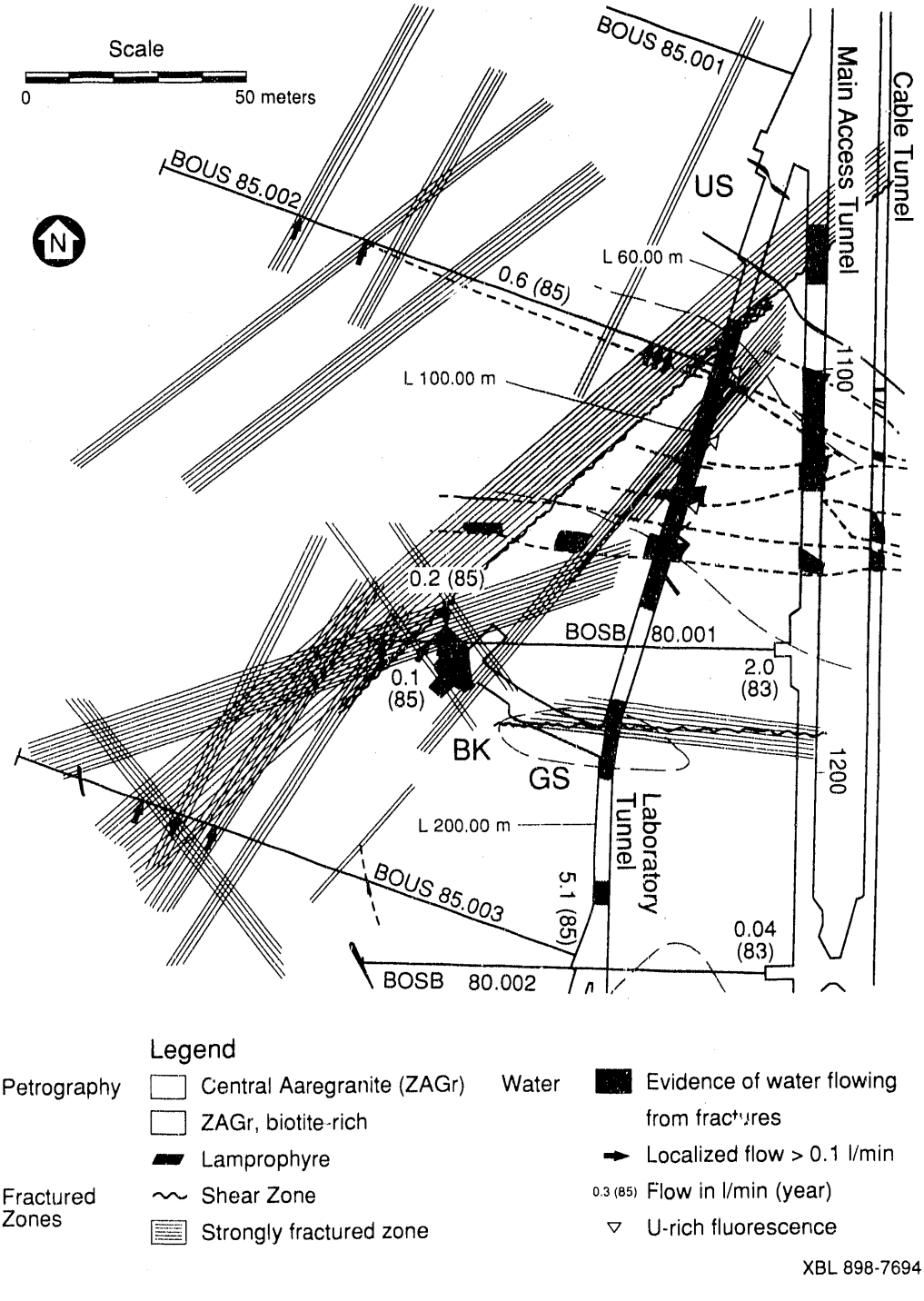

Figure 4.6. Structural interpretation of the US/BK site from NTB 87-14. Numbers along main access tunnel mark distance in meters from its north entrance.

4.1.4. Conclusions from the NAGRA Reports

The structural interpretation near the BK room is similar in NTB 81-07 (Figure 4.1), NTB 85-46 (Figure 4.2) and NTB 87-14 (Figure 4.6). The prominent S2 zone that intersects the laboratory tunnel near the northeast corner of the site and the northwest-striking K1 fractures near the west end of the BK room have essentially the same position and orientation in Figures 4.1, 4.2 and 4.6. The differences in the geologic interpretations of Figures 4.2 and 4.6 are relatively small. The lamprophyres north of the BK room and the fractures west of it are extended further in NTB 87-14 (Figure 4.6), and several fractures near the mouth of the room that are shown in NTB 85-46 (Figure 4.2) are not shown in the generalized laboratory map of NTB 87-14 (Figure 4.6).

4.2. Systematics of Major Geologic Structures

4.2.1. Overview

When we began our work, models of the Juchlistock region (Figures 4.3, 4.4, and 4.5) and site-specific models of the fracture structure near the BK room had been prepared (Figures 4.1, 4.2, and 4.6), but the distinguishing attributes of the major fracture zones had not been described in great detail. For that reason we concentrated on defining the systematics of the major geologic structures early in our study, focusing on the surface outcrops with the largest and most complete exposures of fracture zones and lamprophyres. We did not focus on the particular fracture zones directly above the US/BK site because the surface exposures there are poor. Rather, we examined a few zones nearby that are particularly well-exposed.

4.2.2. Fabric of the Granitic Rock

As noted in NTB 87-14, the granitic rock at Grimsel is foliated. The foliation strikes approximately N65°E, dips 65° to 70° to the southeast, and is defined by the alignment of biotite grains in the rock and by deformed bands of granite in which the grain size has been reduced. Our use of the term foliation corresponds closely to the use of the term schistosity in NTB 87-14. In addition, the rock has a linear fabric element. Grains of feldspar in the foliation planes have been elongated in the direction the foliation dips. This can be clearly seen in drill cores from the

from the southern part of the laboratory. This linear fabric is also reflected in the laboratory by inclusions in the granite having smaller cross sectional areas in the roof and floor than in the tunnel walls. The granitic rock at Grimsel is clearly anisotropic.

4.2.3. K-Zones

A 100-m-long section of an exceptionally well-exposed K-zone (Figures 4.7 and 4.8) was mapped at an elevation of ~2000 m on the north side of the Bachlisbach gorge. This zone strikes northwest, nearly at right angles to the foliation. The zone appears to offset a steeply-dipping lamprophyre dike left-laterally by ~20 m; this interpretation is based in part on lamprophyre exposures north of the area of Figure 4.8. The K-zone contains a series of northwest-striking faults. They are linked by smaller fractures that strike east-northeast, oblique to the zone as a whole. Both kinds of fractures dip steeply. Structurally, this zone is remarkably similar to some left-lateral fault zones in the Sierra Nevada of California that developed from fault-parallel joints (Martel et al., 1988; Martel, 1990), and we suspect that the K-zone developed the same way.

The K-zone mapped clearly is not a uniform, planar structure. It has a nonlinear trace, with subparallel segments joining at echelon steps, and varies in width from about one to ten meters. The relative abundance of the internal obliquely-striking fractures varies markedly along strike. They are most abundant at a left echelon step between two faults at the northwest end of the map. The orientation of the internal fractures suggests that the K-zone slipped left-laterally when the axis of maximum horizontal compression was oriented east-northeast or east.

A fracture zone with a fracture pattern similar to the K-zone of Figure 4.8 is exposed at the east end of the BK room (Figures 4.2 and 4.9). This zone contains a series of steeply-dipping fractures that strike east-west, the most prominent being a fault exposed where the north wall of the BK room intersects the laboratory tunnel (Figure 4.9). Several subparallel fractures are exposed in the laboratory tunnel a few meters north of this fault, and another is exposed 11 m to the south (Figure 4.2). On the south side of the fault in the BK room (Figures 4.2 and 4.9) are numerous fractures that strike to the southwest and dip steeply to the southeast. Most of these fractures either splay directly from the fault or are connected to fractures that splay from it. A

Figure 4.7. View to the northwest across the Ratrichsbodensee dam showing the glaciated surface above the north entrance to the main access tunnel. The entrance is below and to the right of the far side of the dam. The lamprophyre dike and K-zone of Figure 4.8 intersect at the dark spot in the center of the photograph. The lamprophyre extends left and up from this spot; the K-zone extends down and to the left. The stream in the prominent gorge at the left edge of photograph is Bachlisbach.

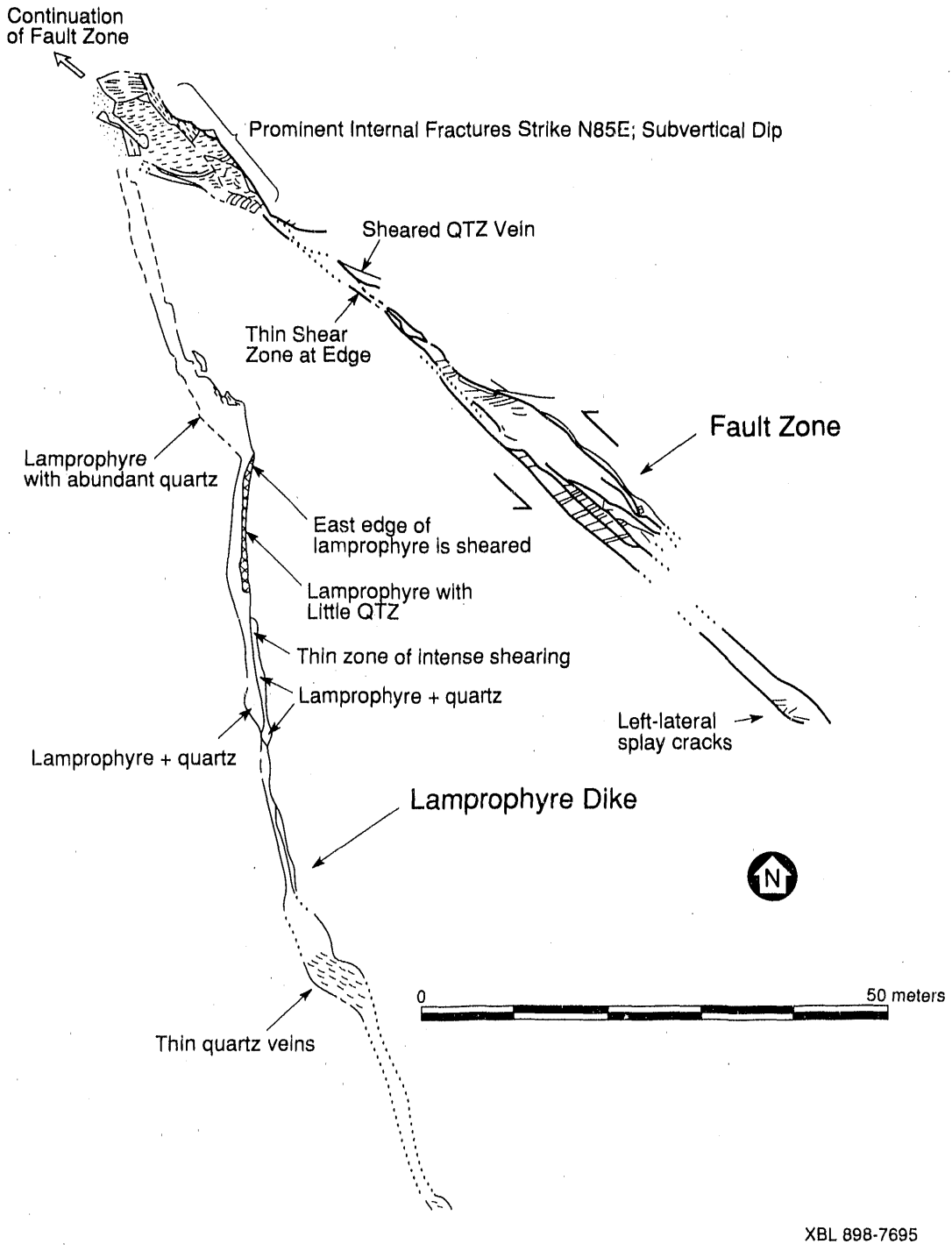

Figure 4.8. Map of part of the lamprophyre dike and K-zone of Figure 4.7. The dark spot of Figure 4.7 is immediately north of the northwest corner of this map.

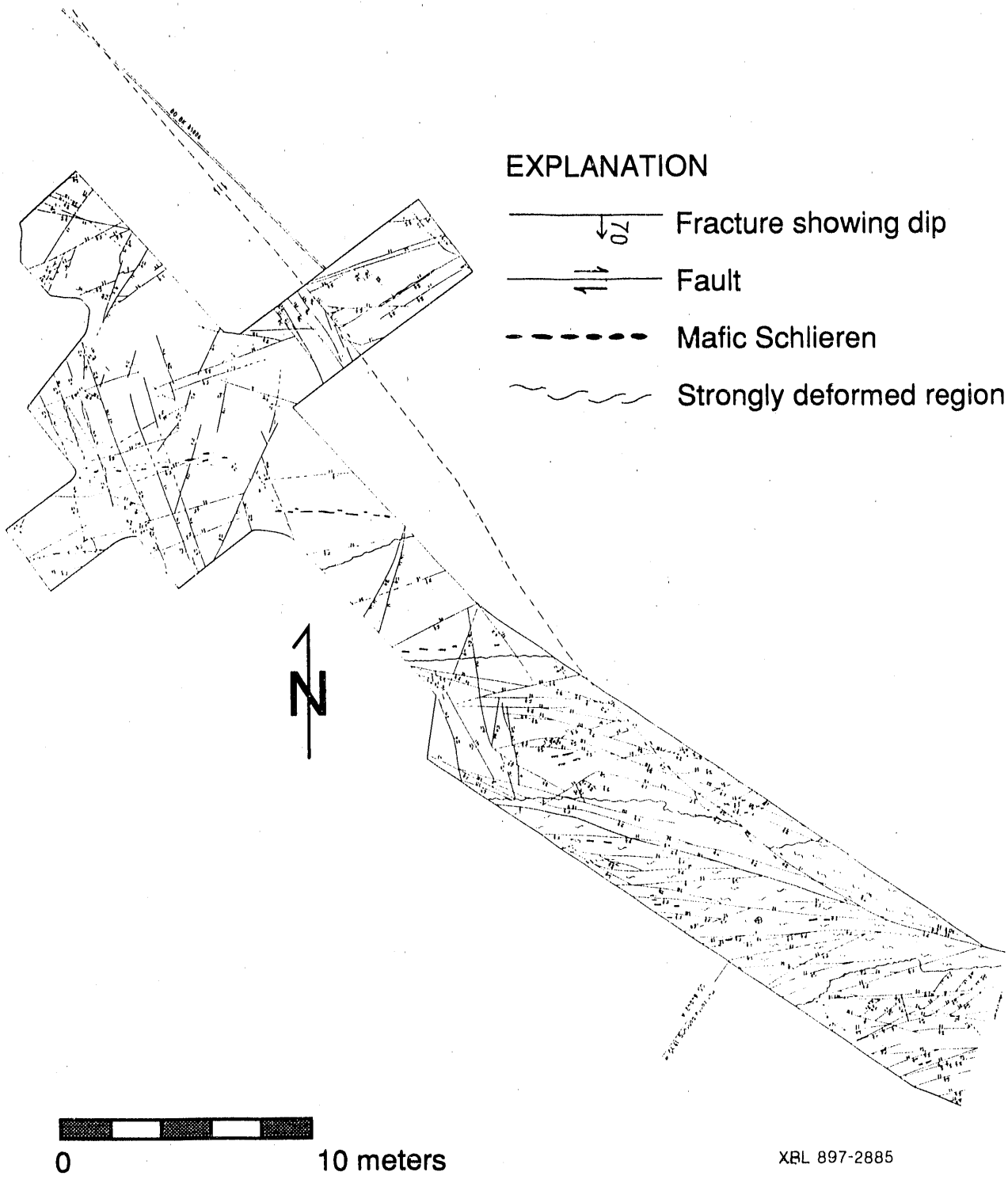

Figure 4.9. Map of fractures in the floor of the entrance drift to the BK room. The floor was covered by concrete after the fractures were mapped. Note the prominent fracture that strikes west-northwest from the east end of the room towards the north arrow. This fracture is interpreted to be a fault. The numerous fractures that splay from that fault strike west; the splay fractures splay to the left from the fault (see Figure 4.12). This is analogous to the fractures in the K-zone of Figure 4.8.

few southwest-striking fractures are mapped on the north side of the fault, and a few occur in the adjacent part of the laboratory tunnel. This fracture pattern is remarkably similar to that at the major step in the K-zone of Figure 4.8, and we suggest that the southwest-striking fractures in the BK room link two west-striking faults, one at the mouth of the room and the other 11 m to the south. Although an apparent right-lateral offset is mapped across the fault (Figure 4.9), the fracture structure indicates that the fault is part of a left-lateral fault zone; perhaps the fault has slipped in two different senses at different times. The laboratory tunnel is damp adjacent to this inferred structural step, suggesting that the step is a preferred conduit for fluid flow. This area coincides with an area of unusually dark granite (Figure 4.6), so an alternative interpretation is that the southwest-striking fractures are primarily related not to the faults but instead to the dark granite.

4.2.4. S-Zones

In contrast to the K-zones, the S-zones display a braided structure. This pattern is revealed at the surface (Figure 4.10; also see Figure 3.12 in NTB 87-14), in the roof of the laboratory tunnel at L75, and in the laboratory tunnel walls between L80 and L103 north of the BK room (Figure 4.11). The traces of S-zone fractures on tunnel walls resemble fish gills (Figure 4.12). In some cases a subsidiary fracture is nested within a more prominent fracture (Figure 4.12a), whereas in other cases the more prominent fracture is nested within a subsidiary fracture (Figure 4.12b). The two scenarios reflect cases where the subsidiary fracture strikes from the more prominent fracture in different directions. Fractures between L80 and L103 appear to splay to the right (Figure 4.12a) about as commonly as they splay to the left (Figure 4.12b). The overall pattern thus appears to be braided. Because we see repeated evidence of a braided structure in the S-zones we consider them to characteristically have a braided character in plan view (Figure 4.13). Surface and subsurface exposures at Grimsel suggest that a braided pattern of S-zone fractures is also present in the down-dip direction but is less pronounced.

The structure of the S-zones is clearly tied to the anisotropy of the granitic host rocks. At a macroscopic scale the S-zones parallel the foliation in the rock. In some places S-zone fractures

Figure 4.10. View along the strike of an S zone (15-cm-ruler for scale). Note the braided fracture structure. The macroscopic structure mimics the microscopic structure in the granite.

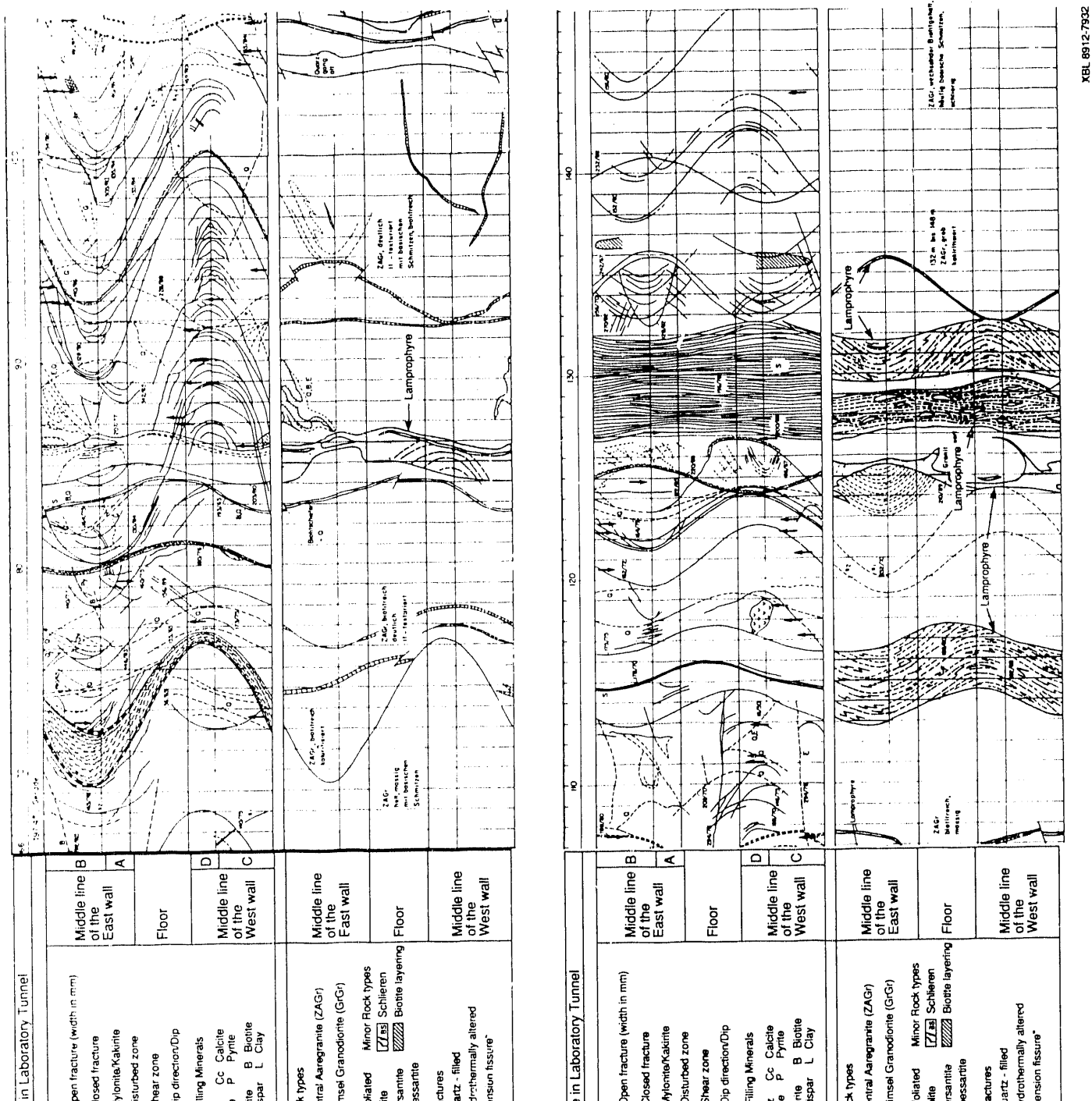

Figure 4.11a. Log of the fractures in the portion of the laboratory tunnel between L66 and L230 (from the preliminary volume of NTB 87-14).

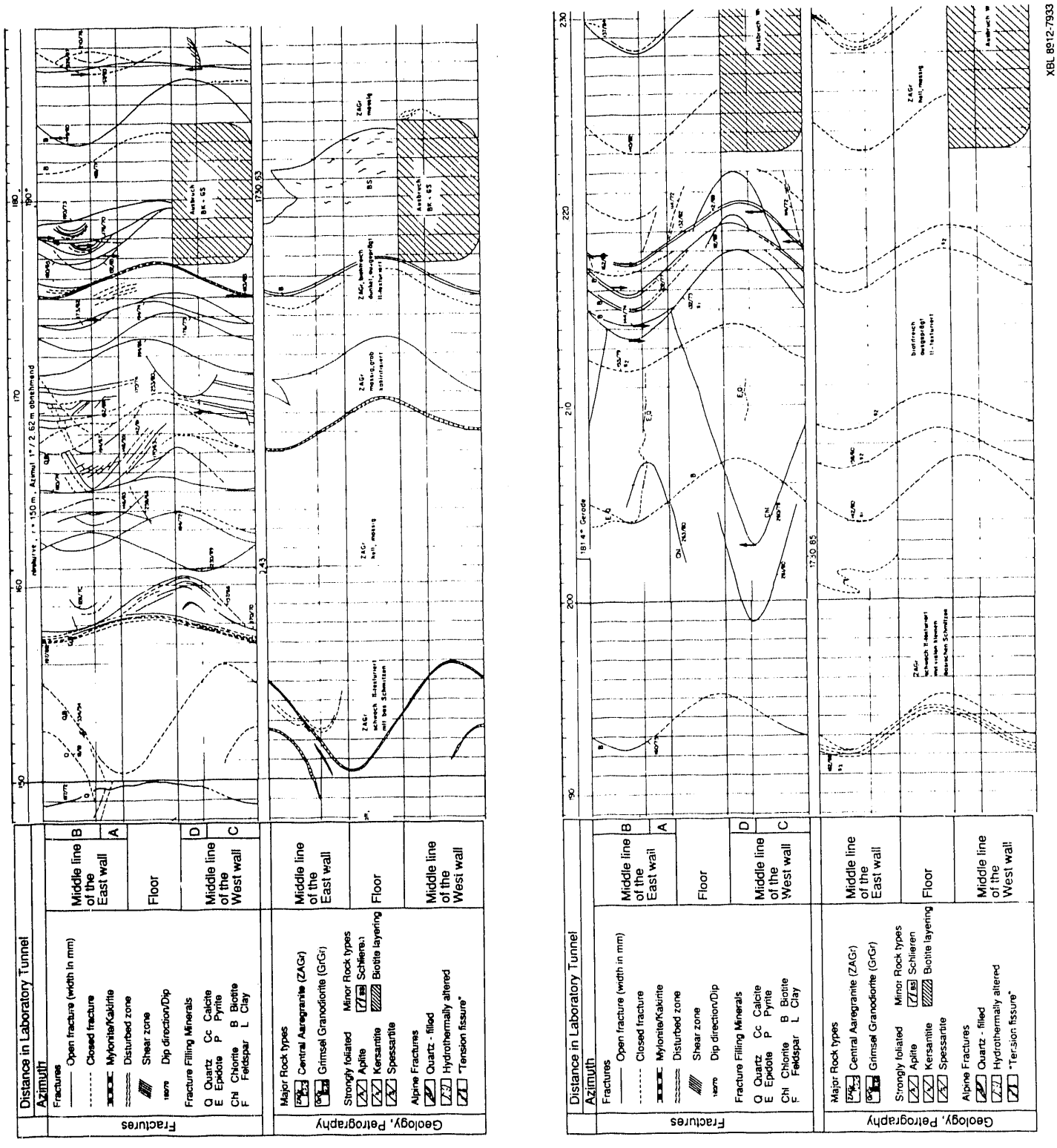
Distance in Laboratory Tunnel
Azimuth
Fractures
Open fracture (width in mm)
Closed fracture
Mylonite/Kakirite
Disturbed zone
Shear zone
Dip direction/Dip
Fracture Filling Minerals
Q Quartz Cc Calcite
E Epidote P Pyrite
Chl Chlorite B Biotite
F Feldspar L Clay
Middle line of the East wall
Floor
Middle line of the West wall
A
B
C
D
Geology, Petrography
Major Rock types
Central Aaregranite (ZAGr)
Grimsel Granodiorite (GrGr)
Minor Rock types
Strongly foliated
Aplite
Kersantite
Spessartite
Schlieren
Biotite layering
Alpine Fractures
Quartz - filled
Hydrothermally altered
"Tension fissure"
Middle line of the East wall
Floor
Middle line of the West wall
XBL 8912-7933

Figure 4.11b.

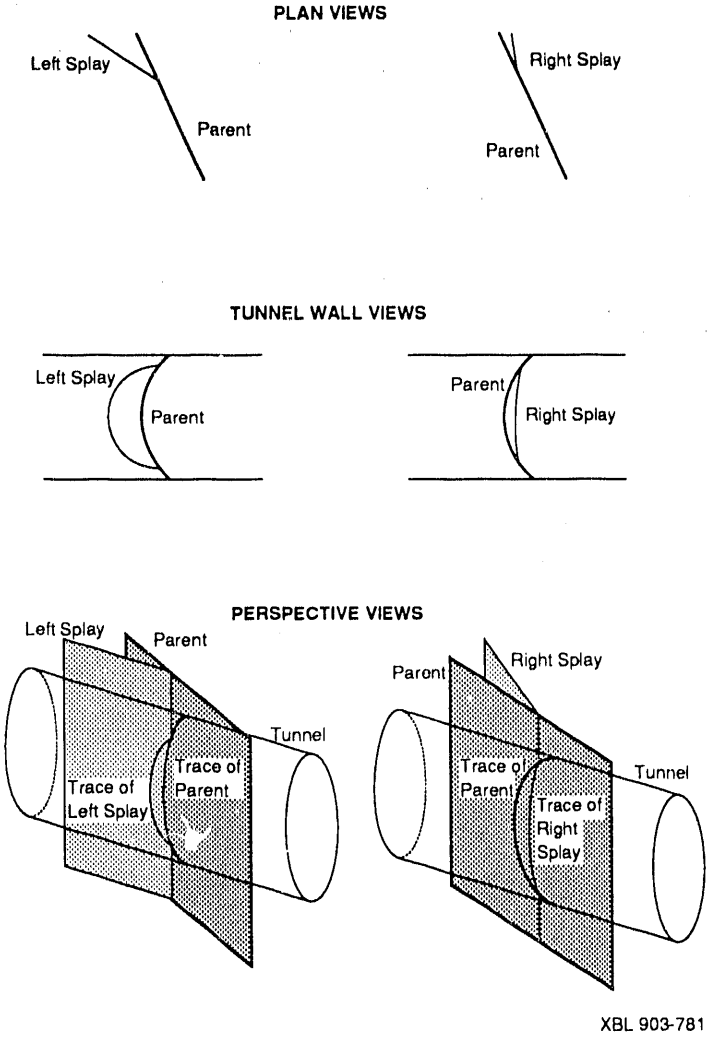

Figure 4.12. "Fish-gill" diagram showing projections of the traces of a parent fracture and a splay fractures in a horizontal map view, in a vertical view of the wall, and in a three-dimensional perspective view. The plan views show the intersections of the fractures with a horizontal plane through the axis of the tunnel. The tunnel wall views show the fracture traces as projected orthogonally from the tunnel wall onto a vertical plane; this is how the fracture traces appear in the tunnel wall to an observer standing in the tunnels. For the case of a left splay, the tunnel wall trace of the parent fracture is nested inside the tunnel wall trace of the splay fracture. For the case of a right splay, the tunnel wall trace of the splay fracture is nested inside the tunnel wall trace of the parent fracture. Compare the tunnel wall views here with the fracture traces in the west wall of the laboratory tunnel between L80 and L103 in Figure 4.11.

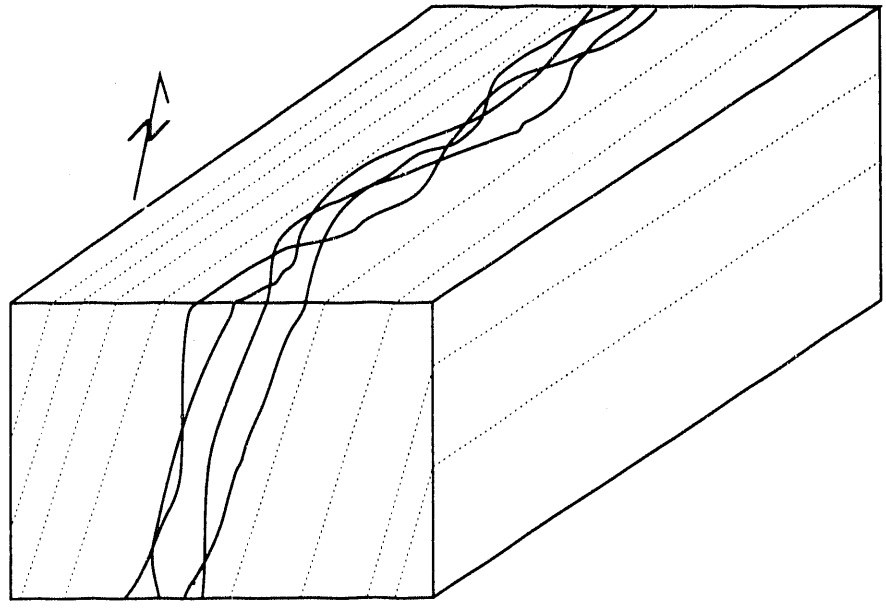

XBL 903-782

Figure 4.13. Block diagram showing the braided structure of S-zone fractures in plan view and in a vertical cross section. The braided structure is more pronounced in plan view than in cross section. Dashed lines mark the orientation of the foliation in the rock.

occur along mylonites (bands of concentrated ductile shear deformation) that parallel the foliation (Frick et al., 1988). The macroscopic fracture structure of the S-zones also mimics the microscopic arrangement of the biotites, which largely define the foliation. The S-zone fractures commonly parallel the biotites and are particularly well developed where biotite is concentrated. In plan view the biotites form a braided pattern as they wrap around feldspar and quartz grains in the rock, analogous to the braided pattern formed by the S-zone fractures. The feldspars tend to be elongated parallel to the dip of the foliation, so in cross sections perpendicular to foliation strike the braided pattern is more drawn out; this too is analogous to the pattern formed by the S-zone fractures.

Subhorizontal slickenlines within the S-zones indicate strike-slip faulting along the zones. Several surface exposures at the edges of S-zones contain steeply-dipping veins that are plastically sheared in a left-lateral sense (Figure 4.14), whereas in subsurface exposures veins are sharply offset across S-zones in a right-lateral sense (e.g. Figure 4.11, tunnel floor at L84). We infer that some S-zones may have first slipped left-laterally under elevated pressure-temperature conditions and then right-laterally under lower pressure-temperature conditions.

4.2.5. Structural Relationship Between K- and S-Zones

We have not definitively identified any consistent structural relations between the K- and S-zones. It is not clear in general whether the K- and S-zones offset each other, what their relative ages are, or what the structure of their intersections is. However, several surface exposures contain individual northwest-striking and northeast-striking fractures that offset each other. One exposure is less than 100 m west of the entrance to the Grimsel Laboratory. These relationships suggest that the zones may offset each other. The zones may have been active at the same time.

The distinctly different structures of the K- and S-zones (Figure 4.15) appear to reflect differences in the flaws from which the zones developed. The K-zones apparently developed from an irregular distribution of pre-existing west or northwest-striking fractures, whereas the S-zones developed upon the foliation in the rock. The most prominent fractures in the K-zones strike at high angles to the foliation. In contrast, the S-zone fractures parallel the foliation.

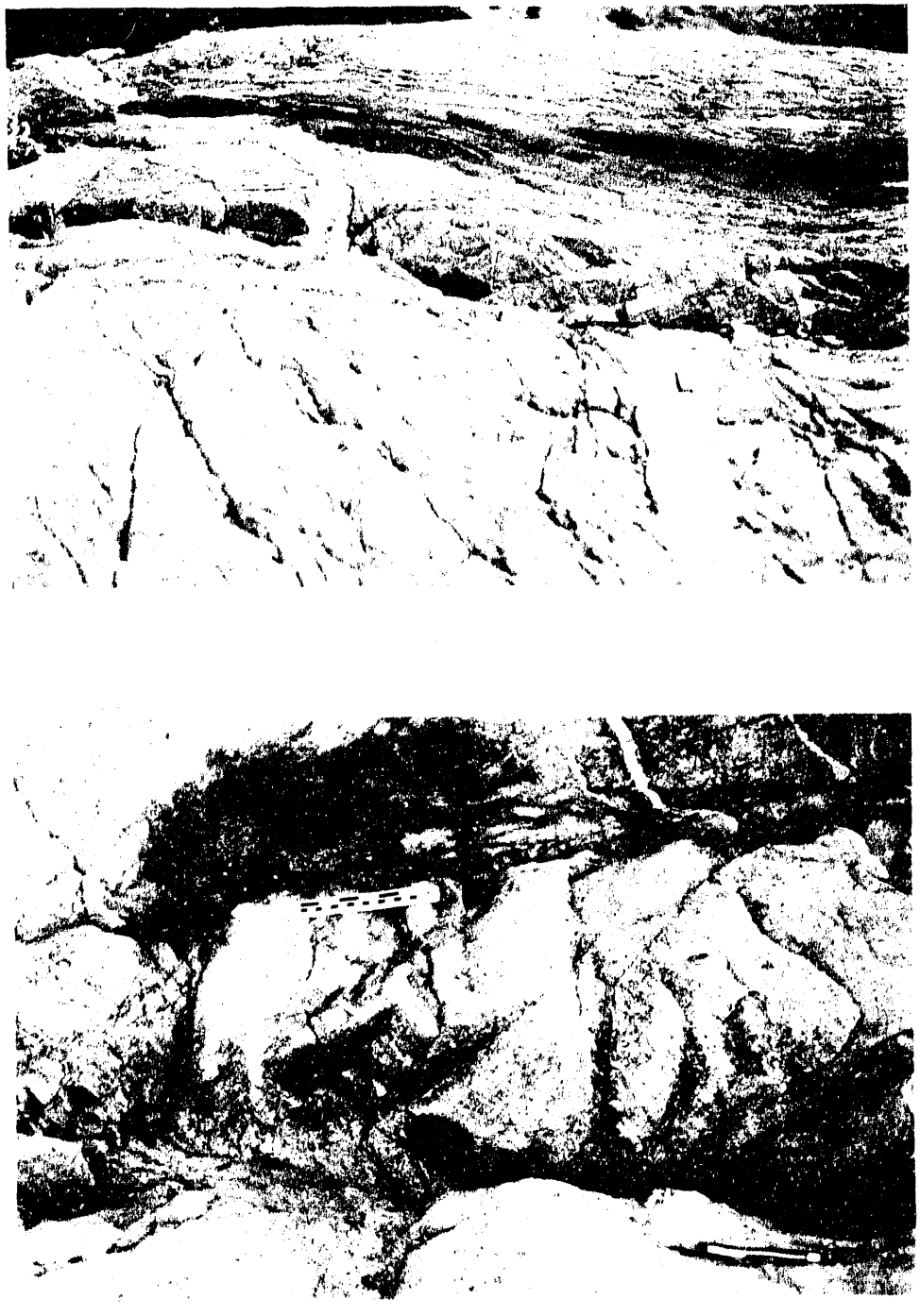

Figure 4.14. Photographs of plastically deformed veins offset left-laterally across northeast-striking S-zone fractures along the west shore of the Ratrichsbodensee. The veins dip steeply and become progressively more deflected as they approach the fractures. 15-cm-ruler for scale.

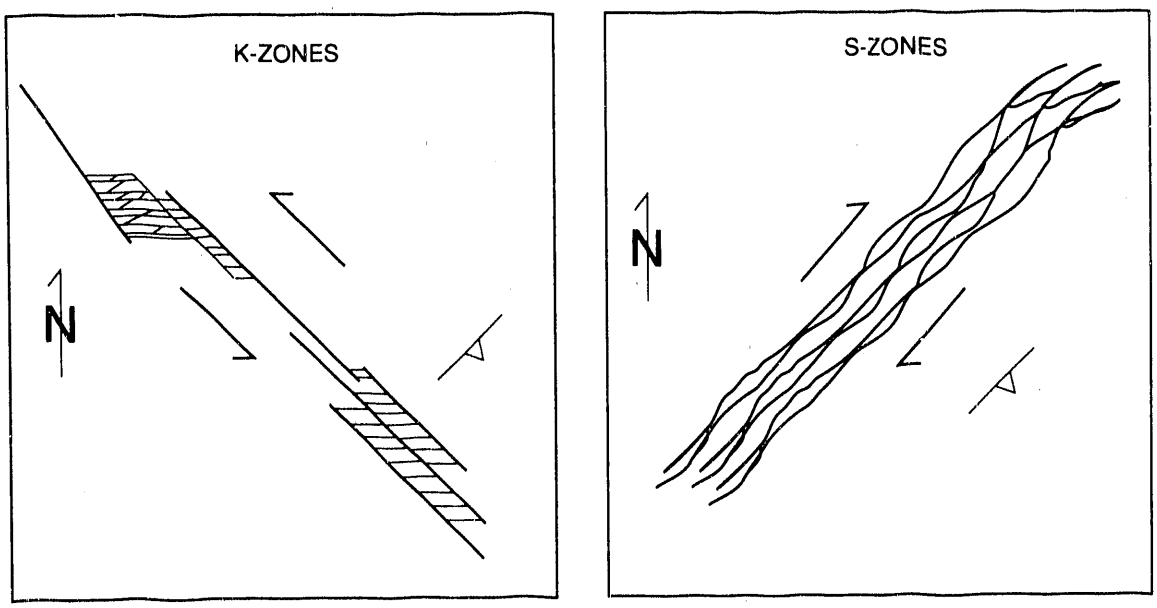

Figure 4.15. Schematic diagrams comparing the arrangement of fractures in a K-zone and an S-zone. The foliation in the rock dips steeply to the southeast, at a high angle to the K-zone but parallel to the S-zone.

4.2.6. Lamprophyres

Lamprophyre dikes are superbly exposed at several places in the laboratory tunnels and exhibit a variety of spectacular deformational structures including mullions and Alpine tension fissures. In general the dikes strike to the west or northwest (like the K-zones), dip steeply to the south, and contain abundant micaceous material with little quartz. As indicated in Figure 4.6, it is difficult to trace some lamprophyres along strike as planar structures for more than 10-20 m. Some of this discontinuous structure may reflect deformation (stretching) of the lamprophyres. The lamprophyre edges commonly are highly sheared. Many lamprophyres that strike northwest contain an internal foliation that strikes approximately east-west.

Several of the steeply dipping, northwest-striking lamprophyres in the southern half of the laboratory have developed a pronounced mullion structure, that is a series of periodic cusps at their edges (Figure 4.16a, Figure 4.17; see also Figure 4A, NTB 87-14). Mullions are visible in the roofs and floors of the tunnels, but not in the walls. This indicates that the mullions are approximately vertical. The formation of mullions results from differences in how the granite and lamprophyre flowed during ductile deformation and reflects the lower viscosity of the lamprophyres relative to the adjacent granite (Ramsay, 1967; Smith, 1975, 1977). Mullions develop in response to shortening approximately parallel to the deformed layer and form at approximately right angles to the direction of maximum shortening.

Many and perhaps most of the Alpine tension fissures exposed in the tunnels extend from lamprophyres (Figure 4.17); some are more than a meter tall and extend several meters from the lamprophyres. These fissures are subhorizontal and are exposed in tunnel walls, but not in roofs or floors. Hydrothermal mineral deposits in these fissures and alteration of the adjacent granite shows that the fissures have served as important conduits for hydrothermal fluids.

Assuming that the remote principal strains and principal stresses had similar orientations, the mullions along the northwest-striking lamprophyres would have formed when the maximum compressive stress was oriented northwest-southeast. If the fissures and mullions formed contemporaneously, the least compressive stress during their formation would have been approximately

Figure 4.16. Deformational features along dark-colored lamprophyres in the laboratory that strike northwest. (a) Asymmetric mullion cusps in a tunnel roof. Note the hand for scale. (b) Subhorizontal alpine tension fissures in a tunnel wall. The distance between the two lamprophyres as measured along the tunnel wall is ≈1.5 meters. Note the hydrothermal alteration halos around the fissures (photograph of fissures courtesy of NAGRA).

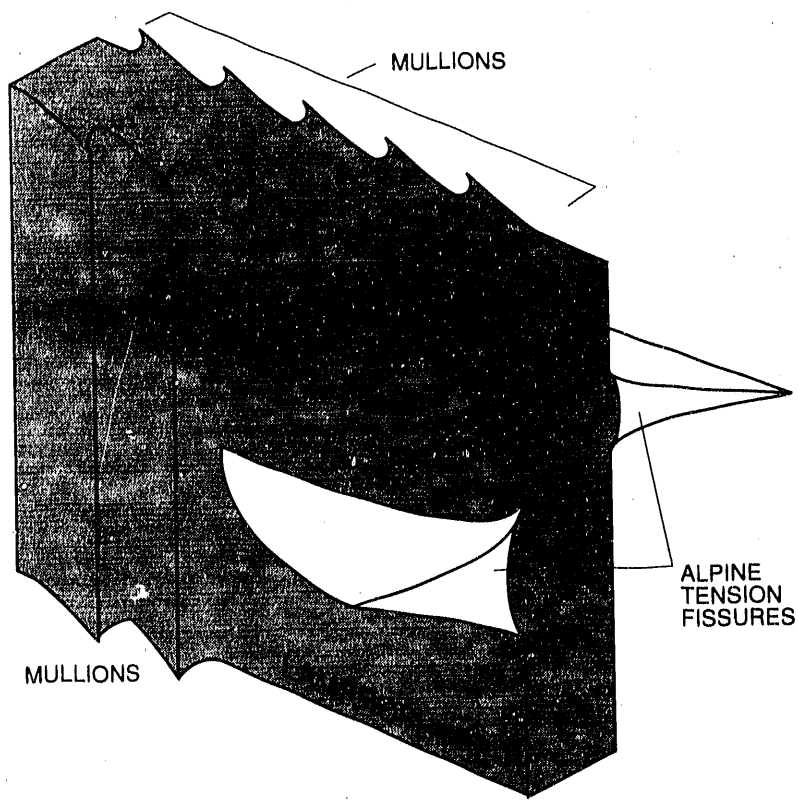

Figure 4.17. Block diagram showing vertical mullions and horizontal Alpine tension fissures extending from a vertical lamprophyre. The fissures are filled with hydrothermal minerals.

vertical.

Shear displacement across some lamprophyres also caused fracturing of the granite. Steeply-dipping splay cracks that strike to the north extend from the ends of northwest-striking lamprophyres in the heater test tunnel at W108.5 and W137 (Figure 4.18). This type of structure indicates right-lateral strike-slip displacement across the lamprophyres (Pollard and Segall, 1987). The splay crack orientation indicates that slip occurred when the maximum compressive stress was nearly horizontal and oriented nearly north-south. The presence of the mullions and splay cracks appear to reflect deformation under two somewhat different stress regimes.

We found one lamprophyre at the surface that is superbly exposed over a distance of approximately 100 m. It appears to be offset by the K-zone of Figure 4.8, with a left-lateral strike separation of perhaps 20 m. The lamprophyre strikes to the north, oblique to the rock foliation. Mullions are much less prominent along this lamprophyre than along those that strike northwest in the subsurface; the degree of deformation along the lamprophyres thus appears to vary as a function of lamprophyre orientation. Along most of the outcrop the lamprophyre appears little-deformed macroscopically, although its margins are locally sheared. However, at echelon steps along strike (Figure 4.8) the lamprophyre appears highly sheared and contains abundant hydrothermal quartz. This suggests that quartz veins may be a sign of particularly large deformation in the lamprophyres.

4.2.7. Evidence for Multiple Deformation Events

There is substantial evidence for multiple episodes of displacement across many of the steeply-dipping structures in the Grimsel area. Across some northeast-striking S-zones, steeply-dipping veins are dragged and offset left-laterally, whereas others offset veins sharply in a right-lateral sense. These observations suggest two episodes of deformation, first one in which the S-zones slipped left-laterally under elevated pressure-temperature conditions and then another in which they slipped right-laterally under lower pressure-temperature conditions (Figure 4.19). Multiple episodes of deformation are also indicated by northwest-striking structures. Left-lateral displacement across the northwest-striking K-zone of Figure 4.8 is indicated by the apparent 20-

Figure 4.18. Splay fractures near the end of a lamprophyre in the laboratory roof; the photograph is printed reversed to show the features as they would appear in plan view. The trace of the lamprophyre is parallel to the long dimension of the photograph. The fractures splay to the right, indicating right-lateral slip across the lamprophyre (the rock to the right of the lamprophyre moved down relative to the left-side). The lamprophyre strikes northwest; the bottom of the photograph is to the northwest. The roof was damp in the vicinity of the splay cracks, indicating relatively high permeability there.

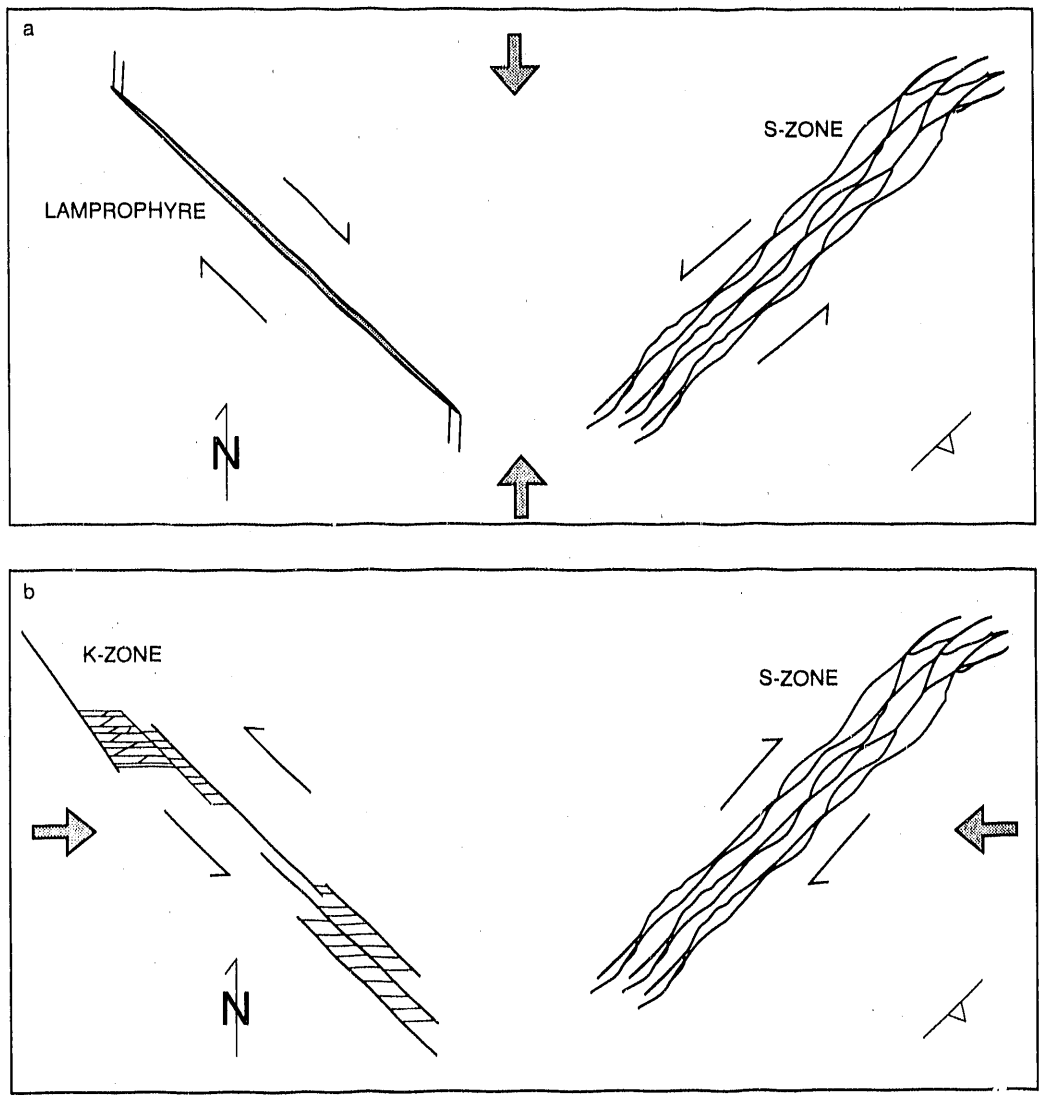

Figure 4.19. Two of the stages of deformation at Grimsel. (a) Left-lateral displacement across the S-zones. Displaced veins are plastically deformed, indicating elevated pressure/temperature conditions. Maximum horizontal compression is oriented north-south. Right-lateral displacement across lamprophyres may have occurred at this stage. (b) Left-lateral displacement across northwest-striking K-zones and right-lateral displacement across northeast-striking S-zones. Fracturing associated with this deformation suggests lower pressure/temperature conditions than in (a).

m left-lateral strike separation of a steeply-dipping lamprophyre and by the fracture structure of the zone. However, the steeply-dipping fractures near the ends of some northwest-striking lamprophyres in the laboratory tunnels indicate right-lateral slip. These observations might be explained by only two episodes of deformation, one in which the maximum compressive stress was horizontal and oriented north-south and another in which it was oriented east-west (Figure 4.19). However, not all the observations are consistent with just two homogeneous deformational events. The fracture structure along the west-striking fault near the mouth of the BK room (Figure 4.9) indicates left-lateral displacement on that fault. This is consistent with slip in which the maximum compressive stress was oriented northeast-southwest, so at least three episodes of strike-slip faulting may have occurred. During strike-slip faulting both the maximum and minimum compressive stresses would have been approximately horizontal. The fabric of the granite, with a steeply-dipping foliation that strike approximately N65°E and a steeply plunging lineation may indicate another stage of deformation in which the maximum compressive stress was oriented approximately N25°W and the minimum compressive stress was oriented approximately vertically. Quartz veins which appear dragged along a fault that dips steeply to the south in the lamprophyre at L114 may reflect normal dip-slip motion on the fault (Figure 4.20), with the maximum compressive stress being oriented approximately vertically and the least compressive stress being oriented roughly north-south. The sequence and number of deformational events is uncertain, but the structures at Grimsel clearly reflect a rather complicated deformational sequence.

4.2.8. Hydrologic Implications

The K- and S-zones are markedly different structures (Figure 4.15) and probably have markedly different fracture flow characteristics. The K-zones appear structurally more heterogeneous than the S-zones and fluid flow may be more heterogeneous along the K-zones than the S-zones. Flow in the K-zones is most likely to be localized at steps, where the fracturing is most extensive. In three dimensions these steps might act as nearly vertical pipes. The principal fractures in the S-zones strike subparallel to the zones, so the permeability probably would be greater

Figure 4.20. View of a white vein offset by a fault in a lamprophyre. This exposure is in the east wall of the laboratory tunnel at L114. The fault extends from the lower right corner of the photograph to the center of the top edge. The offset vein extends down from near the upper right corner towards the fault and hooks back towards the top of the photograph at it near the fault. The vein may be drag folded along the fault. If so, this indicates a component of normal slip, with the north (left) side of the fault up relative to the south side. The pick end of a rock hammer head at the very bottom of the photograph serves as a scale.

along the zones rather than across them. Because S-zone fractures appear more tortuous in plan view than in vertical cross section, we suspect that the average vertical permeability of the S-zones would be greater in the vertical direction than along strike.

Flow along the lamprophyres probably would be concentrated along their edges where deformation of the lamprophyre and the adjacent granite is great. Flow could be particularly high along the Alpine tension fissures that extend from the lamprophyres. The micaceous material in the lamprophyres probably causes permeability across the lamprophyres to be quite low. However, some flow across lamprophyres could occur along foliation planes or where the lamprophyres are discontinuous.

The evidence for multiple episodes of slip suggests that the zones may well offset each other where they intersect. If so, the steeply-dipping zone intersections may be sites of particularly extensive fracturing and preferred paths for fluid flow.

The observations of others (Choukrone and Gapais, 1983; NTB 87-14) indicate that rock deformation is decidedly heterogeneous at the scale of the Grimsel Pass region. Our observations indicate that deformation is also markedly heterogeneous at the scale of the Grimsel laboratory. We expect that flow along fractures will be irregular at the scale of the Grimsel laboratory.

4.3. Site-Specific Model of Geologic Structure: The US/BK Site

We have prepared a site-specific model of the geologic structure at the US/BK site in the northern part of the Grimsel Rock Laboratory. The main laboratory tunnel, which bounds the site on the east, and the BK room, which is located in the southeast part of the site, form the perimeter of the site, albeit a partial one. The site is bounded on the north and south by boreholes BOUS 85.002 and BOUS 85.003 (Figure 4.21). These holes are about 150 m long and are spaced about 150 m apart. About one dozen other boreholes radiate from the BK excavation.

As we developed our interpretation of the geologic structure at the US/BK site we first exploited the exposures in the BK room and the laboratory tunnel. We then identified fracture zones in the boreholes and prepared a preliminary model of the site. Seismic and radar tomo-

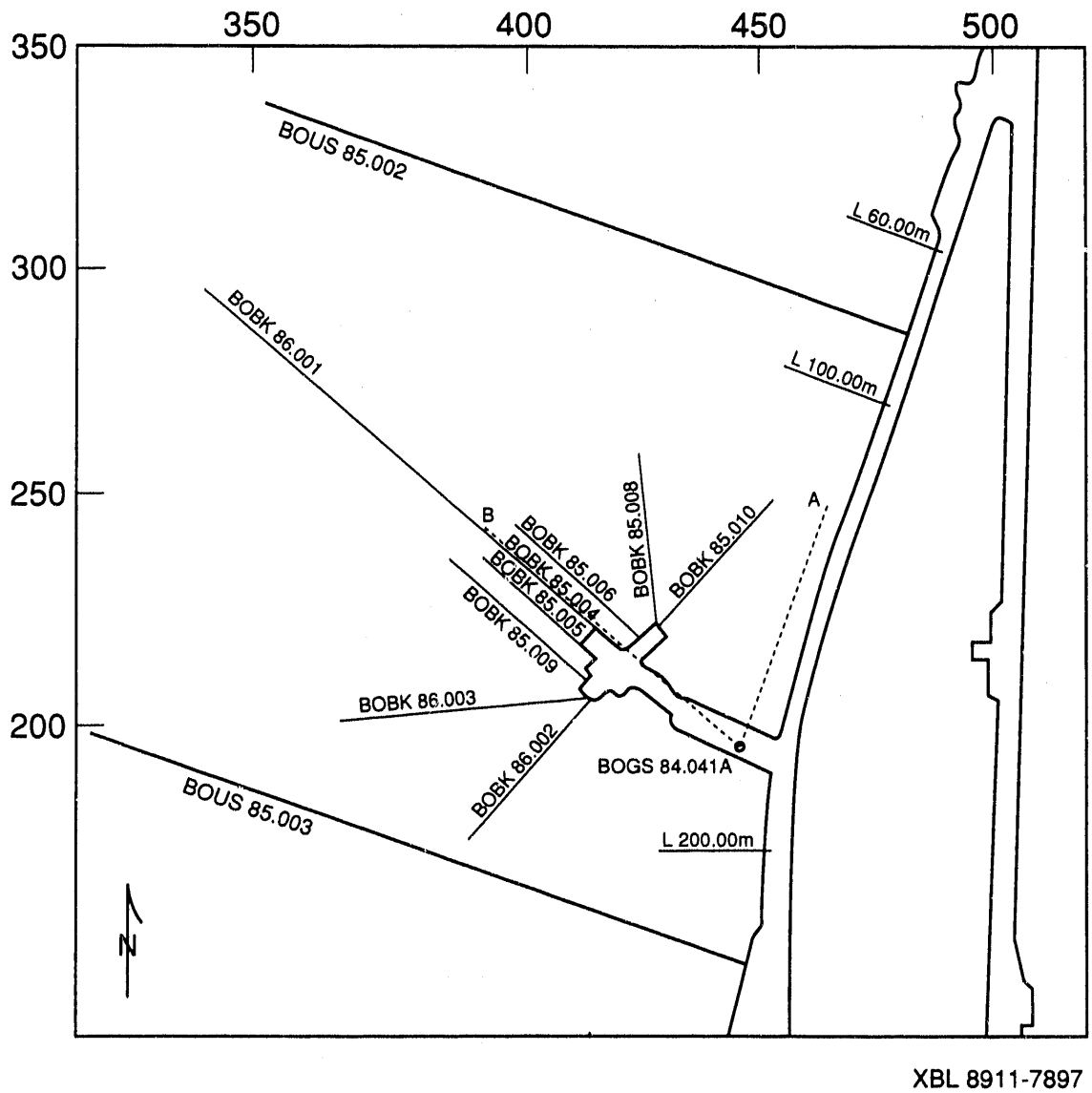

Figure 4.21. Map showing the major boreholes in the vicinity of the BK room. Tick marks are on a 50 meter grid. North is to top of figure. Dashed lines A and B mark lines of cross section shown on Figure 4.23. Borehole BOBK 85.007 is not shown; it projects along borehole BOBK 85.004.

grams were then used to define the structure between the boreholes and the tunnels and to refine our initial model.

4.3.1. Geology Along the US/BK Site Perimeter

BK Room. The fracture structure mapped within the BK room varies considerably (Figure 4.9). The east end of the room is highly fractured and contains the fracture system described in Section 4.2.3. The west end of the room is much less fractured. The fractures in the west end of the BK room generally strike either northeast (S-fractures) or northwest (K-fractures). At least some of the fractures cut, but do not offset, flow structures in the granite. Most of the fractures do not cross the room, and they do not appear to belong to any throughgoing fracture zones. Perhaps the most prominent fracture is a fault that strikes northwest from the fault at the mouth of the BK room (Figure 4.9).

Laboratory Tunnel. The laboratory tunnel reveals three prominent S-zones that strike northeast near the BK room (Figure 4.2). Two of these are north of the BK room, and the other intersects a north-striking joint several meters south of the BK room. Water drains from all of these structures.

The two S-zones north of the BK room (Figure 4.6) are exposed near L76 and between L80 and L103 (Figure 4.11). These dip ~65° and ~80° to the southeast, respectively. Subhorizontal slickenlines are common on fractures in the second zone, indicating some of the fractures have accommodated strike-slip displacement. Lateral displacements across individual S-fractures are usually small. Where offset, quartz veins and other markers are generally offset no more than 20 cm and in a right-lateral sense. However, a gouge-filled fault exposed near L76 appears to offset a steeply-dipping quartz vein much more. The vein is exposed on the southeast side of the fault but not on the northwest side, and we infer that the vein is offset right-laterally by at least 5 m. Northeast of L76, a lamprophyre has been interpreted to make an unusual right-lateral bend where it crosses the projection of this fault (Figure 4.6). We suggest the lamprophyre may be offset right-laterally several meters across the "L76" fault. The second S-zone contains numerous northeast-striking fractures. This zone probably does not extend into the BK room; if

the zone does, it changes character dramatically. Only a few northeast-striking fractures are exposed where this zone would project into the BK room (Figures 4.6 and 4.9), and the zone thickness would decrease from ~21 m in the tunnel to ~7 m in the BK room.

The S-zone south of the BK room (Figure 4.2) is exposed between L213 and L220 (Figure 4.11), within 15 m of borehole BOUS 85.003. If this zone extended on strike twenty meters to the southwest of the tunnel, then it should intersect the borehole within 15 m of the borehole mouth. However, no prominent fracture zone is intersected in that portion of the borehole. The S-zone apparently does not extend to the borehole and is not considered to be a major structure within the US/BK site.

Several lamprophyres that strike to the east occur in the laboratory tunnel north of the BK room (Figure 4.6). They dip steeply to the south and all have been deformed. A few of these lamprophyres contain folded quartz lenses that are faulted. We do not know the sense or amount of displacement across the lamprophyres, but some of the faulted quartz lenses may be drag folded, with the north wall of the fault moving up relative to the south wall (Figure 4.20). That style of deformation is not seen in the more "typical" lamprophyres exposed further south in the laboratory that strike northwest (e.g. Figure 4.16a). Because the east-striking lamprophyres appear to coincide with a prominent K-zone mapped at the surface (Figures 4.3, 4.4, 4.5, and 4.6), we refer to them as K-lamprophyres. Slip along that K-zone may have caused the unusual deformation of the K-lamprophyres.

We have not seen consistent structural relationships between the K-lamprophyres and the northeast-striking S-zone faults. Some northeast-striking faults offset relatively thin K-lamprophyres several centimeters right laterally, whereas others end in K-lamprophyres that are a few meters thick. It is not clear from the tunnel exposures whether the two prominent S-zones cross the K-lamprophyres and offset them, terminate within them, or are offset or deflected across them. The surface mapping (Figure 4.3) and geologic cross section of Figure 4.4 suggests that the S-zone(s) near the US/BK site most likely abut against or are offset by the zone containing the K-lamprophyres, but the block diagram of Figure 4.5 offers an alternative interpretation of the S-

zone(s) crossing the K-lamprophyres exposed in the Strahlchälen gully.

A series of northwest-striking lamprophyres are exposed in the laboratory tunnels south of the BK room (near the 1350- and 1400-m marks in Figure 4.4). Some of these probably extend west of the BK room and come within 100 m of the room.

Some additional structures exposed in the laboratory tunnel strike toward the BK room. A few steeply-dipping joints that strike ~N10°W are exposed between the L199 and L213 marks (Figures 4.2 and 4.11). These joints are not continuous structures, but rather consist of right-stepping echelon segments. The segments typically overlap by several centimeters and the rock bridges between segments are a few centimeters thick.

4.3.2. Borehole Information

We took advantage of independent information on the structural systematics of the major fracture zones at Grimsel when interpreting the borehole data. From the tunnel exposures we knew that a few S-zones, two lamprophyre-bearing zones, and a K-zone occurred at the US/BK site. The S-zones typically strike ~N50E and dip 65° southeast. The K-lamprophyres north of the BK room strike ~N80°W and dip ~80° south, and the lamprophyres south of the BK room strike approximately N20-30° W and dip ~80° west. A steeply-dipping K-zone that appears to lack lamprophyres strikes to the west near the entrance of the BK room. The surface and subsurface geologic mapping demonstrate that these structures are large and relatively planar. Our detailed characterization work demonstrated that the fractures in the S-zones formed a braided pattern. Although the strike of individual S-zone fractures locally differs from the the overall strike of the zone by as much as 20°-30° the overall strike of the S-zone fractures is roughly parallel to the zone as a whole. The average orientation of fractures encountered in a borehole through an S-zone should be a good indicator of the orientation of the zone as a whole. In contrast, the K-zones consist of faults parallel to the zone linked by fractures that strike oblique to the zone; these oblique fractures typically are more numerous than the zone-parallel faults. The average orientation of fractures encountered in a borehole through a K-zone would be a poor indicator of the orientation of the zone as a whole.

We inspected photographs of the cores drilled around the US/BK site and located the intervals of abundant fractures and lamprophyres (see Appendix). The fracture clusters in lamprophyres generally coincide with portions of the core with low Rock Quality Index values (see core logs in preliminary draft of NTB 87-14), and the fracture clusters in granitic rock correspond quite well to slickensided fractures (Bräuer et al., 1989, Figure 4.13). We then assumed that lamprophyres and fracture clusters encountered in the boreholes belonged to one of the types of zones exposed adjacent to the site. We assigned a lamprophyre or fracture cluster to a particular zone based on the location of the cluster and the "average" orientation of fractures in the cluster. The information on the location and orientation of the lamprophyres and fracture clusters were then projected up (or down) dip using the orientation of the appropriate zone to a horizontal plane at an elevation of 1730 m, the elevation of BK room, to form a map (Figure 4.22). The information could also be projected along strike to vertical planes to yield cross sections (Figure 4.23).

4.3.3. Preliminary Geologic Model of the US/BK Site

The major features in our preliminary model (Figure 4.22) based on the exposures in the BK room and the laboratory tunnel and on the borehole data are (from north to south):

(1) a discontinuous series of three northeast-striking S-zone segments,

(2) a lamprophyre-bearing K-zone north of the BK room,

(3) some northwest-striking lamprophyres,

(4) a west-striking K-zone south of the BK room.

We correlate Features 1, 2, and 3 with major structures that are mapped at the surface and shown near the northern border of Figure 4.3. We have not identified a K-zone at the surface that would correspond to feature 4 in our model (Figure 4.22). Our model is different from that in NTB 87-14 (Figure 4.6) which shows the S-zone that contains the fault at L76 as extending continuously across the US/BK site. In our model the S-zone consists of discontinuous segments 1a, 1b, 1c separated by lamprophyres. The two models should have different hydrologic behaviors.

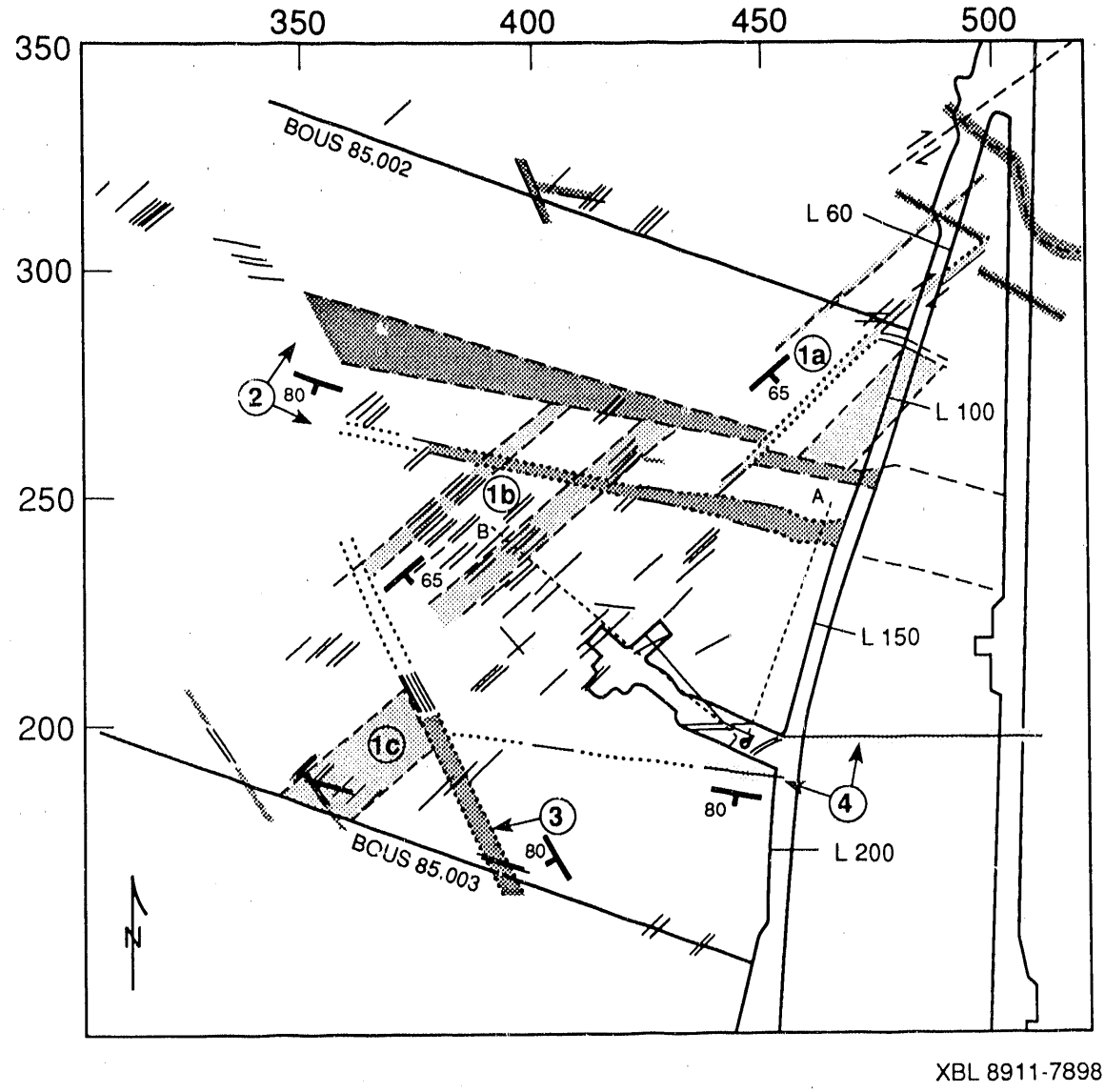

Figure 4.22. Map projection at the 1730 meter level of borehole fractures (fine lines) and associated major structures at the US/BK site. Closely spaced pairs of lines mark edges of fractured zones; single lines mark prominent single fractures. See Appendix for more details. Strike and dip used for projection of fractures shown in heavy line; these attitudes correspond to the attitudes of the major features. Feature 1 (medium screen): S-zone fractures. Feature 2 (dark screen): K-lamprophyres. Feature 3 (dark screen): Northwest-striking lamprophyres. Feature 4 (light screen): K-zone. Tick marks are on a 50 meter grid. North is to top of figure. Dashed lines A and B mark lines of cross section shown on Figure 4.23.

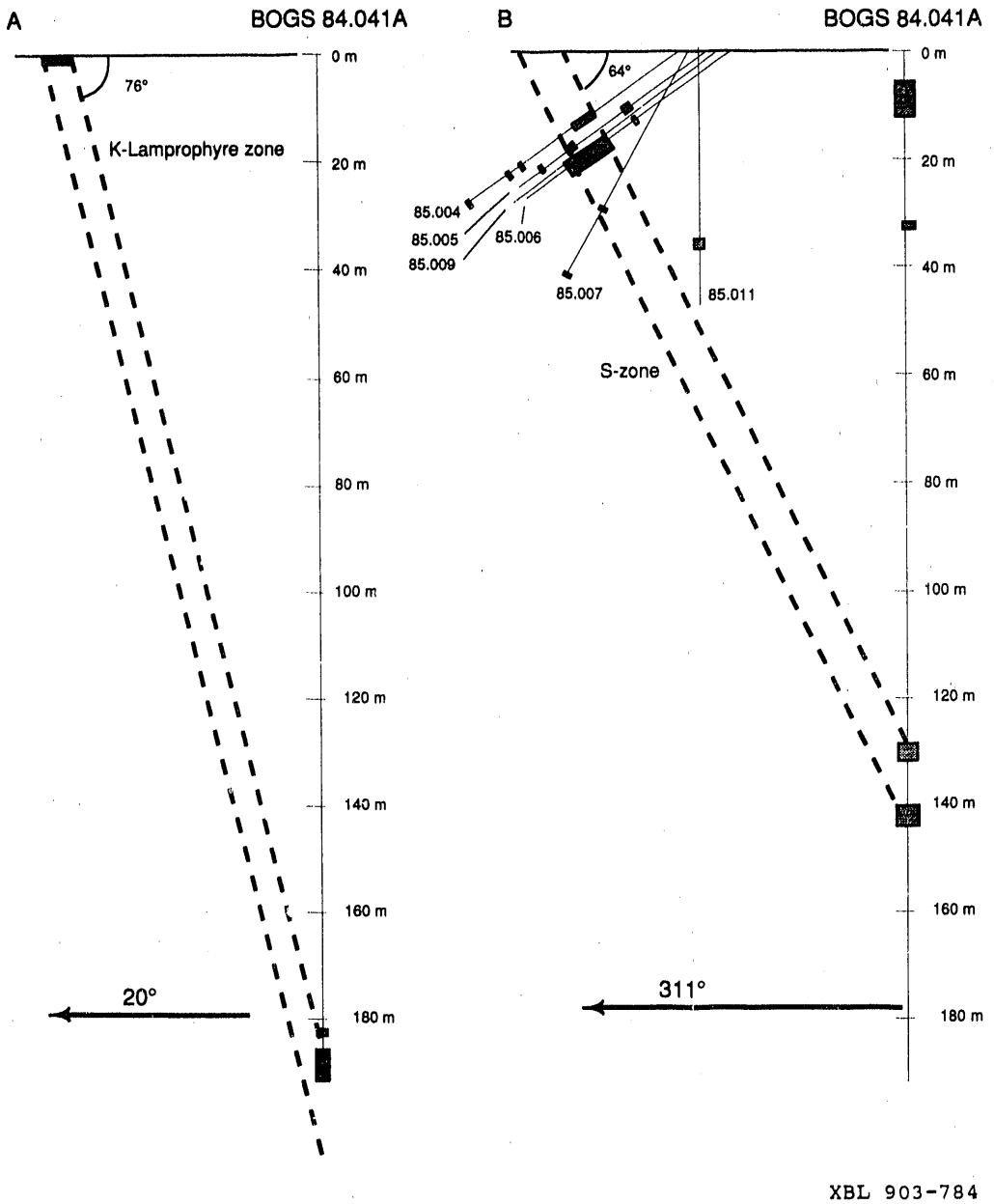

Figure 4.23. Vertical cross sections through borehole BOBK 84.041A. The bottom of the hole is at a depth of 191.5 meters. Horizontal and vertical scales are equal. (a) Cross section along plane that strikes 20°, perpendicular to strike of K-lamprophyres. Dark shading indicates lamprophyres. Dashed line marks inferred edges of K-lamprophyres. (b) Cross section along plane that strikes 311°, perpendicular to strike of S-zone. Dark shading marks intervals with numerous fractures; fractured intervals in non-vertical holes are projected orthogonally onto the cross section plane. Dashed line marks inferred edges of S-zone.

Three lines of evidence suggest the S-zone segment containing the fault at L76 (Feature 1a) does not extend on strike past the BK room as is shown on Figure 4.6. First, within a few meters northwest of the BK room we see only a limited amount of fracturing in boreholes (Figures 4.22 and 4.23) and no trace of the prominent band of mylonite/kakirite that is exposed in the laboratory tunnel near L76 (Figure 4.11). Second, the wide zone of S-fractures between the L80 and L103 does not appear to extend into the BK room. The third point regards the apparent continuity of the east-striking lamprophyres. We show two thick K-lamprophyres (Feature 2) north of the BK room in Figure 4.22. The nearly coplanar alignment of the southern lamprophyre in three boreholes and in the laboratory tunnel strongly suggests that this lamprophyre is not significantly displaced by Feature 1a. Because this S-zone appears to offset features in and near the laboratory tunnel by several meters, the apparent lack of displacement of the southernmost K-lamprophyre indicates that Feature 1a stops at the K-lamprophyres or north of them. The extensive fracturing 25-50 m northwest of the BK room in the boreholes suggests that a second S-zone segment (Feature 1b) occurs there. Segments 1a and 1b would form a right-stepping echelon pair. The south end of Feature 1a and the north end of Feature 1b would terminate at the K-lamprophyres. This interpretation is consistent with the geologic map of the surface (Figure 4.3) and with our own surface observations. Data from borehole BOUS 85.003 (see Appendix) suggests that an S-zone segment intersects the hole at a depth between 90 and 105 m. If the S-zone segment strikes N50° as we interpret, then 1b and 1c would be discontinuous. Northwest-striking lamprophyres (Feature 3) would separate Features 1b and 1c. The S-zone segments may have formed part of a once-continuous structure that was offset by slip across the lamprophyres, but the segments may also have formed part of a structure that was originally discontinuous.

The west-striking K-zone near the BK room (Feature 4, Figure 4.22) is well exposed in the laboratory tunnel and was well exposed in the floor of the BK room before being covered by concrete. The evidence for this feature extending several tens of meters west from the laboratory tunnel comes from a single borehole (BOBK 86.002, Figures 4.21 and 22) and is not particularly strong.

The interval of lamprophyre encountered from 88.3 to 117.3 m in BOBK 86.001 is anomalously thick. It may be that some of this thickness is due to a northwest-striking lamprophyre that projects into the region from the south.

4.3.4. Geophysical Tomography

We used seismic tomograms (Gelbke,1988) and radar tomograms (Niva and Olsson, 1987, 1988a, 1988b) in studying the US/BK site. Both kinds of tomograms are "three-sided", having been produced using signals transmitted between the laboratory tunnel, borehole BOUS 85.002 and borehole BOUS 85.003. These boreholes lie in a plane that strikes approximately north-south and dips 15° to the west beneath the BK room. The technical specifications of the data acquisition systems and the processing and inversions methods are given in detail in the above reports.

The tomograms provide information on the rock mass and the enclosed fractures along their intersection with the plane of the tomography. The tomograms can help not only in extrapolating known features observed at the perimeter of a target site, but also in identifying features within the site which would be difficult to locate using geologic data alone. The tomograms must be interpreted to distinguish between anomalies that are artifacts of the inversion process and anomalies that correspond to features of the rock such as fracture zones or variations in rock type, porosity or fluid content. The pixel dimension of 2.5 meters used in the tomographic inversions provides a lower bound on the resolution of the tomograms. Smearing (distortion of anomaly size, shape and orientation in the inversion process) is likely to be more pronounced where ray coverage is most sparse. For the tomograms presented here smearing will be greatest in the west half of the tomograms and along the edges.

Seismic Velocity Tomography. We have defined several major low velocity anomalies on the seismic velocity tomogram using the 5050 m/sec contour (Figures 4.24 and 4.25). In Figure 4.25, the geologic features are indicated by circled numbers and the seismic anomalies by uncircled numbers. Anomaly S1a is located in the northeast corner of the tomogram. It extends along the laboratory tunnel from BOUS 85.002 (~L80) to ~L120. Anomalies S1a and S2 are linked near the laboratory tunnel at ~L120. Anomaly S2 is a Y-shaped feature. The stem of the Y meets the

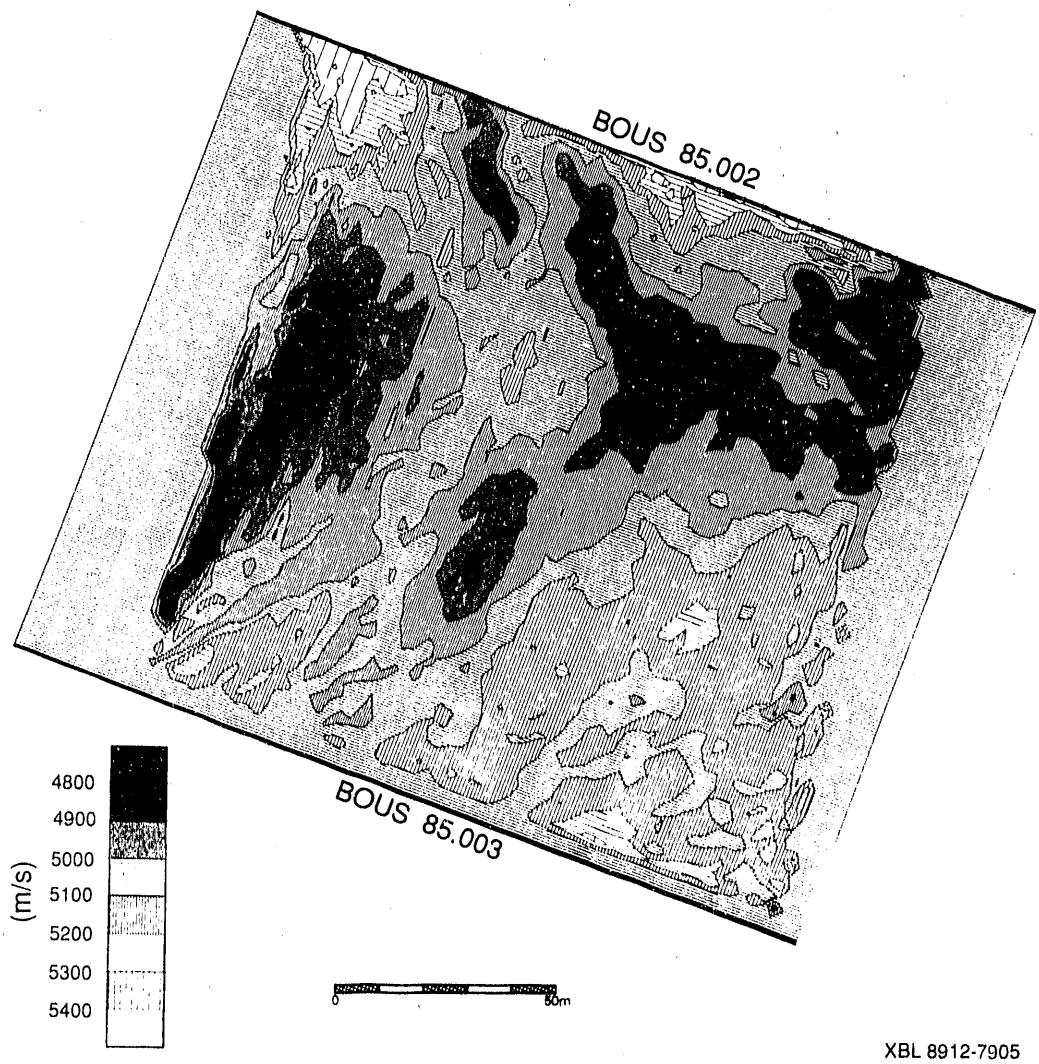

Figure 4.24. Seismic tomogram of the velocity structure between BOUS 85.002 and BOUS 85.003. Modified from NTB 88-06, Figure 65. Boreholes BOUS 85.002 and 85.003 are contained within the heavy lines at the edges of the tomogram, but do not extend along the entire length of the lines. North is to top of page.

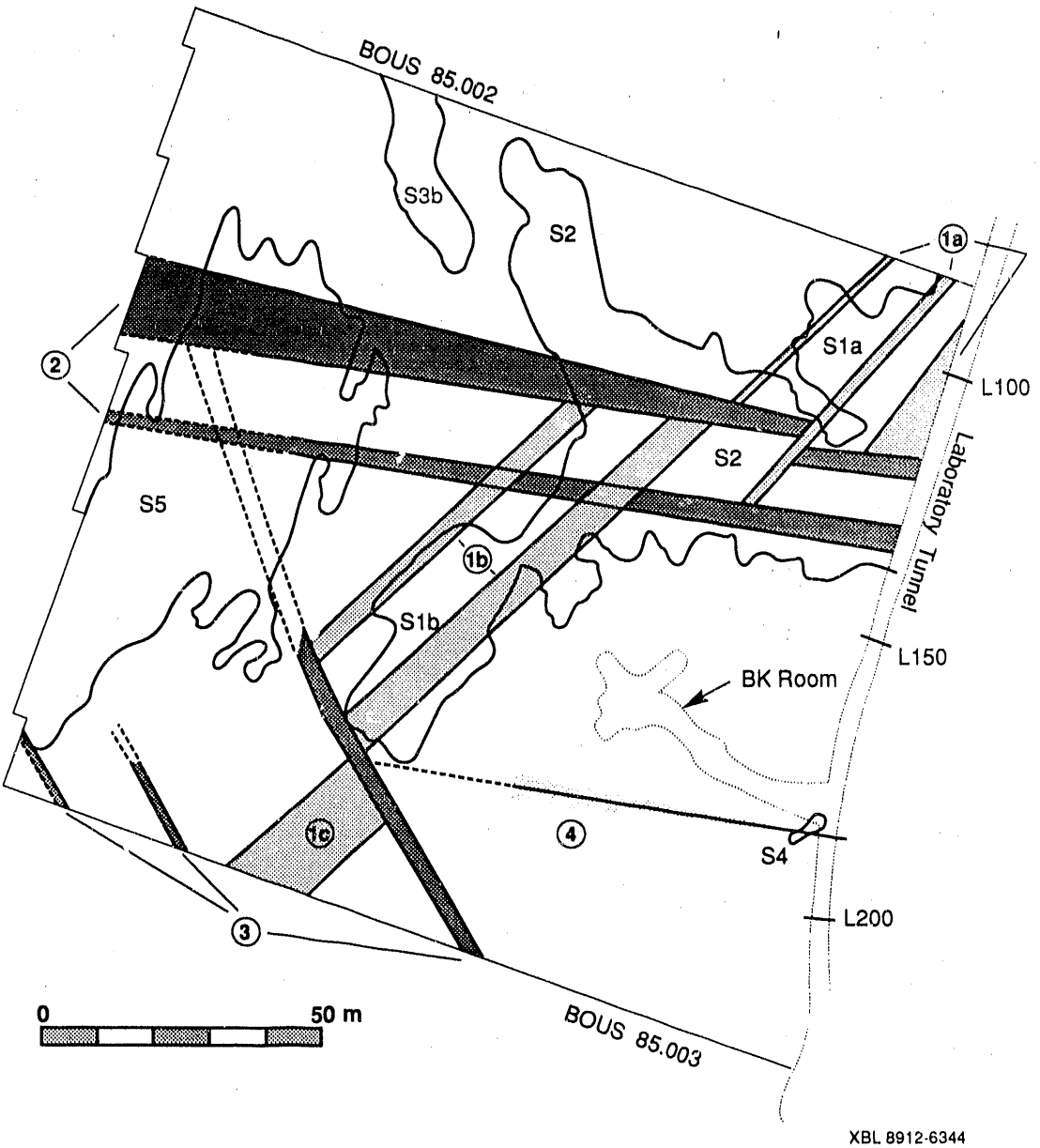

Figure 4.25. Projection in the plane of tomography showing the features of the preliminary structural model of the US/BK site (see Figure 4.22) superposed on the 5050 m/second contour from Figure 4.24. Seismic anomalies S1-S5 are described in the text. North is to top of page.

laboratory tunnel between L122 and L140 and trends approximately east-west. The northwest-trending arm of anomaly S2 would intersect BOUS 85.002 at a depth of 73-87 m. A thin low velocity neck connects the southwest arm of anomaly S2 with anomaly S1b. Anomaly S1b is an oblong feature that trends roughly north-south, but is contained in a region of relatively low velocity that strikes more nearly northeast. Anomaly S3b trends northwest and approaches BOUS 85.002 at a depth of 100-110 m. A small low velocity anomaly (S4) is enclosed by the 5050 m/sec velocity contour just south of the entrance to the BK room. Anomaly S5 occupies a roughly triangular region (Figure 4.24) approximately bounded by the west side of the tomogram and diagonals connecting the corners of the tomogram.

Comparison with Geologic and Borehole Information. The major features inferred from the geologic data are projected into the plane of the seismic tomography in Figure 4.25. Anomaly S1a occurs along a portion of the laboratory tunnel (L70 - L103). The south end of the anomaly coincides with a K-lamprophyre exposed between L113 and L118. The roughly east-west trend of the south end of the anomaly also coincides with the strike of the lamprophyre. We interpret anomaly S1a to reflect S-zone fractures that are bounded by a K-lamprophyre and to match up with Feature 1a in our preliminary model (Figure 4.22). Anomaly S1a does not appear to project on strike to the southwest past anomaly S2 (Figures 4.24 and 4.25).

The K-lamprophyres are associated with a major structure that cuts through the Juchlistock area (Feature 2 of Figure 4.2), and we expect that this zone would extend through the US/BK site. The east end of anomaly S2 coincides with a series of east-striking K-lamprophyres exposed in the laboratory tunnel between ~L120 and ~L140 (Figure 4.11). Because laboratory measurements show that unfractured and undeformed lamprophyre has a higher acoustic velocity than granite, one might expect lamprophyres to have a higher velocity than granite on seismic tomograms. However, the exposures of the K-lamprophyres in the laboratory tunnel are highly fractured and highly deformed, and we expect them to generally have low in-situ velocities. We interpret the eastern "stem" of anomaly S2 (Figure 4.25) to represent fractured K-lamprophyres of Feature 2 (Figure 4.22) The area of slightly above-average velocity between the northwest and southwest

arms of anomaly S2 indicates that the intensity of fracturing may locally be low there. The southwest end of anomaly S2 is discussed below with anomaly S1b. The northwest arm of S2 is discussed below with anomaly S3b.

Perhaps the most striking correspondence of concentrated fractures in Figure 4.22 with a pronounced low velocity seismic anomaly occurs at anomaly S1b and the southwest arm of anomaly S2 (Figure 4.25). These anomalies coincide with Feature 1b of our model. The southwest end of anomaly S1b corresponds in general to the projected intersection of Feature 1b with the northwest-striking lamprophyres encountered in borehole BOBK 86.003 (Feature 3a, Figure 4.22). This suggests that the zone of fractures associated with anomaly S1b may terminate at those lamprophyres. Similarly, S1b does not appear to project on strike to the northeast past the stem of anomaly S2, which supports our interpretation of two echelon S-zone segments that step to the right where they intersect the K-lamprophyres (Figure 4.22). Feature 1c does not have a prominent corresponding anomaly on the seismic tomogram.

The northwest arm of anomaly S2 and anomaly S3b indicate that structures may be present in the northern part of the US/BK site that are not in our preliminary model. The borehole logs of BOUS 85.002 (Figure 4.26) contain ample evidence for fracturing from 69 to 113 m down the borehole, the interval into which the northwest arm of anomaly S2 and anomaly S3b project. However, one can not be sure which geologic features are associated with these anomalies. The northwest arm of low-velocity anomaly S2 appears to stop just short of BOUS 85.002 on the seismic tomogram (Figure 4.25) but would project to intersect the hole at a depth of 73-87 m. The borehole logs (Figure 4.26) show a biotite- and quartz-rich feature, possibly a lamprophyre, with a low acoustic velocity at 69 m. A vein or fissure with quartz, biotite, and chlorite (possibly an Alpine tension fissure) occurs at 76.5-79 m, but this does not show a low velocity in the acoustic log. Numerous fractures bearing quartz and epidote are logged at 86-88m, but there is no pronounced acoustic anomaly there either. A low velocity biotite-chlorite zone, possibly a lamprophyre, occurs at 94-95 m, and numerous northwest-striking chlorite-bearing fractures occur at 95-100 m. Anomaly S3b is shown as intersecting the borehole at ~102-114 m depth. A highly

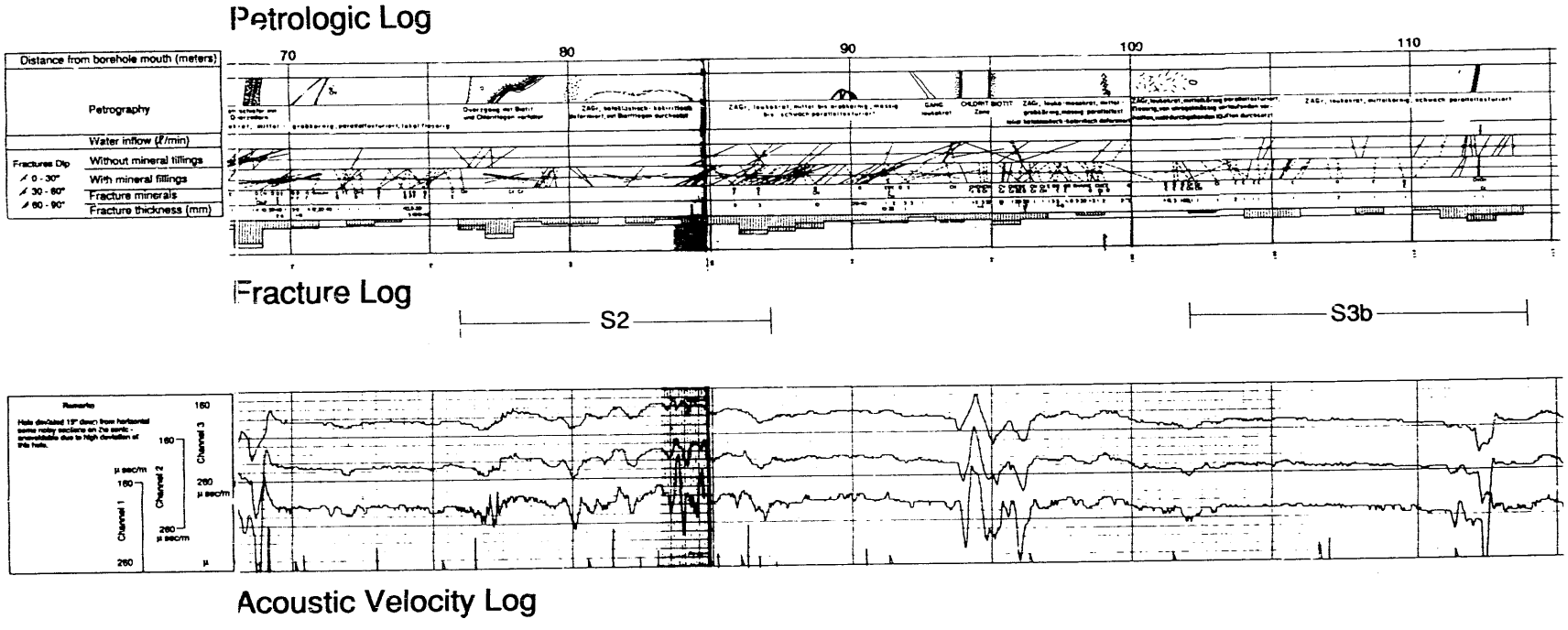

Figure 4.26. Petrologic, fracture, and acoustic velocity logs of borehole BOUS 85.002 from a downhole depth of 68 to 115 meters. The northwest arm of seismic anomaly S2 projects to the interval from 73 to 87 meters. Seismic anomaly S3b projects to the interval from 102 to 114 meters (from preliminary volume of NTB 87-14).

fractured interval with a low velocity occurs at 112.1-112.5 m; this interval would be near the southwest edge of anomaly S3b. We interpret the northwest arm of anomaly S2 and anomaly S3b as corresponding to lamprophyres that strike northwest rather than fracture zones. This interpretation is supported by the geologic map of the surface (Figure 4.3), which shows a northwest-striking lamprophyre intersecting the K-zone containing the K-lamprophyres at an elevation of ~2160 m; this intersection projects downdip to near the intersection of S3b and BOUS 85.002 in the plane of the tomogram.

Anomaly S4 (Figure 4.25) coincides with the entrance to the BK room. This is where numerous fractures have been mapped on the floor of the room (Figure 4.9) and where we have inferred a step in the K-zone of Feature 4 (Figure 4.22). Feature 4 is not represented on the seismic tomogram as a prominent geophysical anomaly west of S4 (Figure 4.25), but we do not expect K-zones to necessarily have prominent tomographic si natures except at steps (see Figure 4.15) or at their ends. It is possible that Feature 4 does not extend to the west of the BK room. In that case anomaly S4 might represent fractures at the west end of Feature 4.

Anomaly S5 (Figure 4.25) reflects artifacts produced by the inversion process in an area where the density of seismic rays is low; no acoustic rays were transmitted from or received along a line connecting the ends of the two boreholes bounding the US/BK site. The rock at S5 may or may not have a low acoustic velocity.

The anomalies on the seismic tomogram are consistent with our structural interpretation based on geology and borehole data. The only significant change the seismic tomogram would suggest is that northwest-striking lamprophyres be added to account for anomaly S3b and the northwest arm of anomaly S2.

Radar Tomography. We now compare our preliminary model to some radar tomograms. Tomographic radar measurements were made at the US/BK site in late 1986 (Phase 1), the spring of 1987 (Phase 2), and late in 1987 (Phase 3). In all three phases the amplitudes and travel times of the transmitted signals were inverted to yield attenuation and slowness tomograms. Slowness is the reciprocal of velocity; high radar slowness equates to low radar velocity.

During the phase two measurements brine was injected into borehole BOBK 85.009 (Figure 4.27). During the phase three measurements brine was injected into borehole BOBK 86.003. The brine serves as a tracer and is discussed in the next section. Tomograms made from data gathered in a single phase primarily reflect the composition and structure of the rock because the brine tracer is relatively weak and is not prominent on the tomograms except near the injection point. Tomograms from the different phases look slightly different for reasons other than the presence of the brine; the data acquisition system and the processing techniques were improved through the course of the tomography experiments. The phase 2 and 3 tomograms look similar. We have relied primarily on the phase 3 tomograms to help model the geologic structure at the US/BK site.

Two major anomalies exist on the phase 3 tomograms (Figures 4.28 and 4.29). The first is a broad belt that trends approximately east-west midway between the BK room and BOUS 85.002. It is essentially in the same position as anomaly S2 on the seismic tomogram (Figures 4.24 and 4.25). We interpret this belt as representing the K-lamprophyres (Feature 2, Figure 4.22). Note that the internal structure of this belt is complicated in both the radar tomograms (Figures 4.28 and 4.29) and the seismic tomogram. More importantly perhaps, the internal structure is different in each of the radar and seismic tomograms. The tomograms thus do not clearly define the internal structure of Feature 2; they do indicate its internal structure is complicated. The second major anomaly occupies a triangular region approximately bounded by the west edges of the tomograms and diagonals connecting the tomogram corners. This anomaly coincides with seismic anomaly S5 and, like anomaly S5, is considered to be an artifact of the inversion process.

Another anomaly can be seen extending southwest from the center of the slowness tomogram (Figure 4.29) towards, but not all the way to, the west end of BOUS 85.003. The magnitude of this anomaly is greatest near its center. A small anomaly occurs at the corresponding spot on the attenuation tomogram (Figure 4.28). These radar anomaly peaks occur near the southwest end of seismic anomaly S1b (Figures 4.24 and 4.25). They also correspond to the intersection of Features 1b and 3 on Figure 3.25 and may indicate that the rock near this intersection is highly

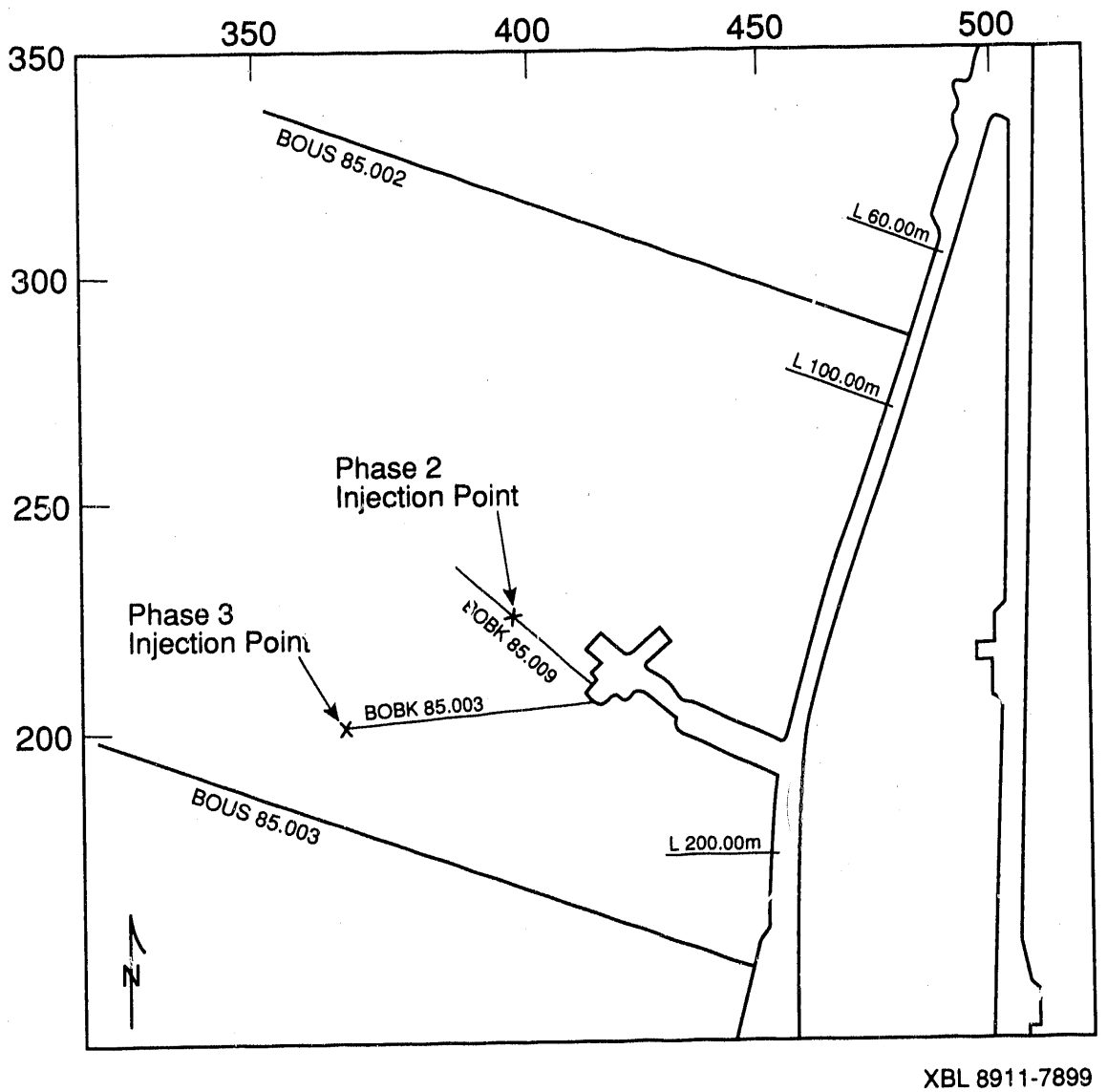

Figure 4.27. Projection in the plane of tomography showing where brine was injected during the phase 2 and phase 3 tomographic measurements. Tick marks are on a 50 meter grid.

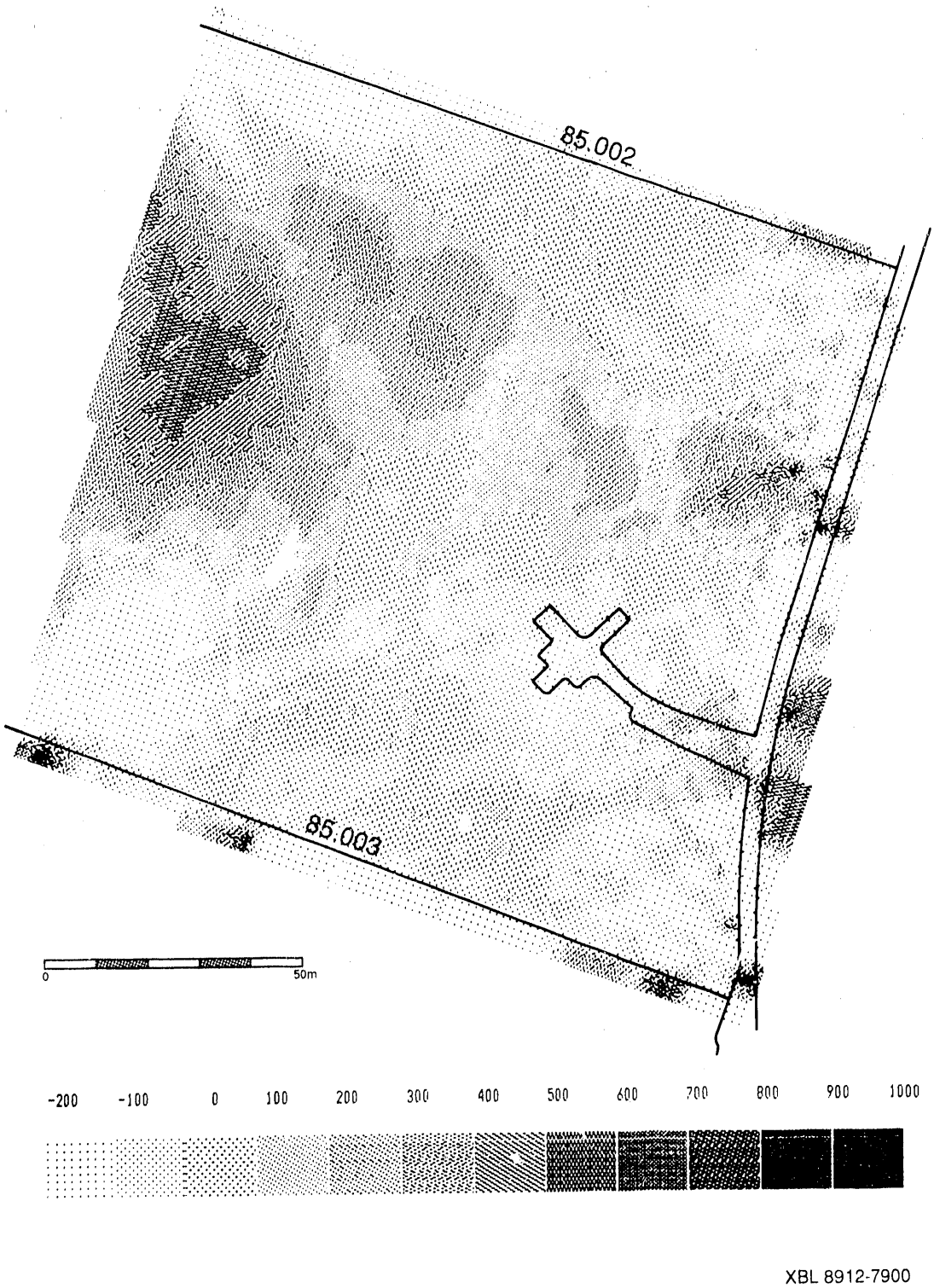

Figure 4.28. Phase 3 tomogram of radar attenuation structure between BOUS 85.002 and BOUS 85.003 (from Niva and Olsson, 1988b, Figure 4.6). Units are dB/m. North is to top of page.

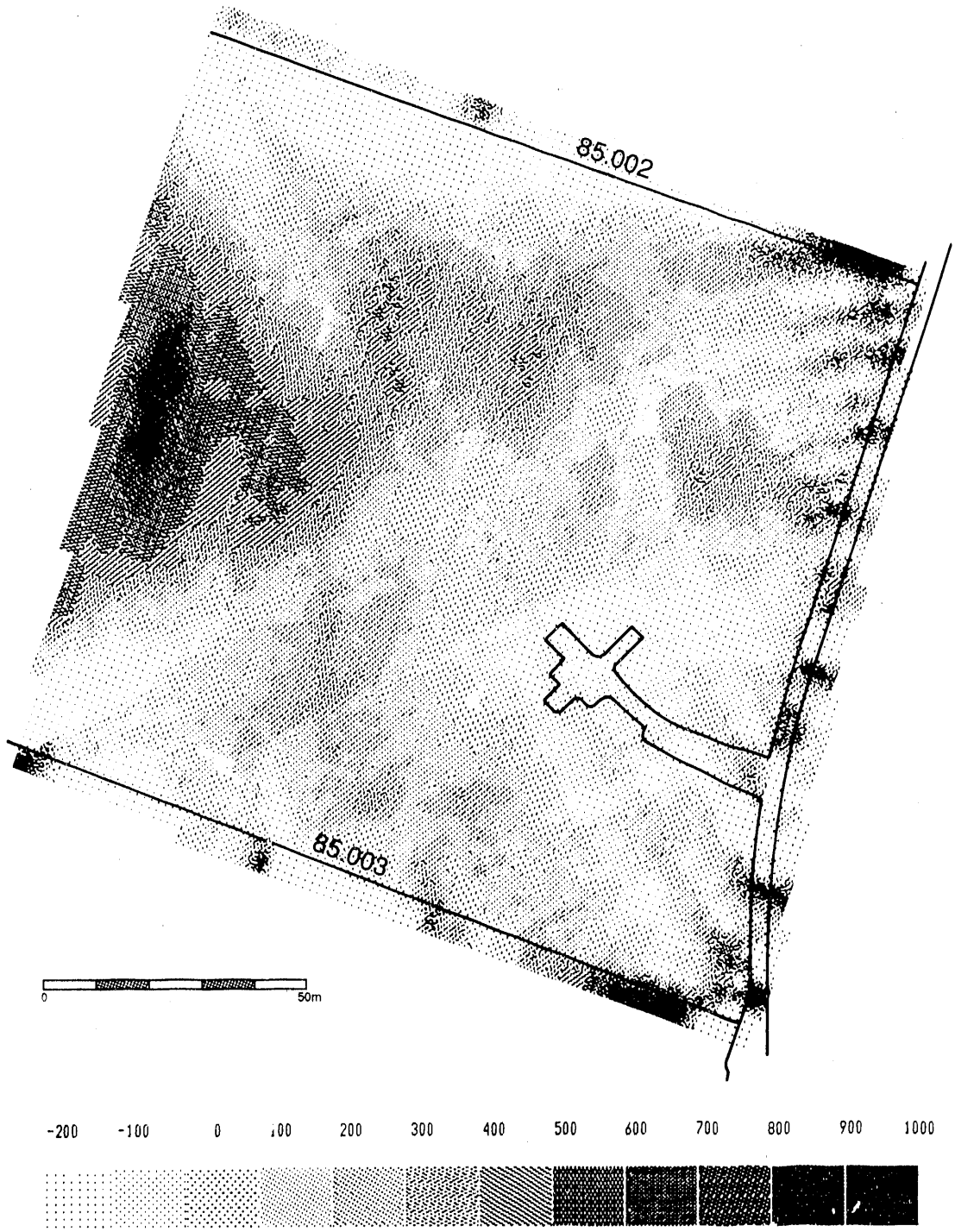

Figure 4.29. Phase 3 tomogram of radar slowness structure between BOUS 85.002 and BOUS 85.003. Values relative to 8050 ps/m standard (from Niva and Olsson, 1988b, Figure 4.2). Units are ps/m. North is to top of page.

fractured.

Numerous minor anomalies occur on the radar tomograms, but the position and orientation of most are different on tomograms from different phases. In a few places small anomalies are persistent in tomograms from different phases. In the northeast corner of the slowness tomogram (Figure 4.29) are several high slowness fingers. The fingers are also present, but in a less pronounced form, on the attenuation tomogram (Figure 4.28). Because these fingers are located near the edge of the tomogram their appearance may not reflect the actual anomalous zone. The location of these fingers coincides with the location of Feature 1a (Figure 4.22) and seismic anomaly S1a (Figures 4.24 and 4.25). Even though the locations of the seismic and radar anomalies coincide with Feature 1a (Figure 4.22), details of the structure can not be resolved. Another minor anomaly occurs in the region southwest of the BK room. The attenuation tomogram (Figure 4.28) shows a broad region of moderately high attenuation there and the slowness tomogram (Figure 4.29) shows a broad moderately slow region. However, the seismic tomogram shows no anomalous zone in this region (Figure 4.24). The geologic evidence does not indicate that a major geologic feature occurs there, and it is not clear what the broad anomalies represent. Feature 4 may extend west through this region, but lacks a distinctive tomographic signature if it is present.

4.2.5. Revised Structural Model of the US/BK Site and Hydrologic Implications

The radar and seismic tomograms support the presence and location of the main features in the preliminary model of Figure 4.22. In particular, the anomalies coinciding with the K-lamprophyres and S-zone segments 1a and 1b have similar positions, shapes and orientations in the seismic velocity tomogram (Figures 4.24 and 4.25) and the two radar tomograms (Figures 4.28 and 4.29). This increases our confidence in the utility of tomography in projecting the major geologic features into the target site. Based on the geophysical tomograms, the structural model of the US/BK site was modified to include two northwest-striking lamprophyres in the north-central part of the site (Figure 4.13).

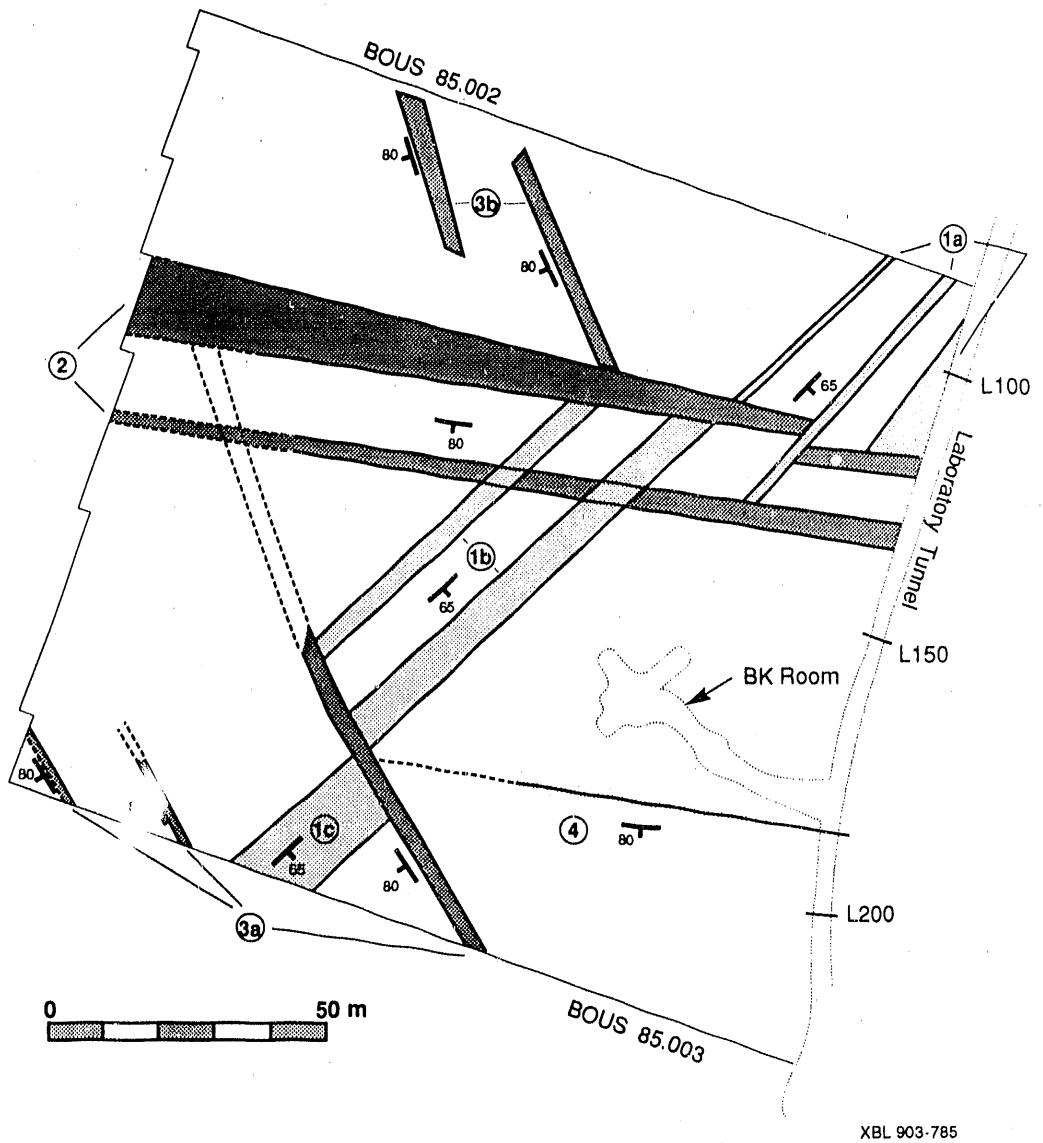

Figure 4.30. Projection in the plane of tomography showing revised model of major geologic structures at the US/BK site. Strike and dip of the major features shown in heavy line. This model includes two lamprophyres near the north (upper) edge of the projection that are not in Figure 4.22. North is to top of page.

We now discuss the hydrologic implications of the model. The results of the subsurface geologic, borehole, and tomographic investigations all indicate that the lamprophyre-bearing K-zone (Feature 2, Figure 4.30) is an especially prominent structure. This feature has nonuniform appearances on both the seismic and radar tomograms, indicating the deformation along this zone is variable within the US/BK site. This is consistent with the complicated appearance of the feature between L112 and L133 in the laboratory tunnel (Figure 4.11). Fracturing and fluid flow along this feature may be quite complex. Because of locally strong fracturing along the K-lamprophyres, they may locally transmit water readily in east-west and vertical directions. We expect that the K-lamprophyres would tend to hydrologically separate the two S-zone segments 1a and 1b. The numerous fractures in the S-zone segments probably form a well connected network. The hydraulic conductivity along these segments probably is high, both along strike and in the vertical direction. The northwest-striking lamprophyres (Features 3a and 3b) probably contain vertical and northwest-trending flow paths. These lamprophyres probably are much thinner and more discontinuous than the K-lamprophyres, and may transmit water across strike more readily especially where intersected by S-zones. The southernmost of these lamprophyres (3a) are interpreted to separate S-zone segments 1b and 1c. The small K-zone (Feature 4) may offer a conduit from the southwest end of Feature 1b towards the laboratory tunnel.

Although the positions of the major structural elements at the US/BK site seem to be fairly well resolved, the nature of the intersections between structures is not well established. For example, although the S-zone appears to consist of discontinuous segments that are separated by lamprophyres, we cannot rule out the possibility that hydraulic connections extend across the lamprophyres where intersected by S-zones. The geophysical tomograms suggest that fracturing may be particularly extensive at such intersections. Hydrologic testing is necessary to firmly establish the nature of the hydraulic connections between the lamprophyres and S-zones.

5.0. BRINE TRACER TESTS AND DIFFERENCE TOMOGRAPHY AT THE US/BK SITE

5.1. Overview

Brine tracers were injected during the second and third phases of the radar tomography surveys (Niva and Olsson, 1988a,b). Difference tomograms (discussed below) allow the brine flow paths to be traced. We have used the difference tomograms to check how well our model (Figure 4.30) identified major flow paths and flow barriers at the US/BK site and to indicate how the model might be improved.

Difference tomograms (Figures 5.1, 5.2, and 5.3) were prepared by inverting travel time- or amplitude-differences between two tomographic surveys. These tomograms show how the region being analyzed changed between test phases. Since the composition and structure of the rock remain constant during the tests, the difference tomograms show the brine and how it migrated in the plane of the tomography. These difference tomograms typically have much better resolution than normal tomograms, because background effects and processing errors are effectively removed. Figure 5.1 was prepared using attenuation data from phases 1 and 2; it shows the flow of brine injected during phase 2. Figure 5.2 was prepared using attenuation data from phases 2 and 3; it shows the flow of brine injected during phase 3. No phase 1-2 radar slowness difference tomogram was available. Figure 5.3 was prepared using slowness data from phases 2 and 3; it shows a rather different picture than Figure 5.2.

5.2 Expected Results of Brine Tracer Tests

The injection points for the tracer tests are nearly in the plane of the tomography and are below and west of the main laboratory tunnel (Figure 4.27). The laboratory tunnel, the BK room, and boreholes BOUS 85.002 and 85.003 were at atmospheric pressure during the injections, and we expect the hydrologic gradient to have been toward these openings. Therefore, we expect

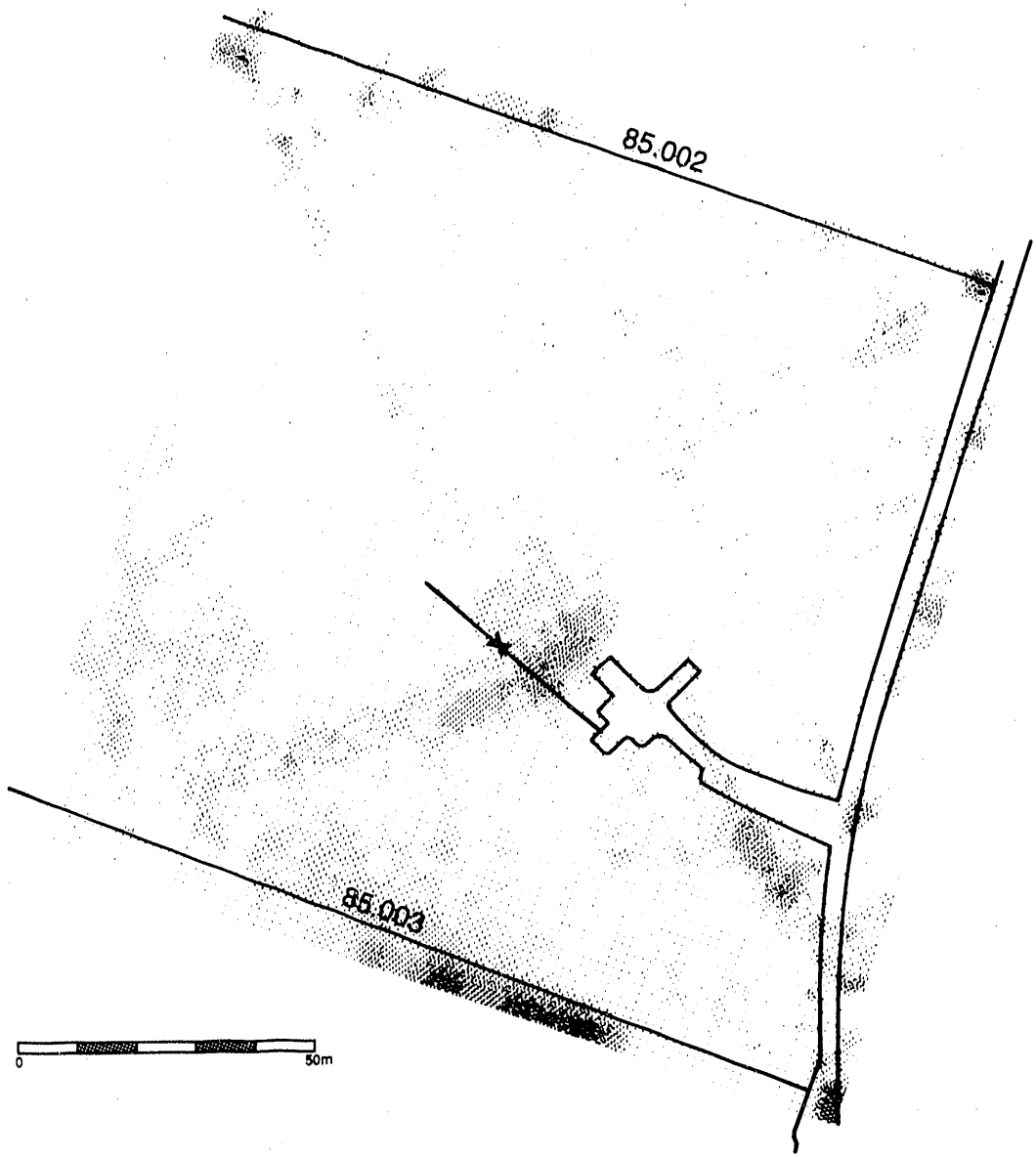

XBL 8912-7902

Figure 5.1. Difference tomogram of radar attenuation structure between BOUS 85.002 and BOUS 85.003 from phase 1 and phase 2 measurements. The tomogram shows the increase in radar attenuation and indicates where brine has migrated during phase 2 (from Niva and Olsson, 1988a, Figure 5.12). Units are in dB/m. North is to top of page.

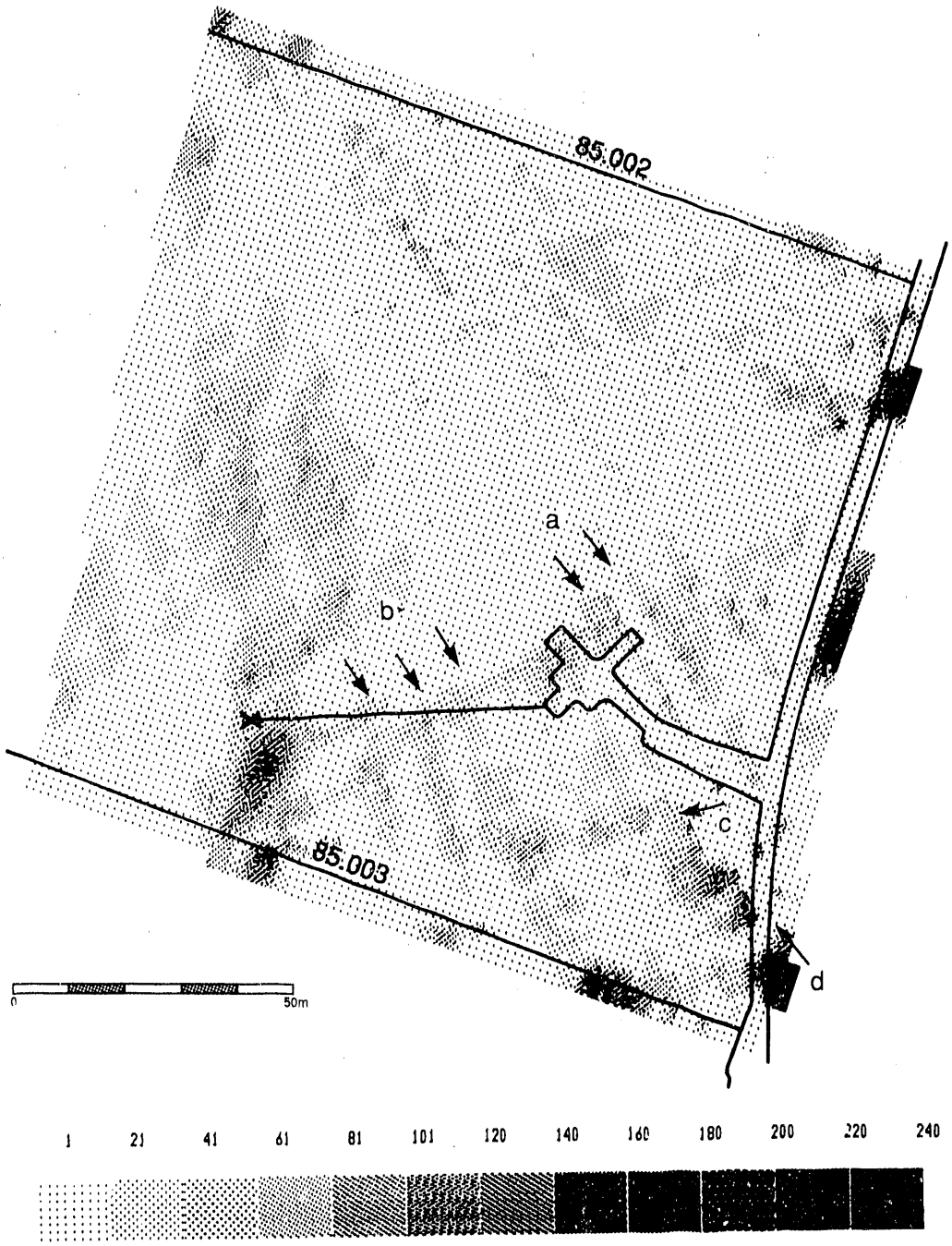

Figure 5.2. Difference tomogram of radar attenuation structure between BOUS 85.002 and BOUS 85.003 from phase 2 and phase 3 measurements. The tomogram shows the increase in radar attenuation and indicates where brine has migrated during phase 3 (from Niva and Olsson, 1988b, Figure 5.26). Units are in dB/m. North is to top of page.

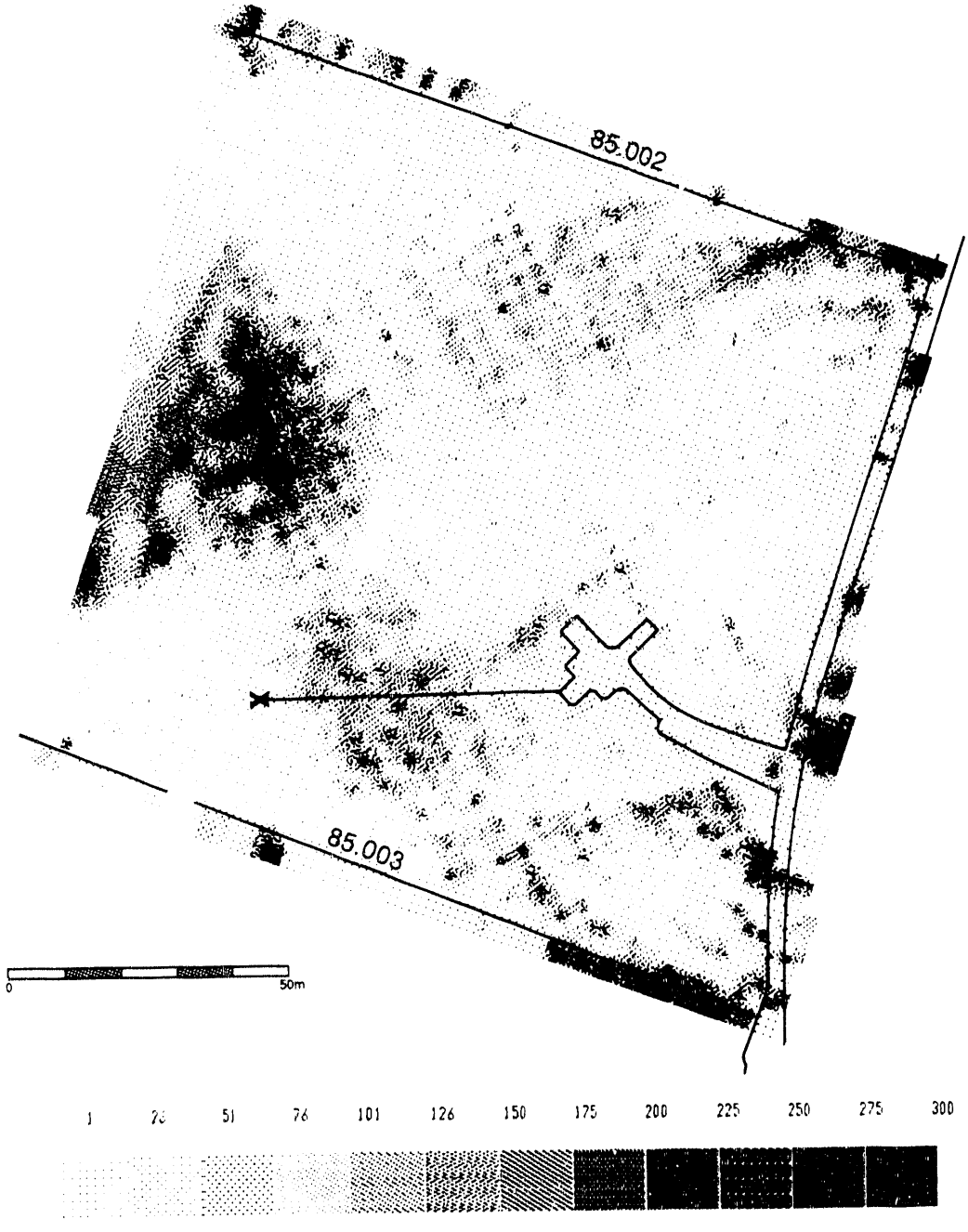

XBL 8912-7904

Figure 5.3. Difference tomogram of radar slowness structure between BOUS 85.002 and BOUS 85.003 from phase 2 and phase 3 measurements (from Niva and Olsson, 1988b, Figure 5.21). Units are in ps/m. North is to top of page.

brine from each test to migrate along major fracture zones identified in our structural model towards the laboratory tunnels and/or these boreholes.

According to our structural model (Figure 4.30), the phase 2 injection point (Figure 4.27) is located near the center of the more southerly S-zone segment (Feature 1b, Figure 4.30). This segment is bounded by lamprophyres about 20 m on either side of the injection point. The S-zone fractures should form a well connected network. We expect that the brine detected in the plane of the tomography would extend northeast and southwest of the injection point towards both sets of lamprophyres. The K-lamprophyres (Feature 2) probably would hydrologically isolate S-zone segments 1a and 1b. Although brine would not be expected to flow northeast of the intersection of the K-lamprophyres with the S-zone, some might flow east along the K-lamprophyres towards the main laboratory tunnel. Brine that flowed southwest along the Feature 1b S-zone might do one of three things once it reached the series of thin lamprophyres (Feature 3a):

(1) flow south across them toward borehole BOUS 85.003;

(2) flow southeast along the lamprophyres towards borehole BOUS 85.003;

(3) flow east along the K-zone south of the BK room (Feature 4).

Because we expect the hydraulic conductivity along the S-zone would be greatest in the vertical direction, the brine might eventually flow out of the gently inclined plane of the tomography.

The phase 3 injection point (Figure 4.27) is located about 25 m north of borehole BOUS 85.003, just south of where the S-zone segment 1b intersects or terminates against the Feature 3a lamprophyres (Figure 4.30). We interpret the injection point as not being in a major geologic or hydrologic feature. We expect that the hydrologic gradient would favor flow toward borehole BOUS 85.003 along one or more of the following paths:

(1) south by way of "background matrix" fractures;

(2) southeast along the lamprophyres;

(3) southeast to Feature 1c and then southwest along it to the borehole.

The last option seems most likely because the hydraulic conductivity along S-zone segment 1c would be highest. Brine is unlikely to flow north across the lamprophyres into Feature 1b against the hydrologic gradient

5.3. Phase 1-2 Difference Tomogram

Two features stand out on the phase 1-2 radar attenuation difference tomogram (Figure 5.1). The first is a northeast-trending feature that extends on either side from the injection point. This anomaly most likely reflects the location of brine, because it is linked to the injection point and it systematically weakens in strength with increasing distance from the injection point. Most if not all of this anomaly should represent the brine injected between phases 1 and 2. The northeast end of this anomaly is well defined and occurs about 20 m northeast of the injection point. This spot coincides with the intersection of Features 2 and 1b in Figure 4.30. The brine apparently did not cross the K-lamprophyres (Feature 2). The anomaly also has a sharp gradient in strength about 20 m southwest of the injection point. This spot coincides with the intersection of Features 1b and 3a in Figure 4.30, and it is along the trend of Feature 4. The gradient in the plume strength may indicate that the northwest-striking lamprophyres of Feature 3a impeded flow of the brine. Anomalies extend southeast and southwest of the intersection of Features 1b and 3a, so some brine may have flowed along the lamprophyres and some may have flowed across them.

The second anomaly on the attenuation difference tomogram (Figure 5.1) strikes northwest beneath the BK room. This anomaly is best displayed just south of the BK room entrance. We assume that this anomaly also represents brine. No feature on the tomogram extends directly from the injection point to the second anomaly, so this anomaly may represent brine that traveled out of the plane of the tomography and collected at a structural step in the K-zone near the entrance to the BK room (Figure 4.30). No major structures are shown in either our structural model (Figure 4.30) or that of NTB 87-14 (Figure 4.6) that would directly link the injection site to that anomaly. We recognize three possible ways that brine may have traveled to a spot just south of the entrance to the BK room. First, the brine may have migrated along a fault and some adjacent fractures that strike northwest through the northern part of the BK room and merge with

the small west-striking K-zone in the eastern part of the room (Figure 4.9). This fault may have been detected by radar reflection measurements (Falk et al., 1988). We did not recognize this fault a potentially being a major hydraulic conductor. A second possible flow path extends north from the south end of Feature 1b along the K-zone of Feature 4. Since the tomogram does not show an anomaly along this path, the flow would occur largely out of the plane of the tomography. A third possibility is that brine either leaked or was dumped from the injection reservoirs in the BK room and seeped into the floor before the phase 2 radar measurements were made.

5.4. Phase 2-3 Difference Tomograms

The second brine injection point is several meters southwest of the inferred intersection of the 3a lamprophyres and the 1b S-zone segment (Figure 4.30). The phase 2-3 radar attenuation difference tomogram (Figure 5.2) shows a pronounced anomaly that extends south-southeast of the injection point towards borehole BOUS 85.003. The anomaly is consistent with the brine flowing along Feature 1c in response to the hydrologic gradient towards the open borehole. The presence of the Feature 3a lamprophyres northeast of the injection point together with the hydrologic gradient towards the hole may have impeded flow to the northeast. The tomogram does not indicate that the brine flowed directly southwest towards the borehole, as would be expected if brine were injected into an along-strike continuation of Feature 1b. The tomogram also shows a series of weak northeast- and northwest-trending features that form a zigzag pattern that extends east from the injection point. This pattern does not seem to reflect flow along the Feature 4 K-zone. The pattern may indicate flow to the east along a network of fractures that do not form a throughgoing fracture zone. The roughly triangular anomaly at the west side of the tomogram probably represents artifacts from the inversion process.

The phase 2-3 slowness difference tomogram (Figure 5.3) looks decidedly different from the phase 2-3 attenuation difference tomogram (Figure 5.2). The most pronounced anomaly on the slowness tomogram is a triangular feature at the west edge of the tomogram. This is a region where the signal ray density is particularly low, and anomalies in this area are regarded as artifacts of the inversion process. This anomaly is much stronger in the slowness difference

tomogram than in the attenuation difference tomogram, indicating that artifacts are more pronounced in the slowness difference tomogram. An anomaly in the north-central part of the slowness difference tomogram (Figure 5.3) may also be an artifact. It is not linked to the injection point and lies north of the Feature 2 K-lamprophyres, which probably have a low across-strike hydraulic conductivity. This anomaly has no counterpart in Figure 5.2. We do not think this anomaly reflects a large amount of brine. The other major anomaly on the slowness difference tomogram (Figure 5.3) occurs east-northeast of the injection point. If this anomaly reflected brine, then we would expect it to be linked to the injection point and to systematically weaken in strength with increasing distance from the injection point. The anomaly does not have these characteristics, and it is not clear that it represents brine. Based on the points cited above, we conclude that the slowness difference tomogram does not reliably indicate the location of brine. Niva et al. (1988, p. 74) also conclude that the slowness difference tomogram is suspect because the pattern of anomalies indicates artifacts are prominent.

5.5. Discussion

The results from the phase 1-2 and phase 2-3 radar attenuation difference tomograms are on the whole consistent with the predictions of our structural model. We interpret the phase 1-2 brine injection to have occurred in a segment of a well-defined northeast-striking S-zone (Feature 1b, Figure 4.30) that is bounded by lamprophyres 20 m from the injection point (Figure 4.27). Most of the brine displayed in the phase 2 radar attenuation difference tomogram appears to be contained within this S-zone segment. We interpret the phase 2-3 brine injection as being outside that fracture zone segment (Figure 4.30). The position and shape of the brine anomaly in the phase 3 radar attenuation difference tomogram (Figure 5.2) indicates the phase 2-3 brine flow was strongly controlled by the hydrologic gradient and Feature 1c. Both radar attenuation difference tomograms are consistent with our interpretation that Feature 1b does not continue on strike to the south across the Feature 3a lamprophyres.

The phase 2-3 radar slowness difference tomogram is not consistent with our model, but we suspect that tomogram does not reflect the flow behavior at the site very well. This may be a

result of the radar signals being more sensitive to the variations in the attenuation properties of the rock/fluid system than the slowness properties. The undifferenced attenuation values range from 5 to 125 dB/100 m, with an average of ~25 dB/100 m, whereas the undifferenced slowness values range from 7850 ps/m to 8850 ps/m, with an average of ~8050 ps/m (Niva and Olsson, 1988b). The maximum differenced attenuation anomalies associated with the brine are 24 dB/100 m; these anomalies are large relative to the average background level of 25 dB/100 m. In contrast, the maximum differenced slowness anomalies associated with the brine are 300 ps/m; those anomalies are small relative to the average background level of 8050 ps/m. respectively. The anomalies are clearly much larger relative to the background values for the attenuation tomograms than the slowness tomograms and may explain why the attenuation tomograms seem to better represent the geologic structure. Although it is unclear from the literature (e.g Sen et al., 1981; Shen et al., 1985) how the introduction of dilute brine changes the radar velocity and radar attenuation characteristics of a water-saturated, low-porosity rock, if the velocity characteristics of brine and water at Grimsel were essentially the same, and if the brine did not invade unsaturated areas, then the anomalies in the phase 2-3 slowness tomogram could very well be artifacts of processing.

There are four places where minor anomalies appear in the radar difference tomograms. All are located in the southeast quadrant of the site. These anomalies do not correspond to throughgoing fracture zones; they all may be artifacts of the inversion process. The first group of anomalies (''a'' on Figure 5.2) occur north of the BK room and trend northwest. These anomalies are not well defined in Figures 5.1 and 5.3. If these anomalies represent real geologic structures, the structures would strike parallel to K-zones and might have carried brine injected prior to the phase 2 measurements southeast below the BK room. Evidence for such structures in the BK room or the laboratory tunnel is lacking.

The second group of anomalies (''b'' on Figure 5.2) occur south of the BK room and would also trend northwest. These anomalies are well defined on Figure 5.2 and poorly defined on Figure 5.1. They may represent a group of thin northwest-striking lamprophyres. One northwest-

striking lamprophyre in that area (Feature 3a, Figure 4.30) had been included in our model based on borehole data; there may actually be more than one.

An anomaly that trends northeast (''c'' on Figure 5.2) occurs south of the BK room in both Figures 5.2 and Figure 5.3. It would extend towards the entrance to the BK room. This anomaly is not defined on Figure 5.1. It is possible that the fractures near the entrance to the BK room (Figure 4.9) which we have interpreted as being in a step along a K-zone (Figure 4.30) could instead be the northeast end of a short S-zone.

A fourth anomaly (''d'' on Figure 5.2) with a north-northwest trend occurs near the laboratory tunnel south of the BK room (Figure 5.1). The position of this anomaly is slightly different in Figures 5.1, 5.2, and 5.3. A single water-bearing joint that strikes north-northwest is exposed in the laboratory tunnel at ~L205 near this anomaly (Figures 4.2 and 4.11). This joint is clearly not a major fracture zone, yet it may have carried enough brine to be detected by the radar differencing technique.

The radar difference tomograms increase our confidence in our interpretation of the geologic structure at the US/BK site. The features which we expected flow along were highlighted, and the features we did not expect flow across seem to have impeded flow. The difference tomograms suggest that not all the hydrologic features at the site are contained in our structural model. If all of the anomalies on the attenuation difference tomograms accurately represent the location of significant amounts of brine, then a detectable portion of flow at the US/BK site is occurring along a network of fractures that that do not form a major throughgoing zone. The distribution of fractures in such a network would not have been identified in our model, which was constructed to identify only the major features, but perhaps should be included in a hydrologic model as ''background matrix'' fractures.

6.0. CONCLUSIONS

The thrust of our effort is to integrate geologic observations and geophysical measurements to identify, locate, and characterize the major geologic structures at a given site. We place a heavy emphasis on the importance of characterizing the fracture zone systematics. This information is particularly important because it helps unite the site-specific geologic mapping, borehole data, and geophysical information and can lend insight into how fluid might flow along the zones. We strongly recommend that detailed mapping be carried out where possible to reveal fracture zone systematics. By resorting to classifying fractures according to their local orientation in a borehole, the systematic structure of a fracture zone tends to be obscured instead of revealed. Maps are perhaps the best vehicle for assembling structural information from fracture zone exposures. This information can subsequently treated statistically if desired. Conversely, it would be difficult if not impossible to reconstruct a map purely from statistical data. A considerable amount of useful information on fracture zone systematics cannot be effectively captured (and may not be collected) without using detailed maps.

The general procedure in our site characterization methodology is to identify and locate major structures that intersect a perimeter around the target site, to project these structures into the site, and to exploit progressively smaller perimeters about the target site as they become available. The process of identifying the major features in the general area of a site first and then focusing in on finer details in smaller areas is a very natural approach, and this aspect of our methodology certainly is not unique. It is much easier to build a site-specific model if a regional model is already in place. The setting of the Grimsel laboratory allowed a regional 3-D model to be developed before rather than during the collection of subsurface information. In many settings the surface exposures would not be as good and regional models would have to be built or substantially modified during the course of the site-specific work. Seismic reflection surveys, vertical

seismic profiling (VSP), and seismic tomography could be used to help build regional models where surface exposures are poor.

For our methodology to work best we need 1) site-specific geologic, borehole, and geophysical data and 2) exposures that allow the systematics of the major fracture zones near the site to be defined. Clearly, these key requirements for our methodology to work were met at Grimsel. A broad multi-disciplinary data base existed when we began our work, and we had ready access to nearly all of it. The general geologic and hydrologic conditions at the site were described in several preliminary site-characterization reports. Regional models of the structure at the laboratory already were prepared. A clean, well-lit, already-mapped tunnel formed part of the perimeter of the site. The key geologic structures there had been identified and located, and they did not have to be projected far into the site. Several boreholes had been logged at the US/BK site and a variety of geophysical tomograms had been prepared. In addition to the studies that had already been conducted, the surface exposures above the Grimsel laboratory and the tunnel exposures in the laboratory are excellent. These exposures not only contributed to the regional modeling but provided a superb opportunity to conduct the detailed mapping we used to characterize the different structures at the laboratory. Finally, the technical staff at NAGRA was very helpful, and this contributed to our effort in no small way.

In many places excellent exposures will not be readily available and it may be extremely difficult (or too expensive) to determine the systematics of the fracture systems. For example, the subsurface fracture systems in many places are not exposed at the surface at all. In such cases, studies of geologically analogous areas may be useful, even if those areas are distant from the target site. Although the features at a given site will be unique to some extent, similar features would probably occur elsewhere. Still, in some locations the fracture systems may be too complex to evaluate their systematics. In cases where the systematics can not be determined, it may be appropriate to consider a number of significantly different geologic models and to treat the fracture systems stochastically.

Some direct sampling of the target site is essential to relate geologic models and tomo-

grams, and small-diameter boreholes are probably the least destructive way to conduct direct sampling. Borehole information at the US/BK site was instrumental in determining that seismic anomaly S1b represented fractured granitic rock and not lamprophyre. Because boreholes sample relatively small volumes, the most reliable information they provide is essentially one-dimensional. Without an advance knowledge of the fracture zone systematics we would have been restricted to using only that one-dimensional component of the borehole data. By using our advance knowledge of the fracture zone systematics we have been able to exploit the 3-D information the boreholes can provide. It would be even more important to exploit that 3-D information at sites where numerous boreholes will not be drilled.

Geophysical tomograms provide a unique way to check geologic models. In places where clusters of boreholes would not be drilled, geophysical tomograms would be relied upon even more heavily than we did here. The usefulness of tomograms is a function of both their resolution and how well the geology is known. Anomalies on tomograms can reflect a wide range of features (different rock types, fractures, zones of hydrothermal alteration, areas of increased porosity, etc.), and an advance knowledge of the geology is essential in order for the anomalies to be interpreted correctly. We have confidence in the positions of the major structures in our US/BK model because their positions are compatible with the different kinds of tomograms and are reasonably consistent with the available geologic information.

Because of differences between the radar and seismic tomograms for the US/BK site we did not try to map details of the internal structure of the major features using the tomograms. There are two main reasons why the details are difficult to interpret and image. First, radar and seismic signals are sensitive to different physical parameters. Radar and seismic tomograms of the same area could be very different. The second problem is one of resolution. Problems of resolution might persist even if the number of source and receiver locations were greatly increased. For example, the large velocity and attenuation contrasts associated with the lamprophyres at the US/BK site dominated the tomograms and obscured other structural details nearby. This effect was aggravated by the tomography boreholes trending parallel to the strike of the lamprophyres.

At present the most practical method to infer details within a fracture zone without drilling into it might be to use geologic information on the relationship between the internal and external structure of a zone. Detailed mapping coupled with mechanical analyses of how key structures developed would aid in doing this. For example, it might be possible to infer whether Alpine tension fissures at Grimsel are likely to be particularly numerous where lamprophyres are closely spaced. Laboratory and small-scale field research that addressed the geophysical signature of well-defined geologic structures would also increase the usefulness of the tomograms.

Judging by the processed tomograms, the seismic velocity tomography appears to delineate the major geologic structures at this site better than the radar attenuation and radar slowness tomography. The radar attenuation difference tomograms used in conjunction with the brine tracer tests seem to be a very effective way to portray fluid flow paths. Implementing three-dimensional tomography or two-dimensional tomography for multiple planes would be a useful next step to increase the geophysical contribution.

The needs of hydrologists motivated us to develop a modeling methodology for locating the major fracture zones at a target site. Those zones may not be the only important hydrologic features at a site; minor geologic structures and the rock matrix may be important also. The nature of the hydrologic connections between conductors may be a critical feature that geologic/geophysical studies are unlikely to define sufficiently well. In many places intersections will be areas of markedly increased hydraulic conductivity; in fact they surely are the most important hydrologic features in some areas. In general, however, fracture zone intersections are likely to be quite complicated features with poor natural exposures, and a clear hydrologic interpretation of them cannot be expected based on the geology alone. The intersections of the S-zones with lamprophyres at the US/BK site is a case in point. Hydrologic field data must be collected to translate a structural model into a hydrologic model.

We close with two general comments. First, there will inevitably be surprises in the course of a site characterization. Reconnaissance studies present the first opportunity to bring important yet previously unforeseen features into the modeling process. With regard to the logging of tun-

nels and boreholes, it seems far too easy for valuable logging observations made early in a project to either be left unrecorded (the form lacks a needed box to check, a feature can't be described well on the form, etc.) or to be buried amidst other data. Furthermore, many tunnels and boreholes might have to be cased for engineering reasons and key exposures could be lost before their significance is realized. Those who collect the initial field data should be encouraged to clearly highlight particularly interesting, important, or unusual features. Regular discussions involving all the different groups making the field observations and conducting the modeling would increase the likelihood that important "surprise" features are recognized and brought into the characterization process early on. Second, it is essential that the geologists and geophysicists be able to work together well if a multi-disciplinary is to be productive. An effective multi-disciplinary approach should cause a particularly large number of useful (and initially unforeseen) to arise in the course of the work; this is a key strength of such an approach. To exploit this advantage, we strongly recommend that those modeling a site personally visit the site, have access to all the original raw data, and be able to collect new data through the course of an investigation.

7.0. REFERENCES

Aydin, A., and Johnson, A. M., 1978. Development of faults as zones of deformation bands and as slip surfaces in sandstone, *Pure and Applied Geophysics, 116*, 931-942.

Berthé, D., Choukrone, P. and Jegouzo, P., 1979. Orthogneiss, mylonite, and non coaxial deformation of granites: the example of the South American shear zone, *Journal of Structural Geology, 1*, 31-42.

Billaux, D., Chiles, J. P., Hestir, K., and Long, J., 1989. Three-dimensional statistical modelling of a fractured rock mass-- an example form the Fanay-Augeres mine, *International Journal of Rock Mechanics and Mining Sciences and Geomechanics Abstracts, 26*, 281-299.

Bräuer, V., Kilger, B., and Pahl, A., 1989. Ingenieurgeologicshe Untersuchungen zur Interpretation von Gebirgsspannungsmessungen und Durchstroemungsversuchen, NAGRA Technical Report 88-37, 53 p.

Choukrone, P., and Gapais, D., 1983. Strain pattern in the Aar Granite (central Alps): Orthogneiss developed by bulk inhomogeneous flattening, *Journal of Structural Geology, 5*, 411-418.

Daley, T. M., McEvilly, T. V., and Majer, E. L., 1988. Multiply polarized shear-wave VSP's from the Cajon Pass drill-hole, *Geophysical Research Letters, 15*, 1001-1004.

Delany, P. T., and Pollard, D. D., 1981. Deformation of host rocks and flow of magma during growth of minette dikes and breccia-bearing intrusions near Ship Rock, U.S. Geological Survey Professional Paper 1202, 61 p.

Dershowitz, W., 1984. Rock joint systems: Ph.D. Thesis. Massachusetts Institute of Technology, Cambridge, Massachusetts.

Donath, F. A., 1961. Experimental study of shear failure in anisotropic rocks, *Geological Society of America Bulletin, 72*, 985-990.

Dyer, J. R., 1983. Jointing in sandstones, Arches National Park, Utah. Ph.D. Thesis, Stanford University, Stanford, California, 202 p.

Falk, L., Magnusson, K.-Å., Olsson, O., Amman, M., Keusen, H.R., Sattel, G., 1988, Analysis of radar measurements performed at the Grimsel Rock Laboratory in October 1985: NAGRA Technical Report 87-13.

Frick, U., Baertschi, P., and Hoehn, E., 1988, Migration Investigations, in Güntensperger, M., ed., NAGRA Bulletin 1988, 23-34.

Gelbke, C., 1988. Seismische durchschallungstomographie, NAGRA Technical Report 88-06.

Howard, J. H., and Nolen-Hoeksema, R.C., 1990. Description of natural fracture systems for quantitative use . petroleum geology, *American Association of Petroleum Geologists Bulletin, 74*, 151-162.

Ingraffea, A. R., 1981. Mixed-mode fracture initiation in Indiana limestone and Westerly granite, U. S. Symposium on Rock Mechanics, 22nd, Massachusetts Institute of Technology, Proceedings, 186-191.

Lawn, B. R., and Wilshaw, T. R., 1975. *Fracture of Brittle Solids*, New York, Cambridge University Press, 204 p.

Long, J. C. S., Remer, J. S., Wilson, C. R., and Witherspoon, P. A., 1982. Porous media equivalents for networks of discontinuous fractures, *Water Resources Research, 18,* 645-658.

Long, J. C. S., and Billaux, D., 1987. From field data to fracture network modeling: An example incorporating spatial structure, *Water Resources Research, 23,* 1201-1216.

Long, J. C. S., Hestir, K., Karasaki, K., Davey, A., Peterson, J., Kemeny, J., and Landsfeld, M., 1989. Fluid flow in fractured rock: Theory and application, Lawrence Berkeley Laboratory Report No. LBL-27879, 37 p.

Martel, S. J., Pollard, D. D., and Segall, P., 1988. Development of simple strike-slip fault zones in granitic rock, Mount Abbot quadrangle, Sierra Nevada, California, *Geological Society of America Bulletin, 100,* 1451-1465.

Martel, S. J., and Peterson, J. E. Jr., 1989. Fracture-zone structure at the US/BK site, Grimsel Rock Laboratory, Switzerland, Earth Sciences Division Annual Report, Lawrence Berkeley Laboratory Report No. LBL-26362, 89-92.

Martel, S. J., 1990. Formation of compound strike-slip fault zones, Mount Abbot quadrangle, Sierra Nevada, California, *Journal of Structural Geology* (in press).

Muehlberger, W. R., 1986. Different slip senses of major faults during different orogenies: The rule?, in Proceedings, International Conference on Basement Tectonics, 6th, Sante Fe, September, 1985, Salt lake City, Utah, International Basement Tectonics Association, p. 76-81.

NAGRA Technical Report 81-07, Sondierbohrungen Juchlistock-Grimsel, Baden.

NAGRA Technical Report 85-46, Grimsel Test Site: Overview and test programs, Baden, 118 p.

NAGRA Technical Report 87-14, Keusen H. R., Ganguin, J., Schuler, P., and Buletti, M., 1989, Felslabor Grimsel: Geologie, Baden, 120 p.

Niva, B., Olsson, O., 1987. Radar crosshole tomography results form phase 1, NAGRA Internal Report 88-30.

Niva, B., Olsson, O., 1988a. Radar crosshole tomography results form phase 2, NAGRA Internal Report 88-31.

Niva, B., Olsson, O., 1988b. Radar crosshole tomography results form phase 3, NAGRA Internal Report 88-57.

Niva, B., Olsson, O., and Blümling, P., 1988. Radar crosshole tomography with application to migration of saline through fracture zones, NAGRA Technical Report 88-31, 87 p.

Olson, J., and Pollard, D.D., 1989. Inferring paleostresses from natural fracture patterns: A new method, *Geology, 17,* 345-348.

Olsson, O., Falk, L., Forslund, O., Lundmark, L., and Sandberg, E., 1987. Crosshole Investigations - results from borehole radar investigations, SKB Technical Report 87-11, Stockholm, Sweden.

Olsson, O., Black, J. H., Gale, J. E., and Holmes, D.C., 1988. Site Characterization and validation, stage 2 - preliminary predictions, Swedish Geological Company Report ID No. 88.

Peng, S., and Johnson, A. M., 1972. Crack growth and faulting in cylindrical specimens of Chelmsford Granite, *International Journal of Rock Mechanics and Mining Science and Geomechanics Abstracts, 9,* 37-86.

Peterson, J. E. Jr., 1986. Application of algebraic reconstruction techniques to geophysical problems, Ph.D. Thesis, University of California, Berkeley, 188 p.

Pollard, D.D., and Segall, P., 1987. Theoretical displacements and stresses near fractures in rock: with applications to faults, joints, veins, dikes, and solution surfaces, in Atkinson, B.K., ed.,

Fracture Mechanics of Rock, Academic Press, New York, p. 277-349.

Ramsay, J., 1967. *Folding and Fracturing of Rocks*, McGraw Hill, New York, New York, 568 p.

Rouleau, A., and Gale, J. E., 1985. Characterization of the fracture system at Stripa with emphasis on the ventilation drift, Lawrence Berkeley Laboratory Report No. LBL-14875, 115 p.

Robinson, P. C., 1984. Connectivity, flow, and transport in network models of fracture media, Ph.D. Thesis, St. Catherine's College, Oxford.

Schoenberg, M., 1980. Elastic wave behavior across linear slip interfaces: *Journal of the Acoustical Society of America, 68*, 1516-1521.

Schoenberg, M., 1983. Reflection of elastic waves from periodically stratified media with interfacial slip, *Geophysical Prospecting, 31*, 265-292.

Segall, P., and Pollard, D. D., 1983a. Joint formation in granitic rock of the Sierra Nevada, *Geological Society of America Bulletin, 94*, 563-575.

Segall, P., and Pollard, D. D., 1983b. Nucleation and growth of strike slip faults in granite, *Journal of Geophysical Research, 88*, 555-568.

Segall, P., and Simpson, C., 1986. Nucleation of ductile shear zones on dilatant fractures, *Geology, 14*, 56-59.

Sen, P.N., Scala, C., and Cohen, M.H., A self-similar model for sedimentary rocks with its application to the dielectric constant of fused glass beads, *Geophysics, 46*, 781-789.

Shen, L.C., Savre, W.C., Price, M.J, and Athauale, K., Dielectric properties of reservoir rocks at ultra-high frequencies, *Geophysics, 50*, 692-704.

Sibson, R. H., 1977. Fault rocks and fault mechanisms, *Journal of the Geological Society of London, 133*, 191-213.

Sibson, R. H., 1981. Fluid flow accompanying faulting: field evidence and models, **in** Simpson, D. W., and Richards, P. G., eds., *Earthquake Prediction: An International Review, 4*, 593-603, American Geophysical Union, Maurice Ewing Series.

Sibson, R. H., 1986a, Brecciation processes in fault zones: Inferences from earthquake rupturing, *Pure and Applied Geophysics, 124*.

Sibson, R. H., 1986b. Earthquakes and rock deformation in crustal fault zones, *Annual Reviews of Earth and Planetary Science, 14*, 149-175.

Smith, R. B., 1975. Unified theory of folding, boudinage, and mullion structure, *Geological Society of America Bulletin, 86*, 1601-1609.

Smith, R. B., 1977. Formation of folds, boudinage, and mullions in non-Newtonian materials, *Geological Society of America Bulletin, 88*, 312-320.

Stewart, R. R., Turpening, R. M., and Toksoz, M. N., 1981. Study of a subsurface fracture zone by vertical seismic profiling, *Geophysical Research Letters, 8*, 1132-1135.

Swanson, M. T., 1988. Pseudotachylyte-bearing strike-slip duplex structures in the Fort Foster Brittle Zone, S. Maine, *Journal of Structural Geology, 10*, 813-828.

Sylvester, A. G., 1988. Strike-slip faults, *Geological Society of America Bulletin, 100*, 1666-1703.

Telford, W. M., Geldart, L. P., Sheriff, R. E., and Keys, D. A., 1976. *Applied Geophysics*, Cambridge University Press, Cambridge, 860 p.

Terzaghi, R. D., 1965. Sources of error in joint surveys, *Geotechnique, 15*, 287-304.

Wallace, R. E., and Morris, H. T., 1986. Characteristics of faults and shear zones in deep mines, *Pure and Applied Geophysics, 124*, 107-125.

APPENDIX

BOUS 85.001

Depth in borehole	Mine Coordinates x	y	z	Comment	Strike of Feature	Dip of Feature	Coordinates of Projection Normal to strike at 1730 level x	y	z
13.1	667488.6	159361.5	1724.7	Lamprophyre	100.0	80.0	667488.7	159362.4	1730.0
13.4	667488.3	159361.5	1724.7	Same as above	100.0	80.0	667488.5	159362.5	1730.0
18.8	667483.4	159363.3	1723.2	Kakirite??	50.0	65.0	667481.4	159365.8	1730.0
19.6	667482.7	159363.6	1723.0	Same as above	50.0	65.0	667480.6	159366.1	1730.0
41.4	667462.9	159370.8	1717.4	Lamprophyre	100.0	80.0	667463.3	159373.0	1730.0
74.2	667433.1	159381.6	1708.9	Bleached core	50.0	65.0	667426.8	159389.2	1730.0
76.0	667431.5	159382.2	1708.4	Same as above	50.0	65.0	667425.0	159389.9	1730.0
78.5	667429.2	159383.1	1707.8	White, fractured	50.0	65.0	667422.6	159391.0	1730.0
79.0	667428.8	159383.2	1707.7	Same as above	50.0	65.0	667422.1	159391.2	1730.0
129.0	667383.4	159399.7	1694.7	Small cavity?	50.0	65.0	667372.8	159412.3	1730.0

BOUS 85.002

Depth in borehole	Mine Coordinates x	y	z	Comment	Strike of Feature	Dip of Feature	Coordinates of Projection Normal to strike at 1730 level x	y	z
3.0	667479.3	159288.7	1728.6	L76 zone	50.0	65.0	667478.8	159289.3	1730.0
5.0	667477.4	159289.4	1728.0	Same as above	50.0	65.0	667476.8	159290.1	1730.0
5.0	667477.4	159289.4	1723.0	Lamp + qtz	50.0	65.0	667476.8	159290.1	1730.0
6.7	667475.9	159290.0	1727.6	Same as above	50.0	65.0	667475.2	159290.8	1730.0
14.8	667468.5	159292.7	1725.5	A few fractures	50.0	65.0	667467.2	159294.3	1730.0
15.3	667468.1	159292.8	1725.4	Same as above	50.0	65.0	667466.7	159294.5	1730.0
55.5	667431.6	159306.1	1715.0	Qtz + fractures	50.0	65.0	667427.1	159311.5	1730.0
55.8	667431.3	159306.2	1714.9	Same as above	50.0	65.0	667426.8	159311.6	1730.0
56.2	667430.9	159306.3	1714.8	Qtz + fractures	50.0	65.0	667426.4	159311.8	1730.0
56.8	667430.4	159306.5	1714.6	Same as above	50.0	65.0	667425.8	159312.0	1730.0
68.0	667420.2	159310.2	1711.7	A few fractures	50.0	65.0	667414.8	159316.8	1730.0
68.5	667419.8	159310.4	1711.6	Dark core + frax	50.0	65.0	667414.3	159317.0	1730.0
69.2	667419.1	159310.6	1711.4	Same as above	50.0	65.0	667413.6	159317.3	1730.0
77.3	667411.8	159313.3	1709.3	A few fractures	50.0	65.0	667405.6	159320.7	1730.0
79.4	667409.9	159314.0	1708.8	Lamp/bleached	100.0	80.0	667410.5	159317.7	1730.0
86.2	667403.7	159316.2	1707.0	Same as above	100.0	80.0	667404.4	159320.2	1730.0
93.9	667396.7	159318.8	1705.0	Dark core + frax	160.0	80.0	667400.9	159320.3	1730.0
95.3	667395.4	159319.3	1704.7	Same as above	160.0	80.0	667399.6	159320.8	1730.0
112.4	667379.9	159324.9	1700.2	Fissure	50.0	65.0	667371.0	159335.5	1730.0
142.0	667353.1	159334.7	1692.6	Fractures	50.0	65.0	667341.8	159348.0	1730.0
147.0	667348.5	159336.3	1691.3	Same as above	50.0	65.0	667336.9	159350.2	1730.0

BOUS 85.003

Depth in Borehole	Mine Coordinates x	y	z	Comment	Strike of Feature	Dip of Feature	Coordinates of Projection Normal to Strike at 1730 level x	y	z
8.5	667441.7	159149.4	1728.4	Mylonite on log	50.0	65.0	667441.2	159149.9	1730.0
9.0	667441.2	159149.5	1728.3	Same as above	50.0	65.0	667440.7	159150.1	1730.0
19.4	667431.8	159153.0	1725.6	Bleached	50.0	65.0	667430.5	159154.5	1730.0
20.5	667430.8	159153.3	1725.3	Same as above	50.0	65.0	667429.4	159155.0	1730.0
61.6	667393.5	159166.9	1714.6	Lamprophyre	100.0	80.0	667394.0	159169.6	1730.0
64.0	667391.3	159167.7	1714.0	Same as above	100.0	80.0	667391.8	159170.5	1730.0
64.6	667390.8	159167.9	1713.9	Lamprophyre	100.0	80.0	667391.3	159170.7	1730.0
91.0	667366.8	159176.6	1707.0	Kakirite on log	50.0	65.0	667359.9	159184.8	1730.0
93.8	667364.3	159177.5	1706.3	Fractures	50.0	65.0	667357.2	159186.0	1730.0
95.9	667362.4	159178.2	1705.8	Same as above	50.0	65.0	667355.1	159186.9	1730.0
99.0	667359.6	159179.3	1705.0	Fractures	50.0	65.0	667352.0	159188.2	1730.0
104.3	667354.7	159181.0	1703.6	Same as abc e	50.0	65.0	667346.8	159190.4	1730.0
104.3	667354.7	159181.0	1703.6	Kakirite on log	50.0	65.0	667346.8	159190.4	1730.0
105.0	667354.1	159181.2	1703.4	Same as above	50.0	65.0	667346.1	159190.7	1730.0
105.6	667353.6	159181.4	1703.2	Lamprophyre	100.0	80.0	667354.4	159186.1	1730.0
109.6	667349.9	159182.8	1702.2	Same as above	100.0	80.0	667350.8	159187.6	1730.0
115.2	667344.8	159184.6	1700.8	Lamprophyre	150.0	80.0	667349.3	159187.2	1730.0
115.9	667344.2	159184.8	1700.6	Same as above	150.0	80.0	667348.7	159187.4	1730.0
137.6	667324.5	159192.0	1695.0	Lamprophyre	150.0	80.0	667329.9	159195.1	1730.0
138.9	667323.3	159192.4	1694.6	Same as above	150.0	80.0	667328.7	159195.6	1730.0
148.0	667315.1	159195.4	1692.3	Highly fractured	50.0	65.0	667303.8	159208.9	1730.0
148.5	667314.6	159195.6	1692.1	Same as above	50.0	65.0	667303.3	159209.1	1730.0

BOUS 85.004

Depth in Borehole	Mine Coordinates x	y	z	Comment	Strike of Feature	Dip of Feature	Coordinates of Projection Normal to Strike at 1730 level x	y	z
0.6	667413.7	159223.0	1729.8	Fractures	50.0	65.0	667413.6	159223.1	1730.0
0.7	667413.6	159223.1	1729.8	Same as above	50.0	65.0	667413.5	159223.1	1730.0
20.5	667401.4	159233.7	1718.4	Fractures	50.0	65.0	667397.9	159237.8	1730.0
21.0	667401.1	159234.0	1718.1	Same as above	50.0	65.0	667397.5	159238.2	1730.0
22.0	667400.4	159234.5	1717.6	Many fractures	50.0	65.0	667396.7	159238.9	1730.0
23.6	667399.4	159235.4	1716.6	Same as above	50.0	65.0	667395.4	159240.1	1730.0
24.6	667398.8	159235.9	1716.1	Fractures	50.0	65.0	667394.7	159240.9	1730.0
25.0	667398.6	159236.1	1715.8	Same as above	50.0	65.0	667394.3	159241.2	1730.0
25.7	667398.2	159236.5	1715.4	Fractures	50.0	65.0	667393.8	159241.7	1730.0
36.9	667391.2	159242.5	1709.0	Many fractures	50.0	65.0	667384.9	159250.0	1730.0
38.1	667390.5	159243.2	1708.3	Same as above	50.0	65.0	667384.0	159250.9	1730.0
39.6	667389.6	159244.0	1707.5	Fractures	50.0	65.0	667382.8	159252.0	1730.0
40.3	667389.1	159244.3	1707.1	Same as above	50.0	65.0	667382.2	159252.5	1730.0
48.6	667384.0	159248.8	1702.3	Fractures	50.0	65.0	667375.7	159258.7	1730.0
49.0	667383.7	159249.0	1702.1	Same as above	50.0	65.0	667375.4	159259.0	1730.0

BOUS 85.005

Depth in Borehole	Mine Coordinates x	y	z	Comment	Strike of Feature	Dip of Feature	Coordinates of Projection Normal to Strike at 1730 level x	y	z
0.0	667415.3	159215.0	1730.2	Frax on logs, not	50.0	65.0	667415.4	159214.9	1730.0
5.0	667412.2	159217.7	1727.3	many on photos	50.0	65.0	667411.4	159218.6	1730.0
17.2	667404.7	159224.2	1720.3	Fractures	50.0	65.0	667401.8	159227.7	1730.0
19.4	667403.3	159225.4	1719.0	Same as above	50.0	65.0	667400.1	159229.3	1730.0
23.1	667401.1	159227.4	1716.9	Fractures	50.0	65.0	667397.1	159232.1	1730.0
23.5	667400.8	159227.6	1716.7	Same as above	50.0	65.0	667396.8	159232.4	1730.0
30.5	667396.5	159231.4	1712.7	Fractures	50.0	65.0	667391.3	159237.6	1730.0
30.6	667396.4	159231.4	1712.6	Same as above	50.0	65.0	667391.2	159237.6	1730.0
32.5	667395.2	159232.4	1711.5	Fractures	50.0	65.0	667389.7	159239.0	1730.0
32.6	667395.2	159232.5	1711.5	Same as above	50.0	65.0	667389.6	159239.1	1730.0
38.2	667391.7	159235.5	1708.2	Fractures	50.0	65.0	667385.2	159243.3	1730.0
38.6	667391.5	159235.7	1708.0	Same as above	50.0	65.0	667384.9	159243.6	1730.0

BOUS 85.006

Depth in Borehole	Mine Coordinates x	y	z	Comment	Strike of Feature	Dip of Feature	Coordinates of Projection Normal to Strike at 1730 level x	y	z
21.8	667411.9	159231.2	1717.6	Fractures	50.0	65.0	667408.2	159235.6	1730.0
22.0	667411.8	159231.3	1717.5	Same as above	50.0	65.0	667408.1	159235.7	1730.0
28.6	667407.7	159234.8	1713.7	Many fractures	50.0	65.0	667402.9	159240.6	1730.0
33.7	667404.6	159237.6	1710.8	Same as above	50.0	65.0	667398.8	159244.4	1730.0
34.7	667404.0	159238.1	1710.2	Fractures	50.0	65.0	667398.0	159245.2	1730.0
35.1	667403.7	159238.3	1710.0	Same as above	50.0	65.0	667397.7	159245.5	1730.0
35.8	667403.3	159238.7	1709.6	Fractures	50.0	65.0	667397.2	159246.0	1730.0
36.1	667403.1	159238.9	1709.4	Same as above	50.0	65.0	667396.9	159246.2	1730.0
36.7	667402.7	159239.2	1709.1	Fractures	50.0	65.0	667396.5	159246.6	1730.0
36.9	667402.6	159239.3	1709.0	Same as above	50.0	65.0	667396.3	159246.8	1730.0
37.3	667402.4	159239.5	1708.8	Fractures	50.0	65.0	667396.0	159247.1	1730.0
37.4	667402.3	159239.5	1708.7	Same as above	50.0	65.0	667395.9	159247.2	1730.0

BOUS 85.007

Depth in Borehole	Mine Coordinates x	y	z	Comment	Strike of Feature	Dip of Feature	Coordinates of Projection Normal to Strike at 1730 level x	y	z
0.2	667415.5	159221.5	1729.6	Core is broken	50.0	65.0	667415.3	159221.6	1730.0
0.3	667415.4	159221.5	1729.5	Same as above	50.0	65.0	667415.3	159221.7	1730.0
33.0	667403.1	159232.2	1701.2	Many fractures	50.0	65.0	667394.4	159242.5	1730.0
34.4	667402.5	159232.7	1700.0	Same as above	50.0	65.0	667393.6	159243.4	1730.0
47.5	667397.6	159237.0	1688.7	Fractures	50.0	65.0	667385.2	159251.8	1730.0
48.3	667397.3	159237.3	1688.0	Same as above	50.0	65.0	667384.7	159252.3	1730.0

BOUS 85.008

Depth in Borehole	Mine Coordinates x	y	z	Comment	Strike of Feature	Dip of Feature	Coordinates of Projection Normal to Strike at 1730 level x	y	z
12.1	667427.1	159231.6	1723.2	Frax along core	50.0	65.0	667425.0	15923[illegible].1	1730.0
12.4	667427.1	159231.9	1723.0	Same as above	50.0	65.0	667425.0	159234.4	1730.0
27.3	667426.2	159244.1	1714.4	Fractures	50.0	65.0	667421.6	159249.6	1730.0
27.9	667426.2	159244.6	1714.1	Same as above	50.0	65.0	667421.4	159250.2	1730.0
30.1	667426.1	159246.4	1712.8	Lamprophyre	100.0	80.0	667426.6	159249.3	1730.0
33.0	667425.9	159248.7	1711.2	Same as above	100.0	80.0	667426.5	159252.0	1730.0
33.0	667425.9	159248.7	1711.2	Fractures	50.0	65.0	667420.3	159255.5	1730.0
33.7	667425.9	159249.3	1710.8	Same as above	50.0	65.0	667420.1	159256.2	1730.0
35.5	667425.8	159250.7	1709.8	Many fractures	50.0	65.0	667419.7	159258.0	1730.0
36.1	667425.7	159251.3	1709.4	Same as above	50.0	65.0	667419.5	159258.6	1730.0
36.4	667425.7	159251.5	1709.2	Many fractures	50.0	65.0	667419.5	159258.9	1730.0
37.1	667425.7	159252.1	1708.8	Same as above	50.0	65.0	667419.3	159259.6	1730.0
37.1	667425.7	159252.1	1708.8	Fractures	50.0	65.0	667419.3	159259.6	1730.0
39.7	667425.5	159254.2	1707.3	Same as above	50.0	65.0	667418.7	159262.3	1730.0
39.7	667425.5	159254.2	1707.3	Lamprophyre	100.0	80.0	667426.2	159258.1	1730.0
40.4	667425.5	159254.8	1706.9	Same as above	100.0	80.0	667426.2	159258.8	1730.0
45.9	667425.2	159259.3	1703.8	Broken core	50.0	65.0	667417.3	159268.6	1730.0
46.0	667425.2	159259.3	1703.7	Same as above	50.0	65.0	667417.3	159268.7	1730.0
47.3	667425.1	159260.4	1703.0	Broken core	50.0	65.0	667417.0	159270.1	1730.0

BOUS 85.009

Depth in Borehole	Mine Coordinates x	y	z	Comment	Strike of Feature	Dip of Feature	Coordinates of Projection Normal to Strike at 1730 level x	y	z
0.0	667414.0	159209.6	1730.2	Core loss	50.0	65.0	667414.1	159209.5	1730.0
0.4	667413.8	159209.8	1729.9	Same as above	50.0	65.0	657413.7	159209.8	1730.0
0.4	667413.8	159209.8	1729.9	Many fractures	50.0	65.0	667413.7	159209.8	1730.0
0.8	667413.5	159210.0	1729.7	Same as above	50.0	65.0	667413.4	159210.1	1730.0
22.6	667400.0	159221.7	1717.2	Frac in foliation	50.0	65.0	667396.2	159226.3	1730.0
27.8	667396.9	159224.5	1714.2	Fractures	50.0	65.0	667392.1	159230.1	1730.0
27.9	667396.8	159224.6	1714.1	Same as above	50.0	65.0	667392.0	159230.2	1730.0
32.4	667394.0	159227.0	1711.6	Bleached core	50.0	65.0	667388.5	159233.6	1730.0
33.6	667393.2	159227.6	1710.9	Same as above	50.0	65.0	667387.5	159234.4	1730.0
37.5	667390.8	159229.7	1708.6	Many fractures	50.0	65.0	667384.4	159237.3	1730.0
38.5	667390.2	159230.3	1708.1	Same as above	50.0	65.0	667383.6	159238.1	1730.0
43.4	667387.2	159232.9	1705.3	Fractures	50.0	65.0	667379.8	159241.7	1730.0
43.9	667386.9	159233.1	1705.0	Same as above	50.0	65.0	667379.4	159242.1	1730.0
45.9	667385.6	159234.2	1703.8	Frax, core loss	50.0	65.0	667377.8	159243.6	1730.0
46.4	667385.3	159234.5	1703.5	Same as above	50.0	65.0	667377.4	159243.9	1730.0
47.1	667384.9	159234.9	1703.1	Fractures	50.0	65.0	667376.8	159244.5	1730.0
47.2	667384.8	159234.9	1703.1	Same as above	50.0	65.0	667376.8	159244.5	1730.0
48.0	667384.3	159235.4	1702.6	Fractures	50.0	65.0	667376.1	159245.1	1730.0
48.1	667384.3	159235.4	1702.6	Same as above	50.0	65.0	667376.1	159245.2	1730.0
49.0	667383.7	159235.9	1702.0	Fractures	50.0	65.0	667375.3	159245.9	1730.0
49.5	667383.4	159236.2	1701.8	Same as above	50.0	65.0	667375.0	159246.3	1730.0

BOUS 85.010

Depth in Borehole	Mine Coordinates x	y	z	Comment	Strike of Feature	Dip of Feature	Coordinates of Projection Normal to Strike at 1730 level x	y	z
3.4	667431.0	159224.8	1728.1	Fractures	50.0	65.0	667430.5	159225.5	1730.0
3.7	667431.2	159225.0	1728.0	Same as above	50.0	65.0	667430.6	159225.7	1730.0
14.8	667437.2	159231.8	1721.6	Fractures	50.0	65.0	667434.7	159234.8	1730.0
15.0	667437.3	159232.0	1721.5	Same as above	50.0	65.0	667434.7	159235.0	1730.0
19.1	667439.5	159234.5	1719.1	Fractures	50.0	65.0	667436.2	159238.4	1730.0
19.2	667439.5	159234.6	1719.1	Same as above	50.0	65.0	667436.3	159238.5	1730.0
20.2	667440.1	159235.2	1718.5	Fractures	50.0	65.0	667436.6	159239.3	1730.0
20.9	667440.5	159235.6	1718.1	Same as above	50.0	65.0	667436.9	159239.9	1730.0
21.3	667440.7	159235.9	1717.9	Fractures	50.0	65.0	667437.0	159240.2	1730.0
22.0	667441.0	159236.3	1717.5	Same as above	50.0	65.0	667437.3	159240.8	1730.0
30.5	667445.6	159241.5	1712.6	Lamp+qtz+myl?	100.0	80.0	667446.1	159244.6	1730.0
36.4	667448.8	159245.2	1709.2	Same as above	100.0	80.0	667449.4	159248.8	1730.0
38.5	667449.9	159246.5	1708.0	Fractures	50.0	65.0	667443.3	159254.4	1730.0
39.7	667450.6	159247.2	1707.3	Same as above	50.0	65.0	667443.8	159255.3	1730.0
39.7	667450.6	159247.2	1707.3	Many fractures	50.0	65.0	667443.8	159255.3	1730.0
40.7	667451.1	159247.9	1706.7	Same as above	50.0	65.0	667444.1	159256.2	1730.0

BOUS 85.011

Depth in Borehole	Mine Coordinates x	y	z	Comment	Strike of Feature	Dip of Feature	Coordinates of Projection Normal to Strike at 1730 level x	y	z
0.2	667417.0	159220.1	1729.7	Broken core	50.0	65.0	667416.9	159220.2	1730.0
0.3	667417.0	159220.1	1729.6	Same as above	50.0	65.0	667416.9	159220.2	1730.0
34.5	667417.0	159220.1	1695.3	Many frax; Kilger	100.0	80.0	667418.1	159226.1	1730.0
35.5	667417.0	159220.1	1694.3	logged as qtz	100.0	80.0	667418.1	159226.3	1730.0

BOBK 85.001

Depth in Borehole	Mine Coordinates x	y	z	Comment	Strike of Feature	Dip of Feature	Coordinates of Projection Normal to Strike at 1730 level x	y	z
57.7	667378.4	159253.7	1697.1	Possible lamp	100.0	80.0	667379.4	159259.4	1730.0
57.8	667378.3	159253.7	1697.0	Same as above	100.0	80.0	667379.3	159259.5	1730.0
60.8	667376.5	159255.4	1695.3	Fractures	50.0	65.0	667366.1	159267.8	1730.0
61.2	667376.2	159255.6	1695.1	Same as above	50.0	65.0	667365.7	159268.0	1730.0
61.2	667376.2	159255.6	1695.1	Lamprophyre	100.0	80.0	667377.3	159261.6	1730.0
61.4	667376.1	159255.7	1695.0	Same as above	100.0	80.0	667377.2	159261.8	1730.0
63.5	667374.8	159256.8	1693.7	Many fractures	50.0	65.0	667363.9	159269.8	1730.0
64.5	667374.2	159257.3	1693.2	Same as above	50.0	65.0	667363.1	159270.5	1730.0
88.3	667359.5	159270.1	1679.5	Lamprophyre	100.0	80.0	667361.0	159278.9	1730.0
117.3	667341.5	159285.7	1662.9	Same as above	100.0	80.0	667343.6	159297.4	1730.0
118.7	667340.7	159286.5	1662.1	Lamprophyre	100.0	80.0	667342.7	159298.3	1730.0
119.3	667340.3	159286.8	1661.7	Same as above	100.0	80.0	667342.4	159298.6	1730.0
120.5	667339.5	159287.4	1661.1	Many fractures	50.0	65.0	667318.9	159312.1	1730.0
120.9	667339.3	159287.7	1660.8	Same as above	50.0	65.0	667318.6	159312.4	1730.0
120.9	667339.3	159287.7	1660.8	Fractures	50.0	65.0	667318.6	159312.4	1730.0
121.4	667339.0	159287.9	1660.5	Same as above	50.0	65.0	667318.2	159312.7	1730.0
121.4	667339.0	159287.9	1660.5	Many fractures	50.0	65.0	667318.2	159312.7	1730.0
121.8	667338.7	159288.1	1660.3	Same as above	50.0	65.0	667317.9	159313.0	1730.0
122.6	667338.2	159288.6	1659.8	Bleached core	50.0	65.0	667317.2	159313.6	1730.0
123.1	667337.9	159288.8	1659.6	Same as above	50.0	65.0	667316.8	159314.0	1730.0
125.6	667336.4	159290.2	1658.1	Lamprophyre	100.0	80.0	667338.6	159302.7	1730.0
126.0	667336.1	159290.4	1657.9	Same as above	100.0	80.0	667338.4	159302.9	1730.0
126.6	667335.8	159290.7	1657.6	Lamprophyre	100.0	80.0	667338.0	159303.3	1730.0
127.1	667335.5	159291.0	1657.3	Same as above	100.0	80.0	667337.7	159303.6	1730.0
127.1	667335.5	159291.0	1657.3	Fractures	50.0	65.0	667313.7	159317.0	1730.0
132.2	667332.3	159293.7	1654.4	Same as above	50.0	65.0	667309.7	159320.7	1730.0
132.2	667332.3	159293.7	1654.4	Lamprophyre	100.0	80.0	667334.7	159306.8	1730.0
132.3	667332.2	159293.8	1654.3	Same as above	100.0	80.0	667334.6	159306.9	1730.0

BOBK 85.002

Depth in Borehole	Mine Coordinates x	y	z	Comment	Strike of Feature	Dip of Feature	Coordinates of Projection Normal to Strike at 1730 level x	y	z
20.9	667403.2	159193.4	1718.1	Frax + lamp(?)	100.0	80.0	667403.6	159195.5	1730.0
21.1	667403.1	159193.3	1718.0	Same as above	100.0	80.0	667403.5	159195.4	1730.0
35.3	667395.5	159184.5	1709.8	Bleached core (?)	50.0	65.0	667389.4	159191.7	1730.0
36.1	667395.0	159184.0	1709.4	Same as above	50.0	65.0	667388.9	159191.4	1730.0
40.9	667392.5	159181.0	1706.6	Frax, dark core	50.0	65.0	667385.4	159189.4	1730.0
41.1	667392.4	159180.9	1706.5	Same as above	50.0	65.0	667385.3	159189.3	1730.0
43.8	667390.9	159179.2	1704.9	Ragged fracture	50.0	65.0	667383.4	159188.2	1730.0
48.4	667388.4	159176.4	1702.3	Fractures	50.0	65.0	667380.1	159186.3	1730.0
48.9	667388.2	159176.1	1702.0	Same as above	50.0	65.0	667379.8	159186.1	1730.0

BOBK 85.003

Depth in Borehole	Mine Coordinates x	y	z	Comment	Strike of Feature	Dip of Feature	Coordinates of Projection Normal to Strike at 1730 level x	y	z
10.4	667404.9	159206.6	1724.1	Frax along core	50.0	65.0	667403.1	159208.7	1730.0
22.4	667395.1	159205.9	1717.2	Bleached core	50.0	65.0	667391.3	159210.4	1730.0
23.2	667394.5	159205.8	1716.8	Same as above	50.0	65.0	667390.5	159210.6	1730.0
50.6	667372.1	159204.3	1701.1	Lamprophyre	150.0	80.0	667376.5	159206.8	1730.0
52.3	667370.7	159204.2	1700.1	Same as above	150.0	80.0	667375.2	159206.8	1730.0
52.9	667370.2	159204.1	1699.7	Lamprophyre	150.0	80.0	667374.8	159206.8	1730.0
54.3	667369.0	159204.1	1698.9	Same as above	150.0	80.0	667373.8	159206.8	1730.0
54.3	667369.0	159204.1	1698.9	Fractures	50.0	65.0	667359.7	159215.2	1730.0
55.5	667368.1	159204.0	1698.2	Same as above	50.0	65.0	667358.5	159215.3	1730.0
55.5	667368.1	159204.0	1698.2	Lamprophyre	150.0	80.0	667372.9	159206.8	1730.0
55.6	667368.0	159204.0	1698.2	Same as above	150.0	80.0	667372.8	159206.8	1730.0
55.6	667368.0	159204.0	1698.2	Fractures	50.0	65.0	667358.4	159215.3	1730.0
56.4	667367.3	159203.9	1697.7	Same as above	50.0	65.0	667357.6	159215.5	1730.0
59.8	667364.5	159203.7	1695.8	Bleached core	50.0	65.0	667354.3	159216.0	1730.0
60.8	667363.7	159203.7	1695.2	Same as above	50.0	65.0	667353.3	159216.1	1730.0
64.9	667360.4	159203.5	1692.9	Many fractures	50.0	65.0	667349.2	159216.7	1730.0
65.2	667360.1	159203.4	1692.7	Same as above	50.0	65.0	667348.9	159216.8	1730.0

- END -

DATE FILMED

01 / 28 / 91